STUDY OF OZONOLYSIS OF ACOUSTICALLY LEVITATED PROXIES FOR ATMOSPHERIC AEROSOLS

A thesis submitted to obtain the degree of

Doctor of Philosophy

School of Chemistry, Food and Pharmacy

EDNA ROCÍO CABRERA MARTÍNEZ

September 2017

Declaration

I declare this is my own work and the use of all material from other sources has been properly and fully acknowledged.

Signed:

EDNA ROCIO CABRERA MARTINEZ

ABSTRACT

Atmospheric aerosols play an essential role in the climate. They are essential to the atmosphere as they help to form clouds and participate in the radiative balance and regulation of terrestrial surface temperature. Organic aerosols originate from natural and man-made sources. Meat cooking is considered an important contributor of a variety of organic compounds in the atmosphere, such as fatty acids. Oleic, linoleic and palmitoleic acids are the most commonly found long-chain unsaturated fatty acids in urban environments. These fatty acids contribute considerably to the aerosol fraction due to the reactions that they undergo, such as ozonolysis, which yields aerosols that have a notable impact on climate and health. It is known that the presence of water in variable relative humidity environments may affect the reaction of ozonolysis of unsaturated fatty acids since both, the carboxylic acid and the products formed may retain water at the surface, increasing the residence time of dissolved ozone at the surface and affecting the reactive uptake coefficient of ozone. The chemistry involved in the reactions of atmospheric aerosols still remains poorly understood.

In this study, Raman acoustic levitation was used to assess the effect of ozone concentration, relative humidity, droplet size and the presence of surfactants, on the ozonolysis of fatty acids.

It was found that droplet size affected the uptake coefficient, whereas relative humidity had a variable effect in the uptake coefficient depending on additional factors, such as ozone concentration and droplet diameter. The presence of surfactants such as sodium

oleate decreased the uptake coefficient of ozone and induced a phase transformation of the levitated droplets, even under high relative humidity. Palmitoleic and linoleic acids showed more reactivity compared to oleic acid.

Products were analysed by headspace solid-phase micro-extraction (SPME) coupled to gas chromatography mass spectrometry (GC–MS). A mechanism of ozonolysis of palmitoleic acids was proposed, and some products were verified to be formed from the reactions. Products of ozonolysis of fatty acids were identified.

Contents

LIST OF FIGURES

LIST OF TABLES

NOMENCLATURE

The following list contains the most common abbreviations and symbols found in this document.

OA	Oleic Acid
PA	Palmitoleic Acid
LA	Linoleic Acid
FA	Fatty Acid
UFA	Unsaturated Fatty Acid
PUFA	Polyunsaturated Fatty Acid
MUFA	Monounsaturated Fatty Acid
POA	Primary Organic Aerosol
SOA	Secondary Organic Aerosol
VOCs	Volatile Organic Compounds
POM	particle organic matter
CI	Criegee Intermediate
SO	Sodium Oleate
MS	Mass Spectra
m/z	Mass-to-charge
RT	Retention Time
RH	Relative Humidity
$[O_3]$	Ozone concentration
UV	Ultraviolet
US	Ultrasonic
AAHP	α-acyloxyalkyl hydroperoxides
HS-SPME	Head Space Solid-Phase Micro Extraction
CCN	Cloud Condensation Nuclei
a.u.	Arbitrary units
γ	Reactive uptake coefficient
k_2	Second order rate constant of reaction

ACKNOWLEDGEMENTS

I would like to express my gratitude to the Government of Colombia and the Department of Science, Technology and Innovation, COLCIENCIAS, for the financial support to this research project.

I would like to say thank you to my supervisor, Dr. Christian Pfrang for his direction throughout this project. Special acknowledgement to Professor George Marston for giving me the opportunity to come to Reading and start my PhD. Likewise a big thank you to the past and present members of the group for the help provided in different moments I needed, and also to some technicians and staff of the Chemistry Department for their help.

My appreciation to the former MChem students: Harry Ancill for collaborating with the experimental, and Sukhpreet Talewar for helping me with the project and for her invaluable friendship. My gratitude is also to my friends for being supportive in the hard moments I faced during the PhD, they are, in the UK: Elisa Chacón, Stella Perdomo, Natali Ortiz, Jorge Ontaneda, Joana Bustamante, Diego Ramirez, Diego Molina and Diego Fuentealba; in Sweden: Juan David Vasquez; and also in Colombia and around the world.

I am very grateful to my family in the United Kingdom, my sister Rina, my lovely niece and nephews, and my brother in law, for making my life easier and happier during these 4 years, they supported me all the time. Also thank you to my family in Colombia (♥) for all the patience and backup during these hard and busy years.

Thanks God for this opportunity.

INTRODUCTION

Over the past few decades, the interest and concern regarding to the pollution and climate change has increased. The atmosphere that allows life on Earth is a mixture of different components of natural and anthropogenic origin. Nitrogen and oxygen comprise the most abundant gases in the atmosphere, but not only gases are present. Atmospheric aerosols are microscopic solid and liquid particles that are disseminated throughout the atmosphere (Boucher, 2015; Seinfeld and Pandis, 2006) and their reactions have caught attention since it was discovered these aerosols have an effect on health and life on the Earth. Aerosols also play a very important role in the global climate as they can scatter, absorb or emit radiation, having an effect on the radiative balance, affecting the surface temperature. They can also have an impact on precipitation as they serve as the initial nuclei upon which water condenses to form the droplets of clouds, so-called cloud condensation nuclei (CCN) (Rudich et al, 2007).

Aerosols can be organic or inorganic. It is estimated that the organic fraction may comprise between 20 and 90% of fine particulate matter mass found in the troposphere (Kanakidou et al, 2005; Kroll and Seinfeld, 2008; Vesna et al 2008); these organic aerosols are released into the atmosphere as primary organic aerosols (POA), but gas-phase precursors are also converted into secondary organic aerosols (SOA) by means of oxidative atmospheric processes (Finlayson-Pitts and Pitts, 2000). The SOA fraction is prevalent among organic aerosols and comprises roughly 66% of the organic aerosol mass in urban areas, whereas in rural areas this amount may be greater than 90% (Hallquist et al, 2009, Song et al, 2007). The organic aerosols fraction consists of a complex mixture that includes saturated and unsaturated hydrocarbons, terpenes,

aromatic compounds, carbonyl compounds and carboxylic acids. It is believed that approximately 10 % of the organic aerosol fraction corresponds to carboxylic acids (Gallimore et al, 2011), characterised by the presence of one or more carbon -carbon double bonds, one or more carboxylic group, and either short or long carbon chains. Examples of fatty acids found in the aerosol fraction are maleic, palmitic, stearic, linoleic, palmitoleic and oleic acids, and the source of these species may be both anthropogenic and biogenic, marine, forest, car exhaust and cooking emissions being some examples (Kawamura, et al, 2003; Moise and Rudich, 2000; Petters et al, 2006).

Many studies have aimed to investigate the conversion of the emitted aerosol to form activated particles. Meat cooking is considered one of the most important source of organic aerosol in urban environments, contributing roughly 20% of the particulate matter in big cities such as Los Angeles, Hong Kong, and Beijing (He et al, 2010). Oleic acid, linoleic acid and palmitoleic acid are the main long-chained unsaturated fatty acids (UFA) found in the emissions from meat cooking in rural and urban regions in China, with a total of 6.46 ng/m3 of UFA measured during autumn 2009, corresponding to 71.5% OA, 26.9 % LA and 1.6 % PA (Zhao et al, 2014). To a great extent, the reaction of ozonolysis of oleic acid has been the model system to study the heterogeneous oxidation of organic atmospheric compounds, following a mechanism that involves the formation of Criegee intermediates, to produce azelaic acid, nonanoic acid, 9-oxononanoic acid and nonanal (Zahardis and Petrucci, 2007).

Studies using linoleic acid suggest an additional mechanism at atmospheric relevant ozone concentrations (20 to 40 ppb in rural regions and 200 to 400 in urban sites), observing an autoxidation induced by ozone, with the formation of products different than carboxylic acids and carbonyl compounds (Lee and Chan, 2007a). Although the general mechanisms of ozonolysis of linoleic acid has been reported and it is believed

that it involves the formation of radicals and diene structures, the full mechanism is still not completely understood. With respect to palmitoleic acid, it is expected that ozonolysis of this fatty acid follows the same mechanism as oleic acid, with the formation of species including carbonyl and carboxylic groups in the structure (Spencer and Kleiman, 1978), also this fatty acid has shown faster reactivity compared to oleic acid (Huff Hartz et al, 2007; Weitkamp, 2008); however there is not sufficient information that confirms the products and mechanism of ozonolysis of palmitoleic acid.

Atmospheric reactions involve several chemical and physical processes that take place either in solution or gas phase, starting with the diffusion of gas particles to the droplet surface, followed by the transport of the gas across the air-water interface; then the solvated gas is diffused into the bulk phase of the droplet, to complete the process when the species either in the aqueous phase or on the interface undergo chemical reactions (Finlayson-Pitts and Pitts, 2000). Factors such as ozone concentration, particle size and relative humidity may have an effect on these processes, by affecting the composition of aerosols and therefore the rate of reactions. Raman spectroscopy is one of the techniques that has been reported to measure hygroscopic properties, and also to elucidate the impact of phase transformation of levitated aerosols droplets and investigate both physical and chemical changes in aerosols (Lee et al, 2008).

As the main sources of carboxylic acids could be direct emission as well as oxidative reactions of their precursors in the atmosphere, the study of reactions that involve their formation and decomposition has generated interest, because a deeper knowledge of physical and chemical processes involved in oxidative ageing of aerosol is necessary in order to understand atmospheric phenomena related to cloud condensation nuclei, precipitation and therefore, climate.

The aims of this thesis are: Despite the appreciable amount of research related to ozonolysis of organic aerosol, the understanding of oxidative ageing processes of many atmospheric aerosols is still considered insufficient (Zahardis and Petrucci, 2007). Therefore, this study attempts to understand the chemical and physical processes involved in ozonolysis of unsaturated fatty acids.

- To carry out the reactions of ozonolysis of unsaturated fatty acids by means of acoustic levitation linked to Raman microscopy.
- To understand the effect of different ozone concentrations, size of droplet and the role of the relative humidity on the oxidative processes.
- To propound the most plausible mechanisms of ozonolysis of fatty acids with the help of analysis of the products formed in the reactions.
- To understand the different processes occurring in both gas and liquid/aqueous phases during the ozonolysis of organic aerosols.
- To establish the atmospheric implications of the obtained results.

This thesis is outlined as follows:

CHAPTER 1: Overview of the chemistry of the atmosphere.

It includes basic concepts regarding to the atmosphere and aerosols, such as: atmospheric aerosols, chemical composition of atmospheric aerosols and reactions, atmospheric ozone, cloud condensation nuclei, organic aerosols and ozonolysis of fatty acids.

CHAPTER 2: Methodology.

This chapter explains the fundamentals of various techniques that have been used to achieve the aims of this research: acoustic levitation and its applications; Raman spectroscopy and instrumentation; Gas chromatography and mass spectrometry. Then, a detailed description of the experimental set-up used to do this research is provided in the last section of the chapter.

CHAPTER 3: Ozonolysis of individual fatty acids.

This chapter introduces the results of ozonolysis of the fatty acids analysed in the research: oleic acid, linoleic acid and palmitoleic acid. Here, two different approaches were followed: the influence of ozone concentration, and the influence of relative humidity. Raman spectra and plots of the ratios of Gaussian area of two peaks (corresponding to C=C stretching and CH_2 bending) obtained from the spectra are shown in this section.

In the second part of this chapter kinetic parameters are calculated, analysed and compared, using the same two approaches (influence of O_3 concentration and relative humidity). The products of the reactions are analysed using GC/MS, then the most probable mechanisms of the reactions are suggest.

CHAPTER 4: Ozonolysis of self-assembled mixtures of fatty acids.

The results of ozonolysis of the mixtures of the fatty acid, sodium oleate and sodium chloride solution in defined proportions as a surrogate of the sea spray in the atmosphere are reported in this chapter. These findings are compared to those reported in Chapters 3 and 4, as well as previous work.

CHAPTER 5 Conclusions and future work.

CHAPTER 1

OVERVIEW OF THE CHEMISTRY OF THE ATMOSPHERE

1.1 EARTH'S ATMOSPHERE

The atmosphere that surrounds the Earth as a protective layer is a mixture of several gases; nitrogen (78.0%) and oxygen (20.9%) are the most abundant gases of the atmosphere, argon comprises 0.9%, and also some trace gases are present in fractions less than 10^{-6}, 1 part per million (ppm) by volume, including carbon dioxide, helium, hydrogen, neon, krypton, methane, xenon and nitrous oxide, among others Brimblecombe, 1996; Seinfeld and Pandis 2006). The atmosphere also contains a variety of other gaseous components, such as sulfur-containing compounds, nitrogen-containing compounds, carbon-containing compounds, halogen-containing compounds, atmospheric ozone and particulate matter which consists on particles resulting from natural or anthropogenic sources, technically named aerosols. They represent an important role in the Earth's radiative balance and in the chemical properties of the atmosphere. Moreover, it has been possible to identify the presence of other atmospheric trace species and also to determine that the composition of the atmosphere is changing over the world. Global concentrations of gases such as carbon dioxide, methane, nitrous oxide and halogen-containing compounds have increased in an alarming way. Those gases, known as "greenhouse gases", act as atmospheric thermal insulators (Seinfeld and Pandis, 2006).

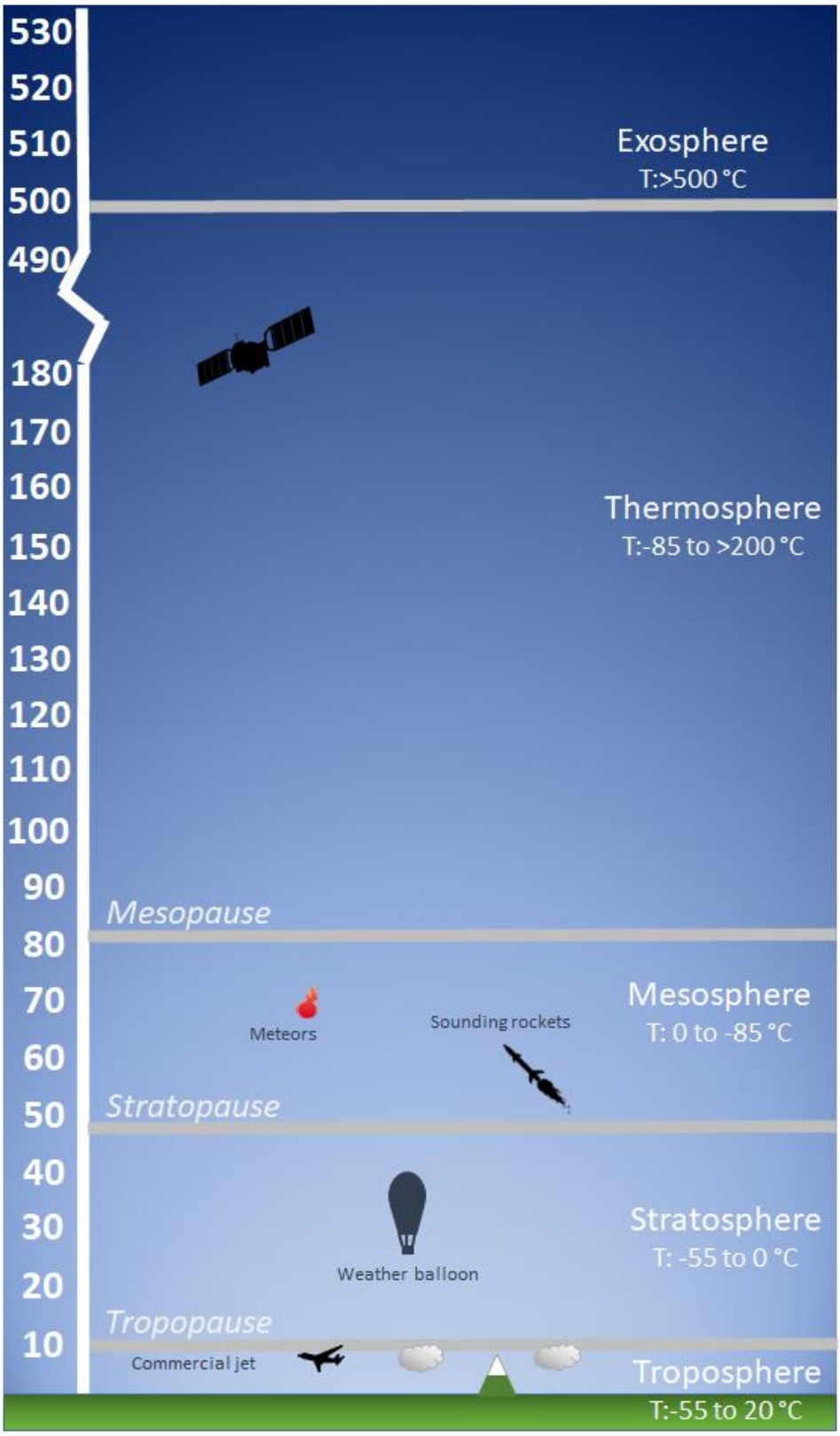

Figure 1.1 Layers of Earth's atmosphere. Given values of the altitudes (in km) and temperatures are approximated (Based on Seinfield and Pandis, 2012).

The atmosphere is divided into several layers, as shown in Figure 1.1. Starting at the Earth's surface, the closest layer is the troposphere, it reaches a maximum altitude of 15 km up to the tropopause, which is a thin boundary zone between the troposphere and the next layer, the stratosphere. In the upper stratosphere lies the ozone layer, a protective gas layer that absorbs dangerous UV radiation, thus it protects life on Earth. The stratosphere is located between the tropopause and the stratopause (from ~45 to 55 km). The upper regions of the atmosphere are mesosphere, thermosphere and exosphere. (Seinfeld and Pandis, 2006).

1.2 ATMOSPHERIC AEROSOLS

An aerosol can be defined in technical terms as a colloidal suspension of fine solid or liquid particles in a gas. This definition can be extended to atmospheric aerosols as microscopic solid particles or liquid droplets dispersed in the atmosphere, to the exception of cloud particles, snowflakes, ice crystals, among other type of hydrometeors (Boucher, 2015), that normally have sizes ranging to 1 nm to 100 μm. Depending on the chemical composition or source, atmospheric aerosols can be classified in different categories, as shown in the schematic in Figure 1.2. A considerable amount of aerosol present in the troposphere comes from human activities, such as car exhaust, industrial emissions, biomass burning, food cooking, etc. Tropospheric aerosols also include sulfate, ammonium, nitrate, sodium, chloride, trace metals, and water vapour (Seinfeld and Pandis, 2006). In addition, the most common inorganic particles found in the troposphere are crustal elements such as oxygen, silicon, aluminium, iron, magnesium, calcium, sodium, potassium, and titanium (Finlayson-Pitts and Pitts, 2000). Natural sources such as windborne dust, sea spray and volcanoes, and also anthropogenic activities such as incomplete combustion of fossil fuels and biomass burning are

sourced atmospheric aerosols.

With respect to organic aerosols, a vast number of organic compounds are present in both urban and remote areas (Hallquist et al, 2009). The organic fraction in the atmosphere is a complex mixture of hundreds of organic compounds that includes n-alkanes, n-alkanoic acids, n-alkanals, aliphatic dicarboxylic acids, terpenes, terpenoids, aromatic polycarboxylic acids, polycyclic aromatic hydrocarbons, steroids, N-containing compounds, etc. (Seinfeld and Pandis, 2006). Part of the organic aerosols is emitted into the atmosphere as Primary Organic Aerosols (POA), that can undergo chemical reactions either in particle or in gas phase. Conversely, Secondary Organic Aerosols (SOA) are formed in the atmosphere as a result of the gas-to particle conversion of volatile organic compounds (VOCs) and some inorganic species (Rudich et al, 2007). The schematic in Figure 1.3 shows the different sources of POA and SOA and their conversion processes in the atmosphere. POA are directly emitted into the atmosphere as liquids or solids from anthropogenic and biogenic sources. Secondary particles are formed in the atmosphere via gas-to-particle conversions when windborne particles are transformed by means of chemical processes, such as homogeneous gas phase, homogeneous aqueous phase, and heterogeneous reactions, or physical processes such as changes in particle size or coagulation (Hobbs, 2000; Pöschl, 2005; Rudich et al, 2007; Seinfeld and Pandis, 2006).

Aerosols are important because they play a role in the absorption and scattering of solar and terrestrial radiation, contributing to the regulation of the Earth's temperature. They have life-times in the atmosphere ranging from hours to weeks (Pöschl 2005), they are also related to the formation of clouds particles, determining visibility and precipitations. Therefore, changing the amount of aerosol may impact the climate.

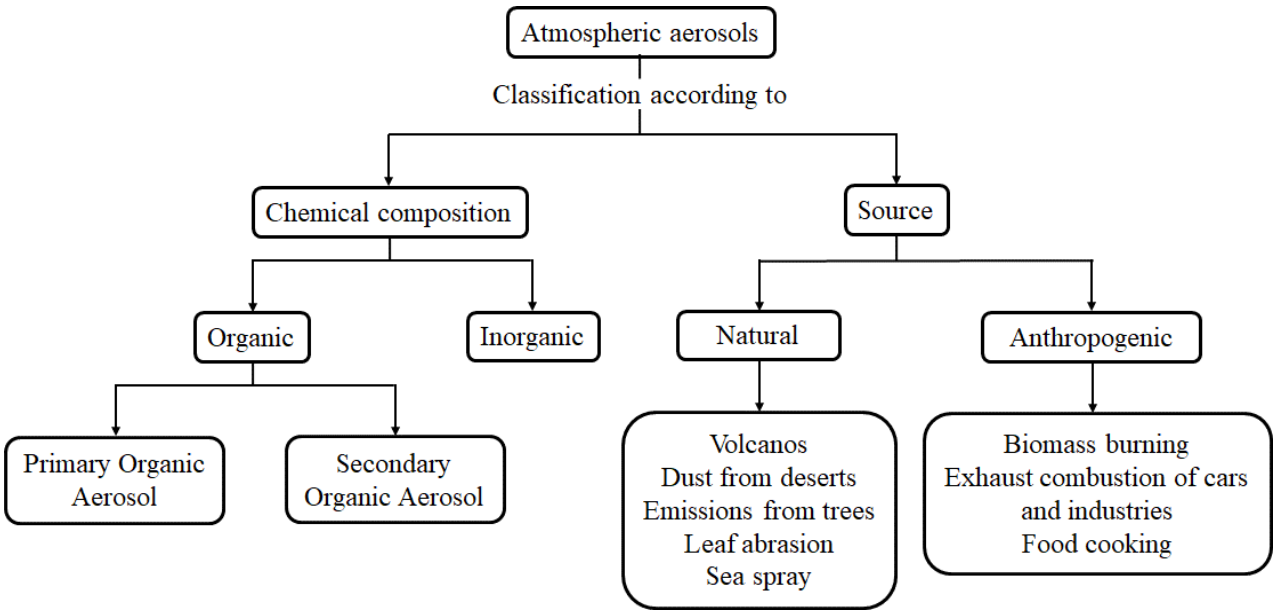

Figure 1.2. Classification of atmospheric aerosols according to origin, source and chemical nature.

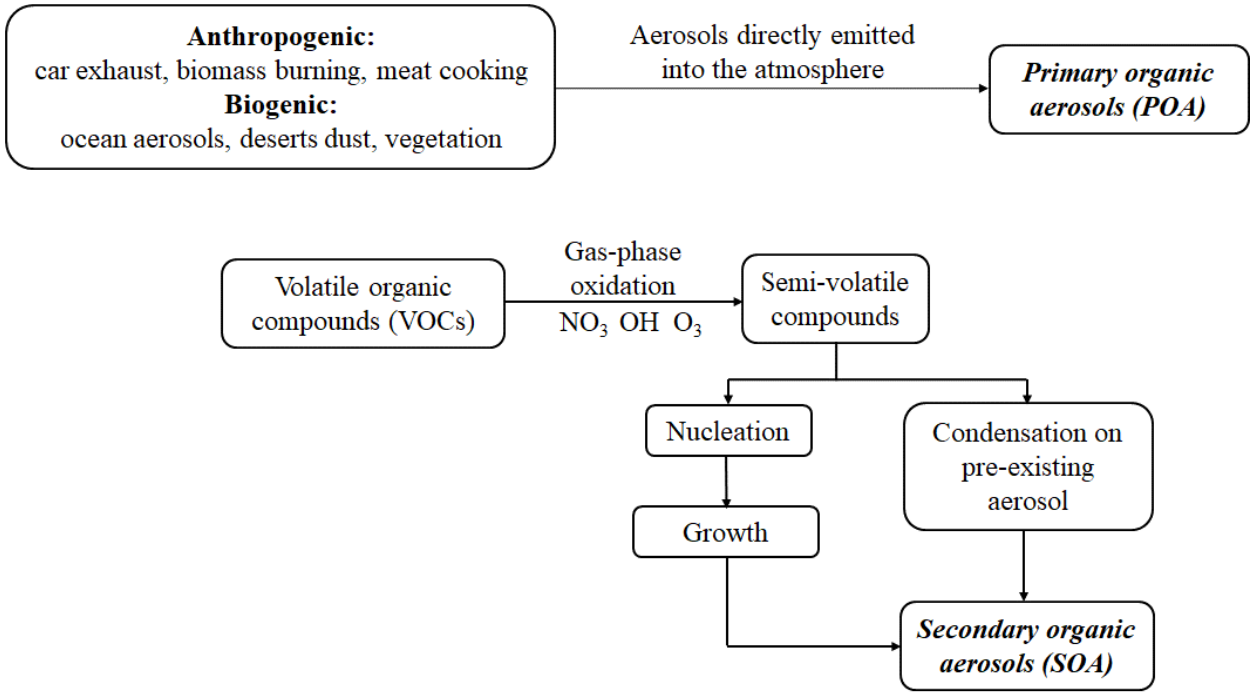

Figure 1.3 Sources of Primary Organic Aerosols and Secondary Organic Aerosol (Rudich et al, 2007)

1.2.1 CHEMICAL COMPOSITION OF AEROSOLS IN THE ATMOSPHERE

Aerosols could be present in both stratosphere and troposphere, therefore the chemical composition varies depending on the place they could remain.

- Stratospheric aerosols: the main components of stratospheric aerosol fraction are sulfur-containing compounds, such as SO_2, CS_2 and H_2SO_4. This aerosol is composed mainly of an aqueous sulfuric acid solution in the range of 60-80% (Hobbs, 2000; Seinfeld and Pandis, 2006).
- Tropospheric aerosols: aerosols present in troposphere are mainly of anthropogenic origin, however the composition of these aerosols is more complex than stratospheric aerosols. They contain both inorganic and organic species, such as sulfate, ammonium, nitrate, sodium, chloride, trace metals, carbonaceous material, crustal elements, and water (Seinfeld and Pandis, 2006). Further information about organic aerosols in the troposphere will be provided in section 1.5.

1.2.2 TRANSFORMATIONS OF TROPOSPHERIC AEROSOLS

a. The *gas-to-particle conversion* of aerosols involves three main species: sulfur, nitrogen, and organic carbonaceous materials. The major processes involved in gas-to-particle conversion are growth of an existing aerosol and nucleation of a new aerosol.

- *Growth aerosols* are formed by condensation onto existing particles, thus an increase in the mass of aerosols (not the number) is achieved (Hobbs, 2000).

- *Nucleation* occurs when low-vapour-pressure species are condensed to form a new particle. When there are two different gas-phase compounds such as sulfuric acid and water, the formation of particles is known as *binary homogeneous nucleation* (Finlayson-Pitts and Pitts 2000).

b. If secondary aerosol is formed by the scavenging of the low-vapour-pressure products onto pre-existing particles, the process is called *heterogeneous condensation* (Finlayson-Pitts and Pitts, 2000).

c. Small aerosol particles (<1 μm in diameter) moving randomly due to collisions with gas molecules and, due to their rapid Brownian motion, collide efficiently with each other causing *coagulation* (Hobbs, 2000).

1.3 CLOUD CONDENSATION NUCLEI (CCN)

Aerosols affect the climate system via several physical mechanisms. Firstly, they scatter and absorb solar radiation, and they also scatter, absorb and emit thermal radiation. In addition, aerosols are essential to the atmosphere as they help to form clouds by acting as cloud condensation nuclei. Cloud condensation nuclei are aerosols that act as the initial sites where water vapour is condensed into cloud droplets or cloud ice particles (Lohmann and Feichter 2005). To form a CCN the aerosols have to be activated thus, as the CCN tend to attract the water vapour present in the atmosphere, they can act as the initial sites for condensation of water vapour into cloud droplets. The formation of a liquid from water vapour starts when a small group of water molecules condensate to

form a cluster over which other gaseous molecules can condense. Given this cluster is very small and the vapour pressure over the cluster is too large, it would instantaneously evaporate at the normal atmosphere supersaturation (about 2%). Therefore, unless there was a particle on which the water can start condensation, clouds and fogs could not be formed (Finlayson-Pitts and Pitts, 2000). Some aerosols have an indirect effect on the formation of clouds from particles which can start such as gaseous water molecules condensation, acting as CCN, which is defined by Kerminen et al (2012) as particles that can activate the growth of a particle due to condensation of water vapor at constant supersaturation. Andreae and Rosenfeld 2008 called these clusters "embryos", they mentioned the influence that some chemical compounds have on the formation of cloud droplets, for example, soluble gases, mainly HNO_3, NH_3, and HCl, can facilitate droplet formation by dissolving in incipient droplets and adding to the solute amount in the droplet. Additionally, organic compounds in aerosols can influence CCN activity via several mechanisms: contribution of soluble matter, reduction of surface tension, and formation of hydrophobic surface films.

1.4 ATMOSPHERIC OZONE

Ozone is a gas present in the Earth's atmosphere in trace amounts; it is produced naturally as a result of the photochemical reaction:

$$O_2 + h\nu \rightarrow O\bullet + O\bullet \qquad \text{Equation 1.1}$$

Ozone is present in both the stratosphere and troposphere. About 90% of the Earth's atmospheric ozone is present in the stratosphere, where it plays a key role in absorbing

damaging ultraviolet radiation from the Sun. Tropospheric ozone is only about 10% of the total mass of the atmospheric ozone (Seinfeld and Pandis, 2006). Given that the troposphere is the closest layer to the terrestrial surface, tropospheric ozone is considered a potent pollutant which causes respiratory problems in humans (Seinfeld and Pandis, 2006). Tropospheric ozone is also involved in the formation of hydroxyl radicals (OH) and hydrogen peroxide (H_2O_2) by means of photochemical reactions. These species are powerful oxidants that reacts rapidly with many atmospheric pollutants, for example, H_2O_2 dissolves in cloud water, where it can oxidize SO_2 into H_2SO_4, while OH radicals have been named the "atmosphere's detergent" because they transform a vast number of tropospheric gases, many of them considered major pollutants (Hobbs, 2000).

Ozone reacts in the atmosphere with unsaturated compounds, such as terpenes and carboxylic acids, by means of a mechanism that involves the formation of Criegee intermediates. The general mechanism of this reaction is shown in Figure 1.4 (Criegee, 1975; Wade, 2013; Zahardis and Petrucci, 2007). The reaction initiates with the 1,3-dipolar cycloaddition of ozone to the double bond to form the molozonide 1,2,3-trioxolane; this primary species reacts to give an aldehyde or ketone and the intermediate energy-rich biradical specie called *Criegee intermediate*, which can be stabilized by collision or can undergo unimolecular decomposition (Horie and Moortgat, 1991). As the double bond involves two carbons, the reaction yields four initial products. However, given the conditions and nature of the compounds that react with ozone, the unsaturated compound yield a mixture of many different products of varying reactivity, according to the general mechanism shown here (Lee and Chan, 2007a; Lee and Chan, 2007b; Vesna et al, 2009).

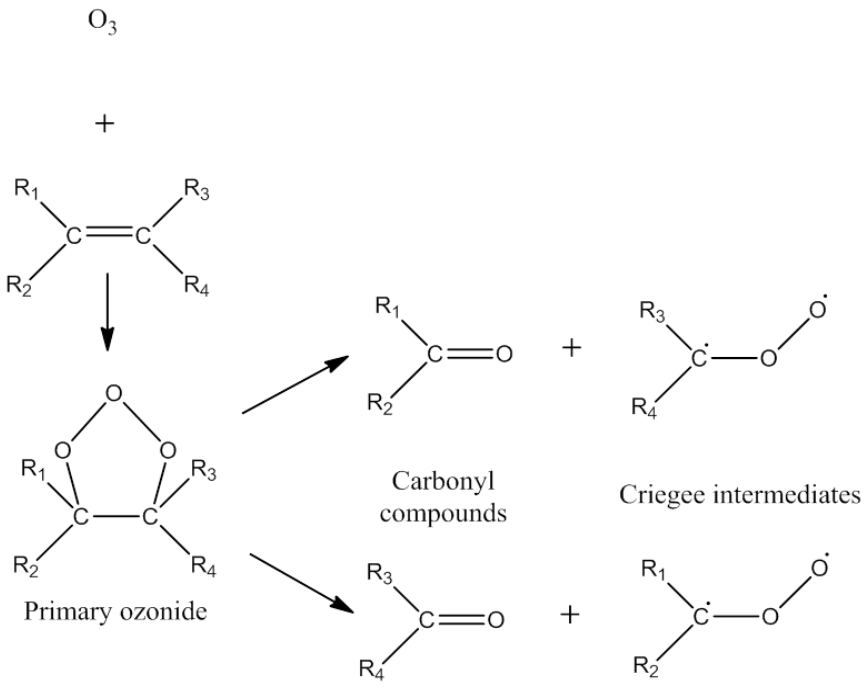

Figure 1.4. Formation of Criegee intermediates by ozonolysis of alkene compound.

The ozonolysis also yield several products derived from the intermediate species. The primary ozonide (molozonide) is an unstable species that is decomposed to form two products, a carbonyl compound, and a Criegee intermediate (carbonyl oxide). The carbonyl oxide is a species positively and negatively charged, similar to a zwitterion that is highly energetic, therefore it is stabilised by resonance, leading to the next step, the stabilization by any of these reactions: 1) dimerization; 2) rearrangements to produce carboxylic acids (Horie and Moortgat, 1991); 3) reaction with aldehydes or ketones to form ozonides, or 4) reaction with proton-active compounds. The overall reaction pathway is illustrated in Figure 1.5, based on the mechanism of ozonolysis published by Criegee (Criegee, 1975).

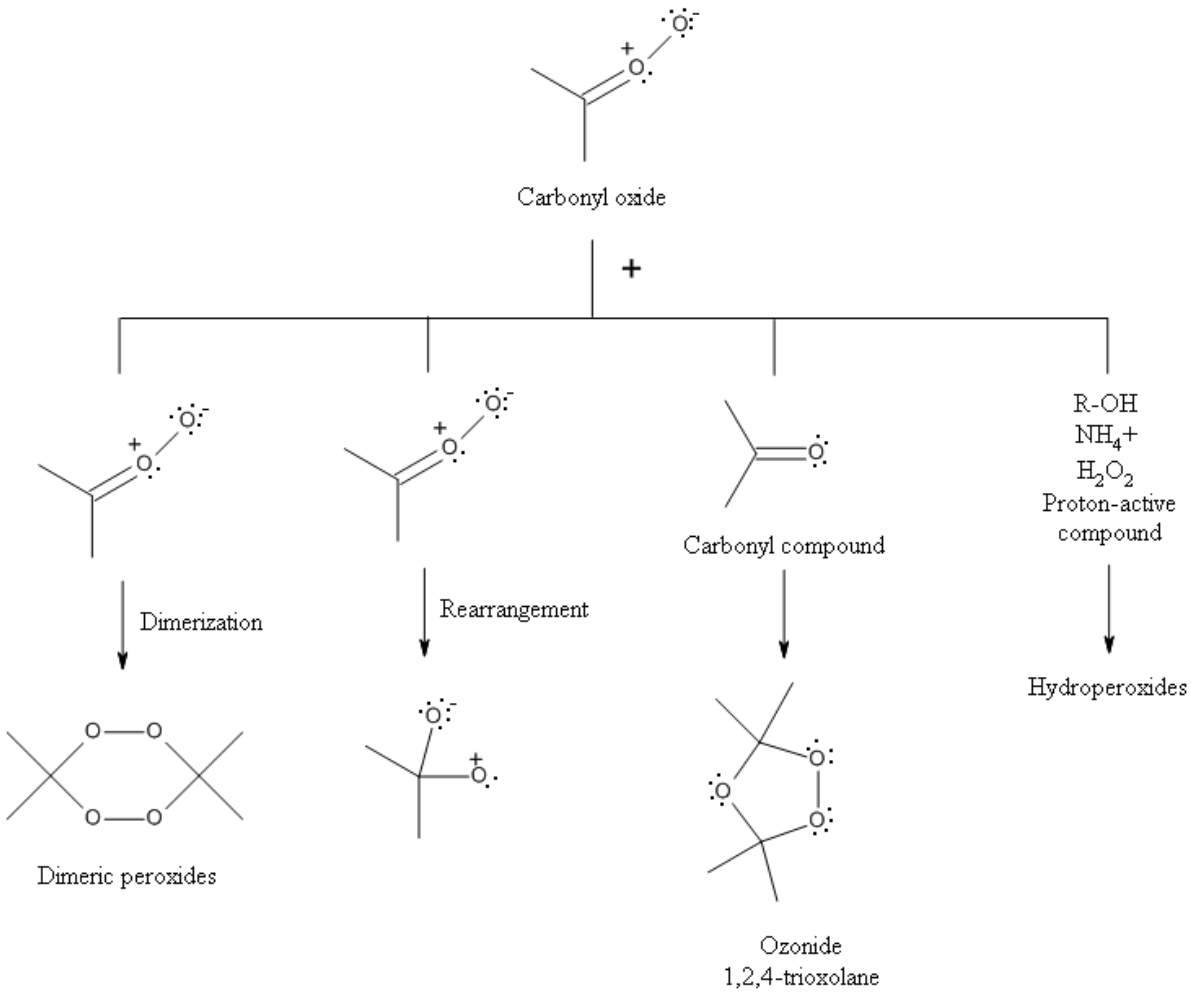

Figure 1.5 Reaction pathways for stabilization of the carbonyl oxide formed during the ozonolysis of an unsaturated compound (based on Criegee, 1975)

1.5 ORGANIC COMPOUNDS IN THE TROPOSPHERE

The atmosphere in different cities around the world has been monitored to establish its composition (Fei et al, 2015; Guo et al, 2012; Limbeck and Puxbaum, 1999; Wang et al, 2006; Zhao et al, 2014). Hydrocarbons such as methane, ethane, propene, acetylene and aromatic species such as benzene and toluene, have been found in the atmosphere

together with many other organic species, for example alcohols (methanol and ethanol), aldehydes (formaldehyde and acetaldehyde), ketones (acetone), organic acids (oxalic, formic, acetic, maleic, tartaric, malic, succinic, palmitic, stearic and oleic acid), peroxides (methylhidroperoxide), and biogenic compounds (terpenes) (Kuo et al, 2011; Limbeck and Puxbaum, 1999; Mochida et al, 2003; Rogge et al, 1991; Zhao et al, 2007a). Some of them are the result of natural sources for example vegetation releases organic compounds into the atmosphere, specifically pine trees emit terpenes such as α- and β-pinene. Additionally human activities can also contribute, either directly or indirectly, to increase the amount of organic species released to the atmosphere. Given that the most of emitted organic compounds released into the atmosphere are in gas-phase, the term *Volatile Organic Compounds* (VOCs) is mainly used to denote the vast majority of gas-phase organic compounds present in the atmosphere. A detailed review and discussion of biogenic volatile organic compounds and their gas-phase reactions in troposphere is presented by Atkinson and Arey (2003).

It is estimated that meat cooking is one of the most important source of organic aerosol in urban environments, providing 20% of the primary organic matter found in organic aerosol fraction in Los Angeles (Schauer et al, 1996) and 10% from Chinese cooking in China (Zhao et al, 2007a). Many studies have been carried out in order to monitor the amount of emissions from this source but also to investigate the conversion of the emitted aerosols into activated particles. The emissions of organic aerosols from Chinese cooking and western-style cooking were compared by Zhao et al (2007b) showing that the released particle organic matter (POM) fraction is a vast set of organic compounds, including carboxylic acids, with oleic acid as the main long-chain unsaturated fatty acid present in the emissions, followed by linoleic acid and palmitoleic acid. By using aerosol mass spectrometer analysis, Mohr et al (2012) identified and

quantified the organic aerosols from meat cooking in Barcelona during the winter, concluding that 17% of POM originated from cooking activities. Other human activities such as biomass burning, vehicle fuel combustion, and trash burning also contribute to the primary organic aerosol load (Mohr et al, 2009; Robinson et al, 2006).

1.6 OZONOLYSIS OF UNSATURATED FATTY ACIDS

It is known that ozone-alkene reactions in gas-phase yields a set of products, principally ketones, carboxylic acids and aldehydes, following the Criegee intermediate mechanism previously mentioned in section 1.4. Long-chain unsaturated fatty acids present in oils are released into the troposphere from cooking activities, and they may undergo ozonolysis to form secondary organic aerosols. Significant amounts of oleic and linoleic acid have been found in emissions from food cooking, and also palmitoleic acid is present in these emissions in traceable quantities. Some other unsaturated fatty acids present in food, such as linolenic and arachidonic acids were not found in significant quantities in the atmosphere (Zhao et al, 2007a; Zhao et al, 2007b).

1.6.1 OLEIC ACID

Vegetable oils such as olive oil contain unsaturated fatty acids (UFA), but this fatty acid is also present in some seeds and animal fats (Czamara et al., 2014). According to Zahardis et al (2006), the prevalent UFA in olive oil is oleic acid (57%) followed by

linoleic acid (15.1%), palmitoleic acid (3.2%) and linolenic acid (1.8%). The use of vegetable oils has been related to presence of oleic acid and methyl oleate in the atmosphere. Carboxylic acids are present in the atmosphere as part of secondary organic aerosol. Recent studies have found that some aerosols could be covered in or contain amphiphilic organic compounds (Davies et al, 2012; Ellison et al, 1999; Latif and Brimblecombe, 2004 Nájera, 2007; Pfrang et al, 2017; Tabazadeh, 2005) and this layer may the affect residence time of particulate matter and its ability to act as CCN, this affects the formation of clouds and thereby precipitations, resulting in variation of the water cycle (Hearn et al. 2005). Methyl oleate is the methyl ester of oleic acid, present in atmosphere due to meat cooking processes. Monolayers of this ester may be present at the air-water interface of droplets acting as a surfactant that reduces the droplet's surface tension, helping the formation of clouds and ultimately precipitation. In their study, Pfrang et al, (2014) determined that ozonolysis removes methyl oleate from the air-water surface faster than its parent oleic acid. As a consequence of this, cloud nucleation properties of water droplets are affected. This is explained by ozone cleavage of carbon-carbon double bond of methyl oleate, such that it loses its ability to remain as surfactant at the air/water interface.

Cis-9-octadecenoic acid, best known as oleic acid (OA), is the most abundant long-chain unsaturated fatty acid found in the POM (Zhao et al, 2014). The reaction of this acid with ozone yields initial products by following the mechanism explained in section 1.4, with the formation of two Criegee intermediates (CI), that finally decompose to form two products, in total, this reaction leads to obtain mainly nonanal, 9-oxononanoic acid, nonanoic acid (from CI II) and azelaic acid (from the CI I), as shown in Figure 1.6 (Zahardis and Petrucci, 2007). This reaction has been extensively benchmarked as a model system to study the heterogeneous oxidation of organic atmospheric compounds.

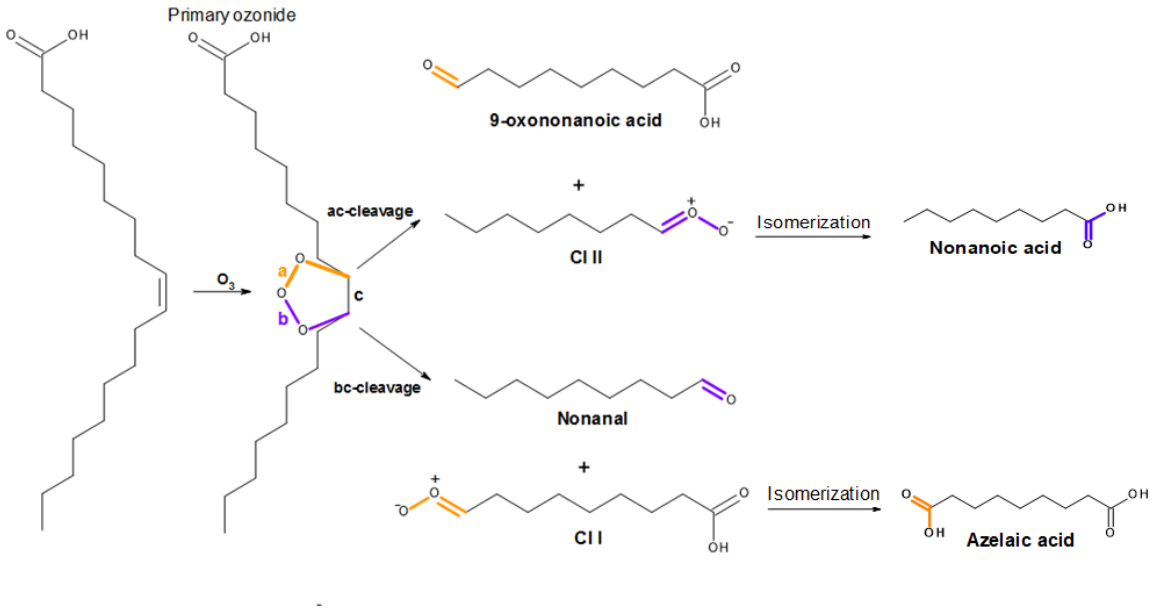

Figure 1.6. Mechanism of ozonolysis of oleic acid (adapted from Zahardis and Petrucci, 2007).

1.6.2 LINOLEIC ACID

C*is*-9,*cis*-12-Octadecadienoic acid, also called linoleic acid (LA), is a long-chain polyunsaturated fatty acid (PUFA), it is the second most prevalent UFA in the atmosphere (Zhao et al, 2014), present in fruits, vegetable, vegetable oils and animal tissue (Czamara et al., 2014; Galliard et al, 1976; Spiteller et al, 2001; Zahardis, 2006). The reaction of ozonolysis of this carboxylic acid may differ from the Criegee intermediate ozonolysis of oleic acid due to the second double bond present in its structure. This compound has shown to follow a mechanism of autoxidation in presence of oxygen, and the evidence from the Raman spectra suggested that the reaction leads to

the formation of dienes and peroxy radicals, to produce a variety of compounds (Lee and Chan, 2007a; Frankel, 1998). Zeng et al (2013) proposed that when ozone is present, the mechanism of ozonolysis is based on Criegee intermediate that produces α-acyloxyalkyl hydroperoxide from carbonyl group.

1.6.3 PALMITOLEIC ACID

The third most abundant unsaturated fatty acid found in the POM from meat cooking is called *cis*-9-hexadecenoic acid, also known as palmitoleic acid (PA). It is a component in many vegetable oils such as olive oil (Zahardis et al, 2006), also in macadamia nuts (80% of fat weight, Hiraoka-Yamamoto et al 2004), and is also present in blood plasma and some tissues, mainly the liver (Czamara et al., 2014). Its abundance in atmosphere is around to 1.7% from the total of UFA (Zhao et al, 2014). Similar to oleic acid, PA is an monounsaturated fatty acid (MUFA), but the carbon chain is shorter by two less carbon atoms. The position of the C=C in PA is exactly the same position as oleic acid, C_9-C_{10}.

In the study by Weitkamp et al (2008), the ozonolysis of PA was compared to the ozonolysis of OA, suggesting that palmitoleic acid reacts roughly 20-30% faster than oleic acid depending on the conditions Nevertheless the evidence in the literature for this reaction is limited. Spencer and Kleimman (1978) reported that the analysis of chromatography for the reaction of ozonolysis of palmitoleic acid suggested the presence of a seven-carbon aldehyde (maybe heptanal) and a nine-carbon aldehyde-ester, while Weitkamp et al (2008) found that azelaic acid is probably formed during this reaction.

1.6.4 SURFACTANTS

Some authors have reported that there are some aerosol particles covered in amphiphilic organic compounds (film-forming compounds, FFCs), also called *surfactants*, which consist of two differentiated parts, a polar head group which is joined to a non-polar chain. When water is mixed with solid surfactants, such as fatty acid salts, the surfactant can: 1) be insoluble, 2) form an aqueous micellar solution as part of the surfactant is dissolved, or 3) form a lyotropic liquid crystal with more dissolved surfactant to obtain an aqueous micellar solution (Tiddy, 1980). Surfactants affect the evaporation of water from droplets, inhibit the transport of some particles or molecules from gas-phase into droplet and reduce the effectiveness in aerosol scavenging particles by clouds and rain (Feingold and Chuang 2002; Finlayson-Pitts and Pitts, 2000; Lohmann and Feichter, 2005).

The physical and chemical properties of aerosol can be influenced by the presence of the surfactants in the atmosphere. It is known that surfactants can form organic aggregates in aqueous solutions but also they can cover the surface of aerosols producing films at the air /water interface, affecting the transportability of water across that interface (Nájera, 2007). Fatty acids such as stearic and palmitic acids have been found in marine environments, as products of the biodegradation of organic matter (Tabazadeh, 2005). It is also believed that aerosols can be covered by organic films, and chemical models to explain the behaviour of long-chain fatty acids as organic films have been proposed; for instance, Ellison et al, (1999) suggested the formation of an inverted micelle of stearate ions covering the surface of marine aerosols. This type of micelle assumes that the organic molecule is not water soluble and it can surround the

inorganic marine particle, with the polar heads in contact with the sea-salt solution in the centre of the micelle whereas the hydrophobic tails are spread out of that centre (Tabazadeh, 2005). The Figure 1.7 depicts the model of a marine aerosol as an inverted micelle which core is composed by salt/water brine covered by a layer of fatty acids settled on the surface of the aerosol (Ellison et al., 1999, Tabazadeh, 2005). In a recent study, Pfrang et al (2017) demonstrated that droplets of mixture of oleic acid, sodium oleate and NaCl solution form 3-D self-assembled phases, with complex nanostructures and arrangements that affect physical and chemical properties of the droplets.

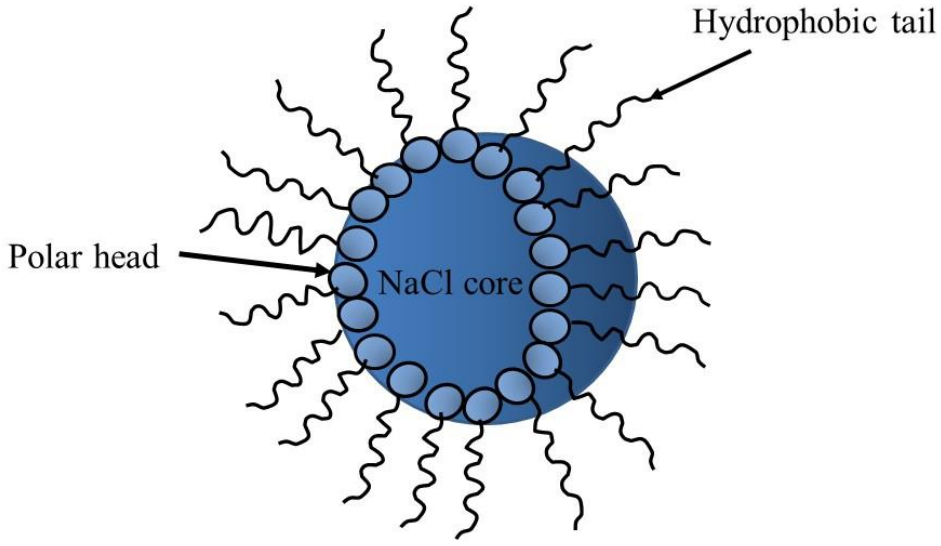

Figure 1.7 Illustration of a model of a marine aerosol as an inverted micelle. The polar heads of the carboxylic acids (light blue) are oriented towards the brine core, whereas the hydrophobic tails (black) are spread out to the micelle.

Long-chain fatty acids, such as oleic and stearic acid act as surface active agents forming a film at the air-aerosol interface in presence of inorganic salt solutions, they can depress the surface tension of aqueous solution depending on the pH, organic

concentration and salt concentration (Schwier, 2012). The oxidation of the organic film may also affect the hygrosocpicity and CCN ability of aerosols (Schwier, 2011).

CHAPTER 2

METHODOLOGY

This chapter will describe all the techniques, instruments and experimental setup that were utilized in the study, starting with the fundamentals of each technique, and then introducing the general methodology and experimental setup.

2. 1 ACOUSTIC LEVITATION

2.1.1 SOUND WAVES

Sound can propagate through gases, liquids and solids. It propagates through the air as longitudinal waves. Sound waves have characteristics, such as amplitude, frequency, wavelength, and velocity. Sound waves have properties, such as refraction, diffraction, and reflection (Priego-Capote, and de Castro, 2006). The sound reflection is produced when the incident waves hit a surface and bounce in opposite direction, with the angle of incidence being the same as the angle of reflection. These reflected waves interfere with the incident waves, forming patterns of constructive and destructive interference, leading to standing waves that are formed when the reflected waves add to the incident waves. Figure 2.1 depicts the parts of a standing wave. During the oscillation the standing wave has sites that are both, the highest and the lowest; the former are called crests and the latter troughs. The points where crests and troughs collide and cancel each other are the nodes (red dots), these remain immobile along the resultant wave and there is no oscillation in those sites, whereas the points of maximum vibration amplitude are the antinodes (blue dots).

2.1.2 FUNDAMENTALS OF ACOUSTIC LEVITATION

Acoustic levitation is achieved by the creation of standing waves that have the antinodes and nodes at equidistant positions each other, by using the adequate frequency to produce waves from a piezoelectric transducer of a ultrasonic radiator that are reflected by the reflector, as shown in Figure 2.2. These waves travel through a fluid, normally a gas (for example, air), and thus equalize the gravity force. Ideally, in an environment subject to microgravity, any particle with the right size, density, and surface tension can be levitated exactly over the pressure nodes (hollow dots), where both acoustic pressure and levitation force are cancelled to zero, but the acoustic velocity is maximal (Vandaele et al, 2005). However, under terrestrial conditions levitation forces depend on the direction of the closest pressure node (See Figure 2.3), thus levitated particles are situated and stabilized below the pressure node, as a result of anti-symmetric acoustic pressure caused by gravity. Standing ultrasonic waves are not perfectly plane, they are rather divergent, and this generates a symmetrical radial force that helps the particle to be centred on the standing wave axis (Ultrasonic Levitator Manual, Tec5).

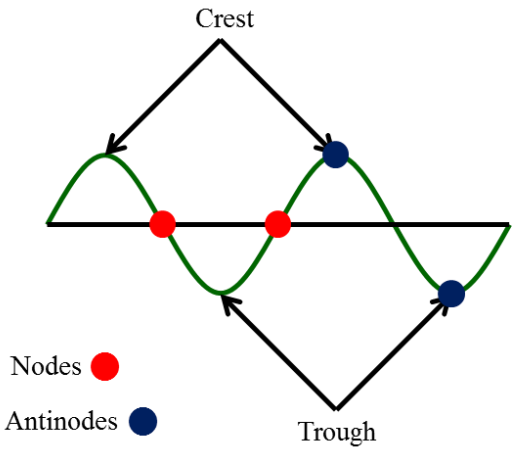

Figure 2.1 Schematic of the parts of a standing wave.

An ultrasonic levitator generally generates between 4 and 5 pressure nodes to accommodate levitated particles, however, not all nodes are sufficiently stable to levitate particles, as the two outer nodes are destabilized by reflections from transducer and reflector. Additionally, stable standing waves are produced at a certain distance between the transducer and the reflector, equivalent to the multiple of half the wavelength, i.e. n x (λ/2), where n is a whole number (Ultrasonic Levitator Manual, Tec5). In this research, the frequency, particle size, and distance between transducer and reflector could be controlled, as they can influence the stability of levitated droplets. This will be explained in section 2.4.2.

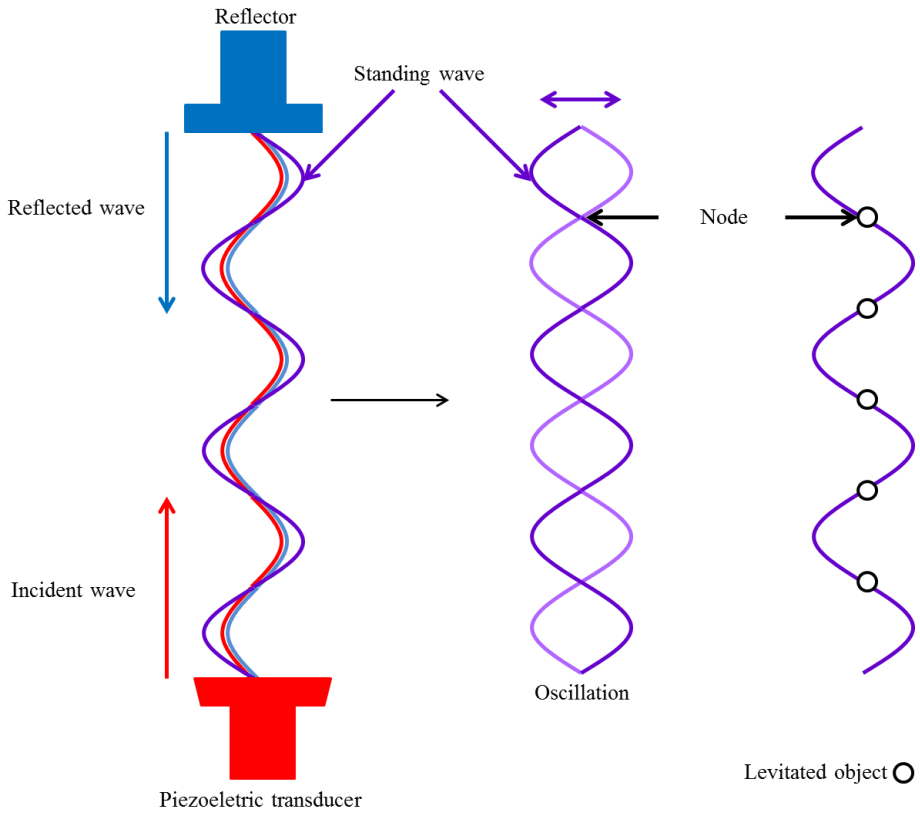

Figure 2.2 Schematic of the acoustic levitation in an environment subject to microgravity (adapted from Ultrasonic Levitator Manual, Tec5)

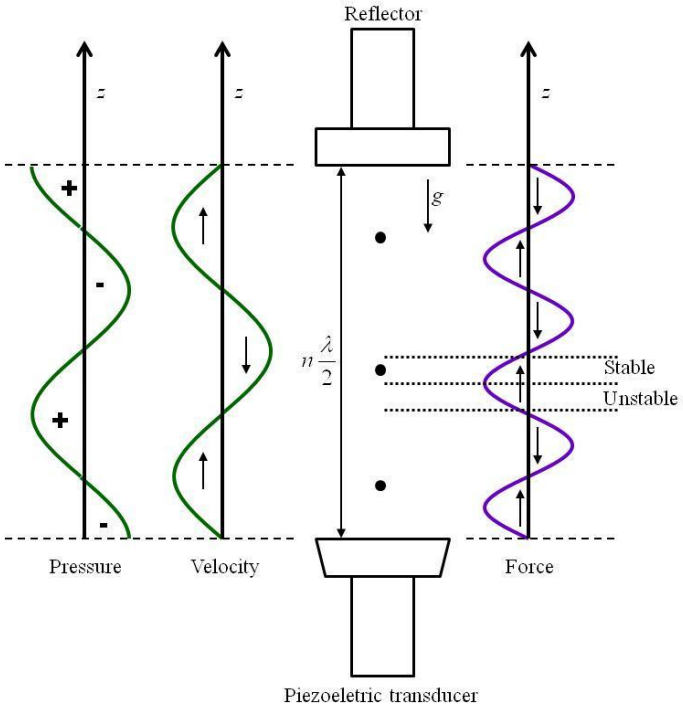

Figure 2.3. Levitation of a sphere in an acoustic standing ultrasonic wave (Adapted from V. Vandaele et al, 2005).

2.1.3 APPLICATIONS OF ACOUSTIC LEVITATION

Acoustic levitation has many applications in the manufacturing of materials with very small sizes to be shaped and used in electronic devices, avoiding the use of very complex and expensive methods (Priego-Capote and de Castro, 2006). It is also useful when the materials are susceptible to corrosion and contamination during reactions, avoiding the contact of the material with contaminants from the walls of containers. In pharmaceutical preparations, acoustic levitation helps to avoid the crystallization of the solution without solidification, contributing to improve and develop more functional

medicines. (Priego-Capote and de Castro, 2006). More applications such as reaction kinetics of liquid-liquid and liquid-gas-systems, study of deformation and disintegration of drops, and chemical trace analysis of concentrated droplets are mentioned by Lierke, (1996).

2.1.4 OTHER LEVITATION TECHNIQUES

Levitation of single droplets or particles can be achieved by a range of methods as briefly summarised below.

- Magnetic levitation: magnetic fields from magnets have been used to levitate objects; this type of levitation is the principle of the high-speed magnetic levitation trains (Schultz et al, 2005). Electromagnetic levitation is mainly used in levitation of materials with high electrical conductivity and superconductivity. It is very useful technique for specific materials with specific characteristics (Priego-Capote and de Castro, 2006).

- Electric levitation: this type of levitation has two different categories: electrostatic and electrodynamic. The former uses static electric fields to suspend small particles, whereas the later makes stable floating charged particles by using both, static (DC) and oscillating (AC) electric fields (Vandaele 2005). The applications of electric levitation are limited to work with specific materials, such as semiconductive, conductive and dielectric. Studies of atmospheric aerosols have used an electrodynamic balance (EDB) to assess the ozonolysis of proxies of fatty acids (Lee et al, 2008; Lee et al, 2012; Lee and Chan, 2007a;

Pope et al, 2010).

- Optical levitation: lasers are applied to levitate small particles, by using the forces of radiation produced from visible laser light. Particles are trapped between laser beams either vertical or horizontal positioned (Brandt, 1989). This technique is limited to very small particles (Priego-Capote) and some restrictions are the transparency of both the particle and its surrounding medium. Studies of aerosol droplets have used optical tweezer to levitate droplets of fatty acids reacting with ozone (Cai et al, 2015; Dennis-Smither, 2012; King et al, 2004).

- Aerodynamic levitation: in this type of levitation, a vertical stream of a liquid or a gas (air) is used to get a spherical particle floating, based on the Bernoulli's principle. In addition to this, the friction of the fluid at the spherical particle surface produces the rotation of the object, which is now under the Magnus force, being responsible for its stability (Brandt, 1989). This levitation technique has been applied to study high temperature reactions (Winborne et al, 2010, Pack et al 2010). However, this method is unsuitable for relevant atmospheric particles.

2.2 RAMAN SPECTROSCOPY

2.2.1 HISTORY

Although the phenomenon of inelastic scattering of light was theoretically predicted earlier by Smekal (1923), C.V. Raman and K.S. Krishnan (1928) published the observed results of the first reported experiments carried out by using very rudimentary instrumentation. They used a telescope objective to converge a sunlight beam through two lenses; the samples were either purified liquids or dust-free vapour, and light-filters were used to detect the presence of what they called "modified scattered radiation". They observed and reported that the track of the light travelling through the sample varied by changing the position of the different filters, showing for the first time the existence of a new type of light scattering. For this contribution, Sir Raman won the Nobel Prize in Physics in 1930. Many challenges were faced in those times due to the lack of more sophisticated resources, such as a good light source and detector, and also the inherent interferences of the phenomenon. The technique caught the interest during the 1960's with the invention of laser, and since then more instrumentation improvements have been made, leading Raman spectroscopy to be a more feasible technique with many applications in different fields.

2.2.2 FUNDAMENTALS OF RAMAN SCATTERING

When the light interacts with molecules, it can be either reflected, absorbed, transmitted,

or scattered. Scattering occurs when the light collides with a particle, and the incident energy is absorbed by the molecule and re-emitted, dispersing that energy in all directions. Figure 2.4 depicts the light scattering, this schematic shows how the photons of the incident light having certain frequency (E_i), are dispersed either of this two ways:

- The energy interacts with the molecule, this interaction causes the electrons in the molecule be moved to the virtual state from the ground state, and then come back to the initial state. If the scattered energy (E_s) remains invariable after the interaction of light with particles, the scattering is elastic, and this is called Rayleigh scattering (a). The colour of the sky is due to the Rayleigh dispersion, which is the elastic scattering of sunlight by air molecules (mostly nitrogen and oxygen), and some different colours on the sky at different times of the day are attributed to the presence of different atmospheric particles dispersed in the atmosphere.

- In contrast, inelastic scattering of light occurs when the molecule is capable to change the frequency of the incident radiation by increasing or decreasing the energy, which corresponds to the energy levels in the particle. This phenomenon is known as Raman scattering, and occurs less frequently than Rayleigh scattering. As shown in Figure 2.4, the molecule can either gain or lose energy from the incident photon. In the first case, the scattered photon has decreased its energy: $\square_0$ - $\square\square$ (b), this is designated as Stokes; on the contrary, when incident photon receives energy from the molecule, the scattered photon has increased its energy: $\square_0$ + $\square\square$ (c), which is named anti-Stokes.

2.2.3 INSTRUMENTATION FOR RAMAN SPECTROSCOPY

It is estimated that in a sample of scattered light only 1 part in 10 million corresponds to Raman shifted light, thus the analysis of that light requires highly sensitive instrumentation. Raman instruments use single coloured light sources, i.e. lasers of different wavelengths, as excitation sources, and also they use a set of lenses to focus the light towards the sample, as well as filters to collect and purify the scattered light. Also they have gratings or a prism to split the light into the component wavelengths; to detect this scattered light the instrument has a light-sensitive device (charge-coupled device, CCD). The system is controlled by a computer that stores and analyses data to finally display the Raman spectra. The instrument can also incorporate a microscope to help focusing the laser beam to a small spot in the sample; this feature allows high spatial resolution of the instrument.

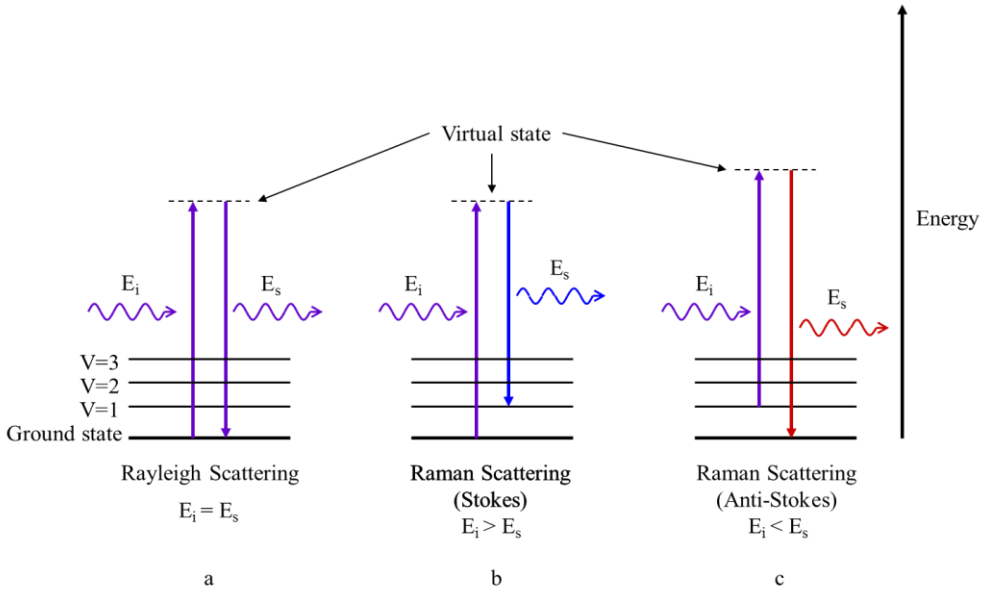

Figure 2.4. Schematic of light scattering: a) in the elastic scattering, energy is unchanged (Rayleigh); however, a minimal fraction of energy has been lost (Stokes) (b) or gained (Anti-stokes) (c) by the incident light (Adapted from Wire 4 Training Modules Compilation).

Modern Raman instruments have a number of features:

- Light sources: different types of lasers are used as sources of light for Raman microscopy, with a variety of wavelength, from UV through the visible to near IR. Ar and Kr ion lasers emit in the blue and green region of the visible spectrum (488 or 514 nm for Ar ion and 530.9 or 647.1 nm for Kr). The short-wavelengths lasers have some disadvantages, for example, they cause fluorescence and also decomposition of the sample. On the contrary, the use of longer wavelengths lasers (Diode at 785 or 830 nm, and Nd-YAG at 1064 nm) minimises the fluorescence and the photodecomposition of the sample (Skoog et al, 2007, p. 477-8).

- Fibre-optic probe: As Raman is based on visible and near-IR radiation, the light can be redirected through optical fibres, to reach samples at longer distances. This accessory is very useful when sampling or experimental work is in remote areas or needs to be interfaced with other bulky instruments (Skoog et al, 2007 p. 477-8)).

- Confocal Raman microscopy: in the wide-field microscopy, the reflection of scattered light in all directions caused the blurriness of the image as the entire sample was exposed to the light source. To solve this, a pinhole aperture was added in front of the laser, in order to direct the light to a single point of the sample. Some instruments have an additional pinhole aperture located between the objective and the image, its function is to filter the scattered rays coming from those points out of the focal point on the sample. Thus, the quality of the

image was substantially improved for instruments using pinhole apertures ("Confocal Raman Microscopy", n.d. para 2,3,4).

2.2.4 RAMAN SPECTRA

A Raman spectrum is the graphical result of the obtained intensities of scattered light (y-axis) for different measurements of frequency of light (i.e. the shift in energy) (x-axis). This frequency is usually measured as wavenumber in cm^{-1}. The information provided in a Raman spectrum allows the identification of Raman-active functional groups, by means of the analysis of intensity and position of Raman bands.

The frequencies of vibration are related to atomic masses and also strength to the bonds they form. In a spectrum, the bands that are shifted to higher values correspond to light atoms with strong bonds between them, whereas heavy atoms involved in weak bonds are shown at low Raman frequencies (Renishaw. (2017). *Raman spectroscopy explained*. [Brochure]). In organic molecules a carbon atom can be present as any of these three hybridization types: sp^3, sp^2 and *sp*. In a single bond C-C the carbon atom is sp^3 hybridized, while in multiple bonds the hybridization of carbon atom is sp^2 and sp for double (C=C) and triple (C≡C) bonds respectively. The contribution of atomic orbitals s and p to the hybrid orbitals formed determine the length and strength of the bond. Thus, the higher *s* character of hybrid orbitals in double and triple bonds reduces the length of bonds and increases their strength The effect of the atomic mass and strength of bonds can be seen in the Raman shift for the common functional groups: C-C (≈600-1300 cm^{-1}), C=C (≈1600 cm^{-1}), C≡C (≈ 2100-2300 cm^{-1}) and C-H (≈ 2700-3100 cm^{-1}). The interaction of the incident light with the molecular vibrations produces

change in energy of photons of the laser light. This information about vibrational modes is obtained and used in the determination of the different types of bonds of a molecule and therefore in the identification of compounds (Skoog et al, 2007; Wade, 2013).

Noise is an inherent problem in any measurement, and Raman spectroscopy is not the exception. Figure 2.5 shows the Raman spectrum of glyoxal, highlighting the three main types of noise that are normally found in a Raman spectrum due to experimental conditions, and light and sample nature. Fluorescence is seen as a slight curve in the baseline and is caused when the molecules interact with the photons of the light source. Shot noise is associated with the effect of incident photons on the detector (Bowie et al., 2002). Cosmic rays cause very sharp and intense peaks; these peaks are visible because cosmic rays are high energy radiation that are detected by the CCD. Data processing allows to improve the signal-to-noise ratio and also remove the unwanted peaks from the Raman spectra. Details of these procedures will be explained in section 2.4.4 of this chapter.

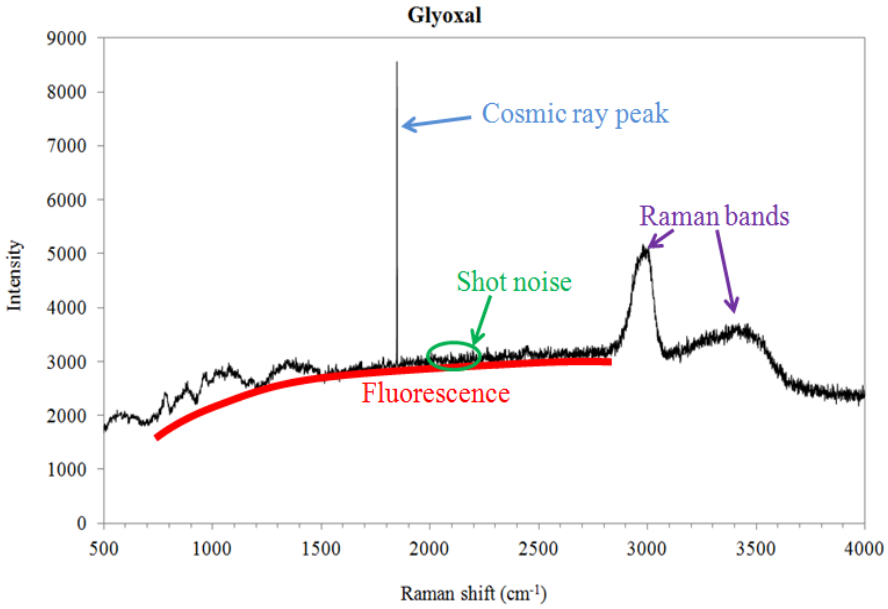

Figure 2.5. Raman spectrum of glyoxal showing the main types of noise. This Raman spectrum was collected using the Raman microscope located at CAF, Department of Chemistry, University of Reading.

2.3 GAS CHROMATOGRAPHY

2.3.1 FUNDAMENTALS

One of the most relevant separation techniques to analyse the composition of a mixture is gas chromatography. The mobile phase should be a chemically inert gas, usually He, however some other gases such as N_2 or Ar are also used. The gas carries the molecules of the sample through the heated column placed inside a thermally regulated oven. This

column contains the stationary phase, which is a packed thin layer of an inert liquid contained in an inert solid support; the length of the column determines the extent of separation, the longer the column the better the separation of the components.

A conventional gas chromatograph is made up of several parts, starting with the injection port where the sample is injected, the column enclosed in the oven, a gas carrier controller system, the detector and a computer that controls the whole system (Skoog et al, 2007, Kitson et al, 1996).

The process starts with the injection of the liquid sample, it is vaporized into the gas phase and then enters onto the column by joining to an inert gas stream. The affinity of compounds present in the mixture to both, mobile and stationary phases determines the retention times, which are the times that every compound spends before leaving the column and reaching the detector.

2.3.2 MASS SPECTROMETRY DETECTORS

There are many types of detectors for gas chromatographs with different applicability depending on sensitivity and nature of analysed compounds. The most common detectors are flame ionization detector (FID), useful to detect organic compounds, especially hydrocarbons; also thermal conductivity detector (TCD), considered a universal detector. Nevertheless, the mass spectrometer detectors (MS) are the most prominent type as they are suitable for any sample. The combination of Gas Chromatography with Mass Spectrometry (GC/MS) allows the separation and identification of components in reaction mixtures and environmental sample

monitoring, among other applications. Figure 2.6 depicts the schematic of a Gas Chromatograph – Mass Spectrometer interface (Kitson et al, 1996; Wade, 2013)

Once the mixed sample is separated into its components by passing through the column on the gas chromatograph, the separated components leave the column at different times and enter to the ion source of the mass spectrometer, here the molecules are ionised and also fragmented. Most of the GC/MS instruments use a quadrupole ion-trap filter, a system that is normally formed by four rods with varying voltages to provide a sufficiently high electric field to separate the incoming ions by mass-selective isolation after the previous ionisation. The voltages produced by ions under the effect of the rods are scanned, measured and then converted into an electrical signal after passing through the detector. Finally, a computer produces the chromatogram and the mass spectra for each GC peak of interest.

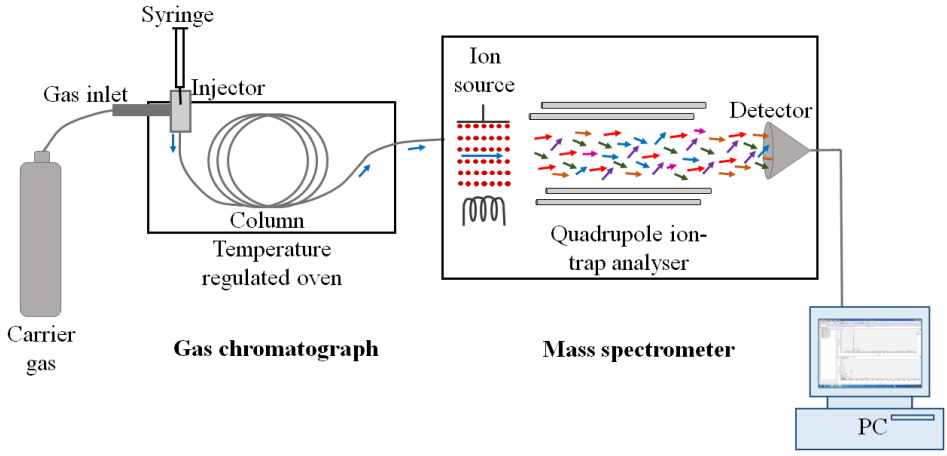

Figure 2.6. Diagram of a gas chromatograph-mass spectrometer.

2.3.3 SOLID PHASE MICROEXTRACTION (SPME)

Solid phase microextraction is a novel, multipurpose, and solvent free sample preparation technique that was developed in the late 80's by Pawliszyn's research group (Arthur and Pawliszyn, 1990), in order to improve its preceding technique, Solid Phase Extraction (SPE).

In SPE, a modified solid support is used to absorb the analyte from the sample, and then the analyte is desorbed by using temperature or solvents. With this technique, the costs are reduced as consumption and disposal of high-purity solvents is reduced. However, SPE method had disadvantages: it required the gas chromatograph injector to be altered; additionally the extractions have blank values, and also the presence of plastic in the cartridges cause interference in the results.

Unlike SPE, the SPME technique does not require use of solvents; also it reduces the blanks and needs less analysis time. This innovative technology consists of a film of a solid sorbent or a liquid coating a fused silica rod fibre (see schematic in Figure 2.7) this fibre is exposed to the sample to extract its components. Then the fibre is injected into the GC and, due to the temperature and the carrier gas, the analyte is desorbed from the fibre and compounds are identified. SPME has been applied e.g. in the identification of polyromantic hydrocarbons in highly polluted cities by combination with other techniques such as Tandem mass spectrometry (Fei et al, 2015). The applications of SPME are diverse, from forensics and toxicology, to environment, food and pharmacy, due to the development of improved fibre coatings selective for specific classes of target molecules (Spitelun et al, 2010)

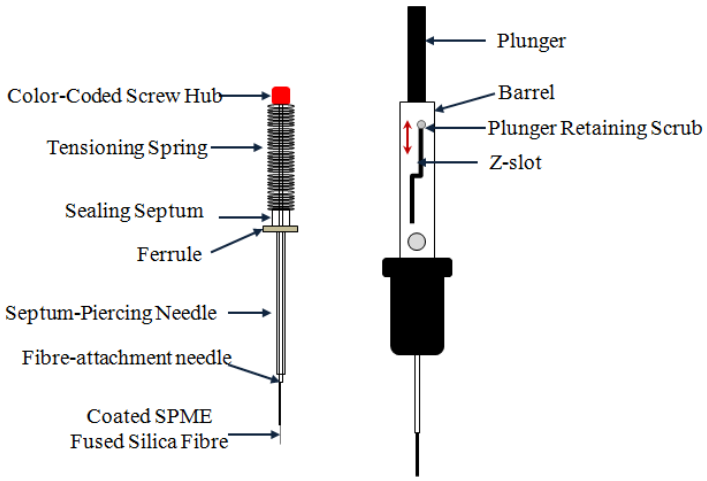

Figure 2.7 Diagram of the SPME device. The retractable fibre is enclosed in the needle, and the type of fibre used depends on the compounds to analyse.

2.4 EXPERIMENTAL SETUP

2.4.1 INTRODUCTION: GENERAL DESCRIPTION OF THE EXPERIMENTAL

In this work, droplets of different diameter ranging from 70 to 350 μm of three unsaturated carboxylic acids (palmitoleic acid: Sigma-Aldrich, analytical standard, ≥ 98.5% (GC), Linoleic acid: Sigma-Aldrich, ≥ 99%, Oleic acid: Sigma-Aldrich, ≥ 99% (GC)) were oxidised by ozone in a flow-through custom-built environmental chamber. Additionally, a solution containing 3% of oleic acid sodium oleate (1:1) and 97% NaCl was prepared by mixing OA with brine and adding SO (Sigma-Aldrich, ≥ 99%). A NaCl solution (analytical reagent grade, Fischer Scientific) was prepared dissolving the salt in deionised water to obtain a solution with a ratio of 10g/L.

Droplets were levitated in a glass reaction stainless steel chamber interfaced with an ultrasonic levitator based on a commercial instrument (Ultrasonic Levitator Manual, Tec5). Several inlet and outlet ports on the chamber allowed the entrance of reactants and carrier gases (sample injection, oxygen and ozone inlet ports) and removal of residual gases (outlet bag port). Once the sample was injected in the chamber, the droplets were levitated by the ultrasonic levitator. The chamber was placed onto an x-y-z moving stage that allows to watch a live video by focusing with help of a height control (up and down) and two micrometer screws (back-forward and left-right). The chamber included a flat glass window placed in front of the optical fibre probe to monitor by video all the process, and also to generate the Raman spectra when the laser beam is shot towards the sample through this window. All the experimental parameters

such as ozone concentration, reaction time, size of droplet, and relative humidity were controlled constantly during every experiment. A schematic of this experimental set up is displayed in Figure 2.8.

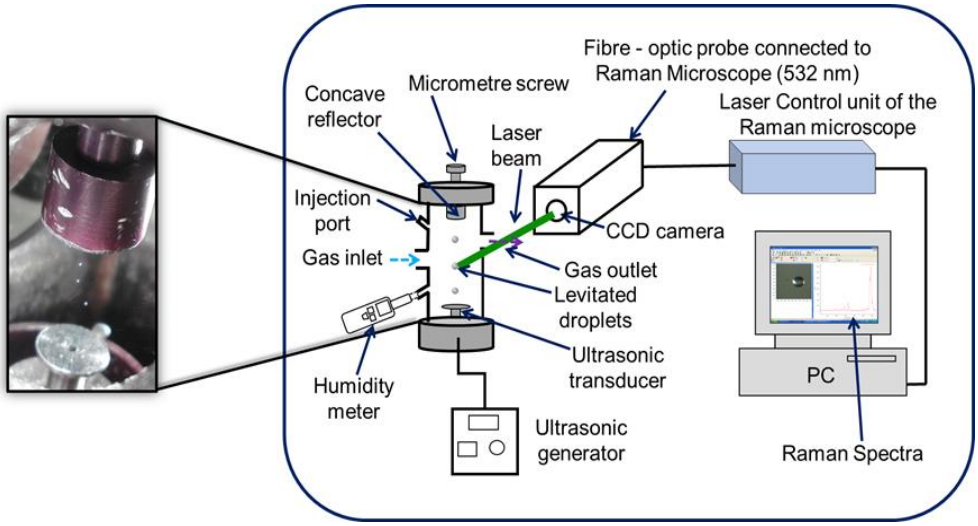

Figure 2.8. Schematic of the experimental setup.

2.4.2 ACOUSTIC LEVITATION OF DROPLETS

The acoustic levitator consists of a source of voltage that uses a frequency of 100 kHz and a wavelength that forms standing waves. The instrument user guide suggests that this acoustic levitator can levitate droplets with diameters between 2.5 mm to 15µm. The voltage passes through a transducer at the bottom of the chamber, whereas a concave reflector attached to a micrometre screw allows to adjust the distance between the transducer and reflector, to levitate particles, by optimizing the sound pressure and distance between transducer and reflector depending on the droplet properties. Almabrok (2012) reported the effect of the sound pressure on the RH and temperature for droplets containing NaCl and ammonium sulfate, concluding that RH decreased and

temperature increased when sound pressure was applied, potentially changing the levitated liquid droplets to a solid phase state. In this study, the frequency applied to levitate stable droplets was in the range of 30 to 70 kHz. Droplets in the range of sizes ranged between 65 and 350 nm were levitated. The fatty acid was injected using a 5 µL syringe inserted in the inlet port set at an angle of 45 degrees, the droplet was detached from the syringe and then stabilised by moving the reflector with the micrometer adjustment screw to adjust the distance between transducer and reflector to obtain a standing wave with suitable pressure nodes and avoid the oscillations of the levitated droplets. The droplets levitated close to the reflector were not stable, because this levitator allows the obtaining of 4 to 5 pressure nodes, however only 2 to 3 pressure nodes are suitable for levitation of particles (inner nodes), while the other 2 nodes are deformed (outer nodes). The droplet close to the transducer was unstable and also out of the range of visibility of the CCD camera. The variability in the size of the droplets was a very difficult factor to control during this stage of the experiment, and few experiments were replicated using the same droplet size in order to obtain the uncertainty for every fatty acid at low and high RH.

2.4.3 PRODUCTION OF OZONE

The ozone was generated by passing a flow of oxygen from a cylinder through a pen-ray ozoniser (UVP Ltd). A ball flow meter with a needle valve controlled the flow of oxygen, which was set to 0.162 L/min, whereas the mixing ratio of ozone was chosen to be in the range from 0.5 to 40 ppm. The exposure to ozone was started once the droplet was stable in size and RH reached the desired value. Times of O_3 exposure were varied,

depending on the nature of the reactant, the concentration of ozone and the RH, ranging from 1 to 8 hours.

To obtain the accurate O_3 concentration, three calibrations of the ozoniser were carried out to ensure that the concentration applied in every experiment was accurate. This calibration followed the procedure described by Almabrok (2012).

Figure 2.9 shows a schematic of the calibration set up. A 10 cm length glass cell was placed onto the Varian Cary 300 UV-Visible spectrometer previously set to record the ozone absorbance at 254 nm. Then, the first measurement was taken (blank) with the empty cell that was evacuated using a manifold system and the baseline adjusted to obtain all the following measurements. Once this absorbance was recorded, ozone was produced by flowing oxygen at 0.162 L/min and displacing the ozoniser bar to different positions in order to generate ozone at the different desired concentrations to fill the cell. Then, three absorbance measurements at 254 nm were taken for each concentration; all the measurements were carried out in random order and the calibration curve was obtained using the Equation 2.1.

$$O_3(ppm) = \frac{10^6 T}{273\ P\ k\ l} \times (absorbance) \qquad \text{Equation 2.1}$$

where T is the temperature in Kelvin, P is the pressure in atm, k is the extinction coefficient of ozone, base 10, 134 cm-1 atm-1 (STP), and l is the path length in cm.

In total, three calibrations were done during the experimental work, and plots of these calibrations, calculations and resultant O_3 concentrations are shown in Figure 2.10

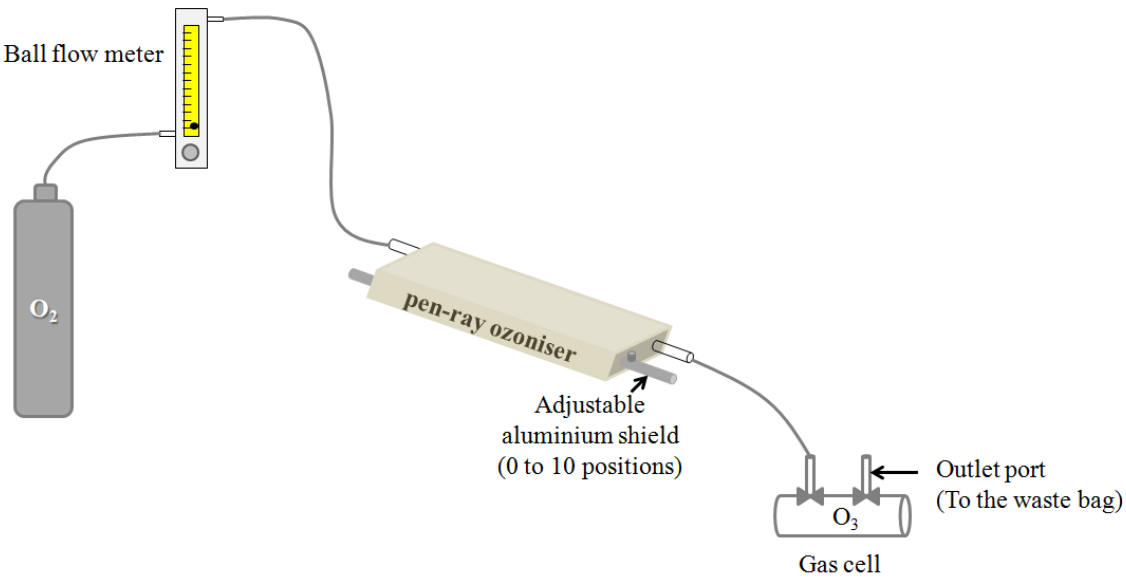

Figure 2.9 Schematic of the ozone calibration set up.

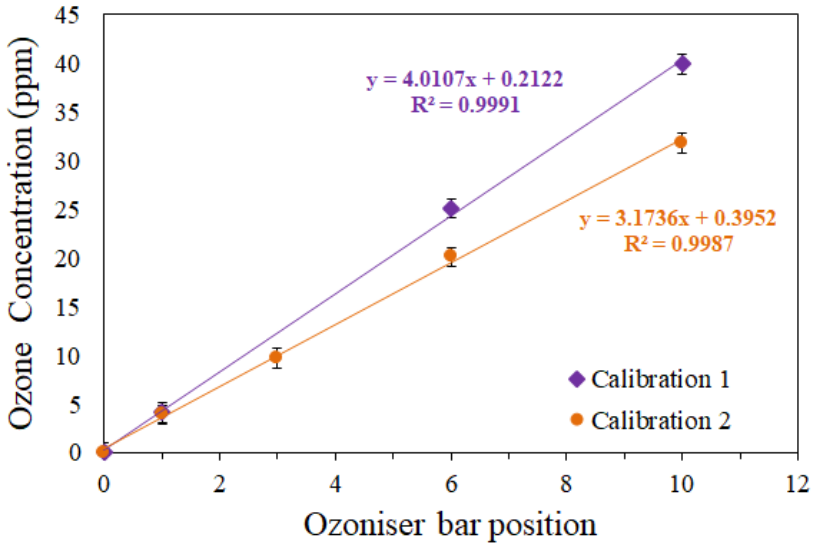

Figure 2.10 Calibration curves of ozone.

2.4.4 ACQUISITION OF RAMAN SPECTRA

The Renishaw inVia dispersive Raman Microscope located in the Chemical Analysis Facility consists of a research grade Leica microscope equipped with four objectives (x5, x20, x50 and x100), and three laser sources with wavelengths of 785, 633 and 532 nm. Additionally, this instrument includes an external fibre optic probe that works with the 532 nm Nd:YAG laser of 300 mW, attached to the CCD camera that is placed in front of the reaction chamber for the study levitated droplet, as shown in the picture of Figure 2.11. Raman spectroscopy requires high sensitivity detectors, therefore the Renishaw InVia Raman Microscope used here has a UV near infrared CCD array detector allowing resolutions over 1 cm^{-1} (Chemical Analysis Facility, University of Reading (n.d.)) This microscope allows confocal measurements, the confocality is set by default, however it is possible to choose a higher confocality, but for all experiments in this study the set up was using the standard confocality.

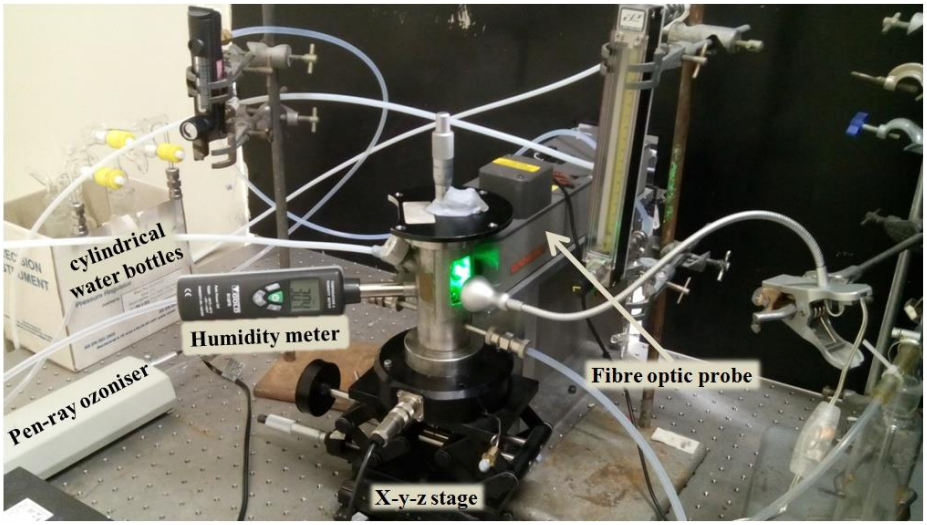

Figure 2.11. Picture of the fibre optic probe, x-y-z stage, and the stainless steel reaction chamber

Reference calibration of the laser was carried out by using a Si reference located inside the Leica microscope. Once this was done, the laser is guided to the fibre optic probe. Then the droplet was levitated and stabilised, a first spectrum was taken before starting the reaction. When the reaction started, time was controlled by using a stopwatch and one spectrum was taken approximately every five minutes. The scan conditions were:

- The chosen scan grating type was extended, with a range of spectrum set between 100 and 3200 cm^{-1} in some experiments, but the majority of experiments were carried out in a range of 100 to 4000 cm^{-1}.
- During the acquisition the detector is exposed to a Raman signal, this feature is called exposure time and it was set to 1s for most of the experiments.
- The accumulations are the number of times a scan is repeated. By using many accumulations of a short scan the signal-to-noise ratio is improved; this is highly recommended when the sample has high fluorescence background (Renishaw. *Wire 4 Training Modules Compilation* [Brochure]). However, as the acquisition time increased when the accumulation is high, this parameter was set to 1 in the experiments, and spectra with sufficient resolution, signal-to-noise ratio, and no fluorescence noise were obtained.
- The percentage of laser power depends on the sample and the laser used in the analysis. The signal-to-noise ratio is improved when laser power is high, but some samples might be damaged. However, given that the samples were levitated droplets of liquids of certain viscosity, and solids dissolved in water or brine, the laser power was set to be 100%, as no damage was detected. This percentage allowed obtaining high resolution for the majority of the spectra.

- The 532 nm laser had to be used for all experiments since the other lasers could not be coupled to the fibre optic probe. The grating was set to 2400 l/mm.
- Although the user manual recommends to use cosmic ray removal to eliminate automatically these peaks, as the instrument spend long time in taking three spectra to obtain the average of them, in this study these feature was not selected, but all the cosmic ray peaks that were visible in the spectra were removed manually when data processing was performed, the procedure is explained below.

Processing data: cosmic ray removal and curve fit.

When cosmic rays appear in the spectrum (see Figure 2.12 (a)), they are removed using the tool zap; then the spectrum can be smoothed if required, as the shot noise can interfere with the data analysis.

Once the spectrum is ready to analyse (Figure 2.12 (b)), the selected peak is zoomed, and the Gaussian area under the curve is calculated using the tool curve fit. To adjust the curve to Gaussian, the band is deconvoluted into several sub-bands (Figure 2.13), they are set to be in the same place to follow the same procedure for all spectra, and thus the number of sub-bands will be constant.

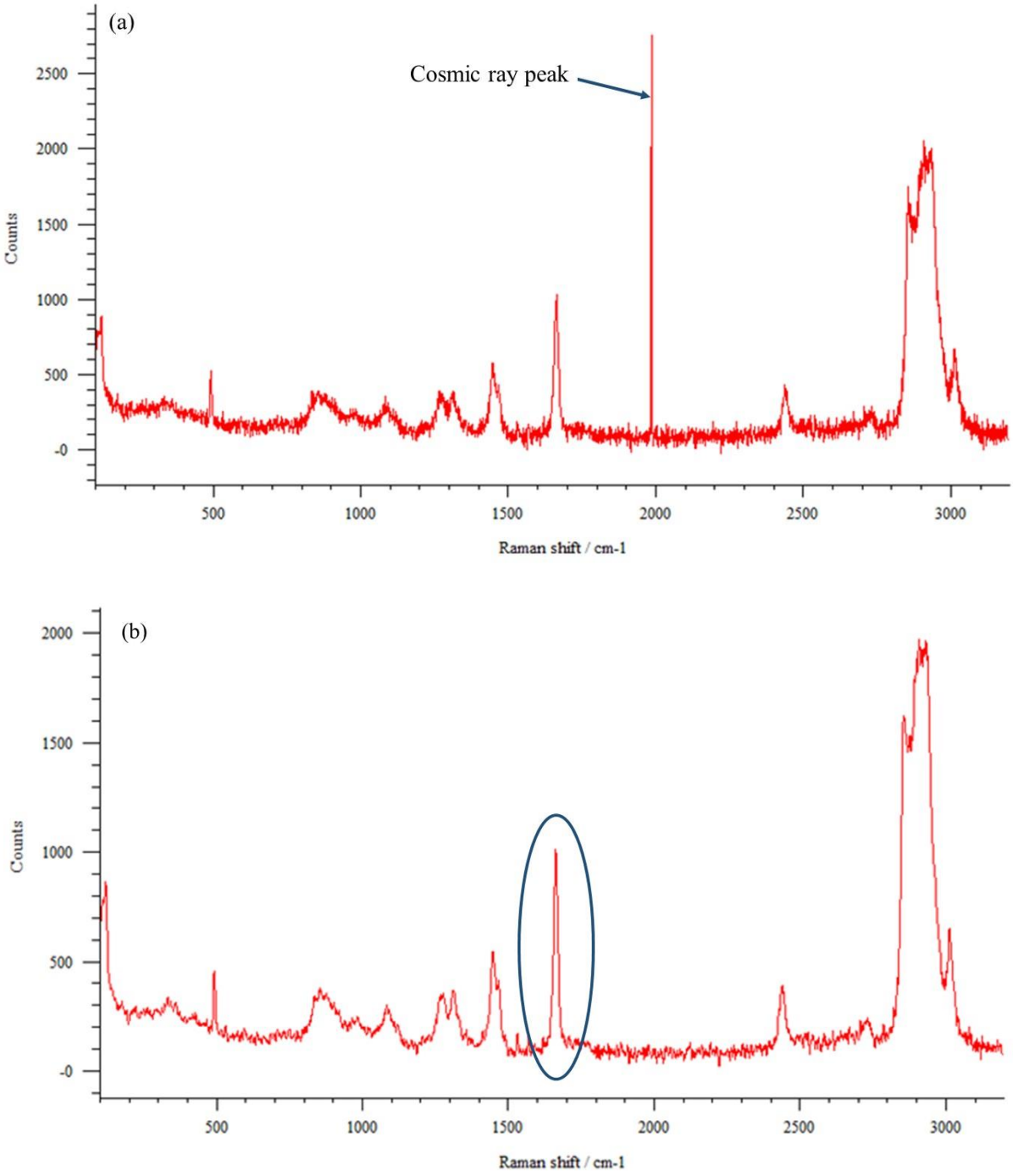

Figure 2.12 (a) Raman spectrum of a levitated droplet of linoleic acid, showing the characteristic cosmic ray peak. This peak is removed using the tool zap of the Wire software. (b) Raman spectrum of a levitated droplet of linoleic acid after removing cosmic ray peak and shot noise. The peak in a circle is used in Figure 2.13.

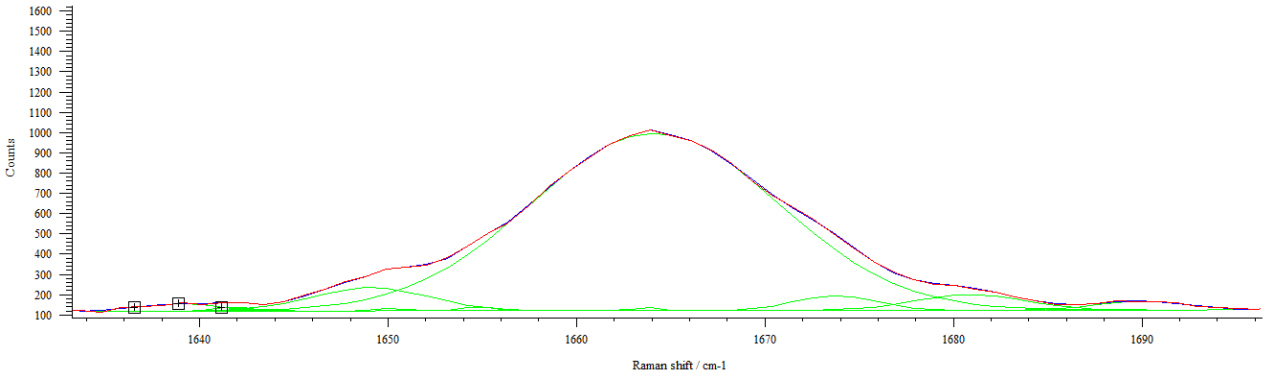

Figure 2.13 Gaussian deconvoluted Raman spectrum taken from a levitated droplet of LA. The peak corresponds to C=C.

The ratio of the Gaussian area obtained from the Raman spectra is calculated dividing the area under the curve of the peak corresponding to C=C *cis*-C=C bond stretching located at ≈ 1663 cm^{-1} by the area under the curve of the peak corresponding to CH_2 in-plane deformation.

$$\text{Ratio of Gaussian area} = \frac{\text{area under curve of peak C=C}}{\text{area under curve of peak } CH_2} \qquad \text{Equation 2.2}$$

2.4.5 RELATIVE HUMIDITY SETUP

Different values of relative humidity between 0 and 90% were controlled by balancing dry and wet flows of oxygen, and measured in close proximity to the levitated droplet throughout the experiment by using a humidity meter.

A coupled three cylindrical Pyrex water bubbler system was used to control humidity in the chamber (see Figure 2.11), this system was attached to a flow meter with a needle valve to control the entering flow to the reaction chamber and keep the humidity at the desired value. RH was variable for the experiments, with values ranging from 0 to 15% for low RH experiments and 60 to 90% for high RH experiments. For the experiments involving self-assembled mixtures, the RH was always maintained over 50% as RH below this value led to phase transformation from liquid to a solid phase state of the droplets. The experiments were made at ambient temperature, ranging from 22 to 30°C. To monitor the relative humidity and temperature, a humidity meter (Precision Gold N18FR Temperature and humidity meter probe, Maplin Electronics.) was attached to a port at one side of the chamber (see Figure 2.11).

2.4.6 ANALYSIS OF PRODUCTS BY GC/MS AND HS-SPME

The analysis of gas products of various reactions of ozonolysis of oleic, palmitoleic and linoleic acids was carried out by means of Gas chromatography and mass-spectrometry. The instrument used was the ThermoFisher Scientific Trace Ultra GC coupled to a ThermoFisher Scientific ITQ1100 Ion trap Mass analyser at the CAF, which allowed injecting the sample contained in the solid phase microextraction fibre. As shown in

Figure 2.14, the SPME fibre was inserted in the inlet port of the chamber.Once the needle containing the coated fused silica fibre was close to the droplets, the plunger was pushed allowing the fibre to be exposed to the vapour phase products above or in the vicinity of the liquid sample; this technique is known as headspace SPME (HS-SPME). Then the fibre was inserted in the injection port of the GC, the setup of this analysis is explained below.

- The coated fused silica of the SPME fibre was prepared before extracting the sample. To do this, a mixture of water/methanol 1:1 was prepared, then the fibre was immersed in the solution by pushing the plunger and sonicated for 30 min. After this, the fibre was injected in the injection port of the GC to desorb the solvents and any contaminant that could have been trapped in the fibre. The GC was set with a specific temperature programme to desorb the extracted compounds; the conditions of this programme are shown in Figure 2.15(a).
- Once the fibre was ready to use, ozonolysis of the fatty acid of interest was initiated. The rate of reaction determined the extraction times of samples. The analysis of products was carried out for the three fatty acids at ozone concentrations of 4 and 40 ppm, at high and low RH values; The formation of products was detected by inspection of Raman spectra, in order to know when to insert the fibre in the inlet port of the chamber. Once the extraction of sample was initiated by introducing the fibre and pushing the plunger to expose the coated silica fibre to extract the gases, it was left for the required time (30 – 60 min) to reach the equilibrium between sample and fibre.

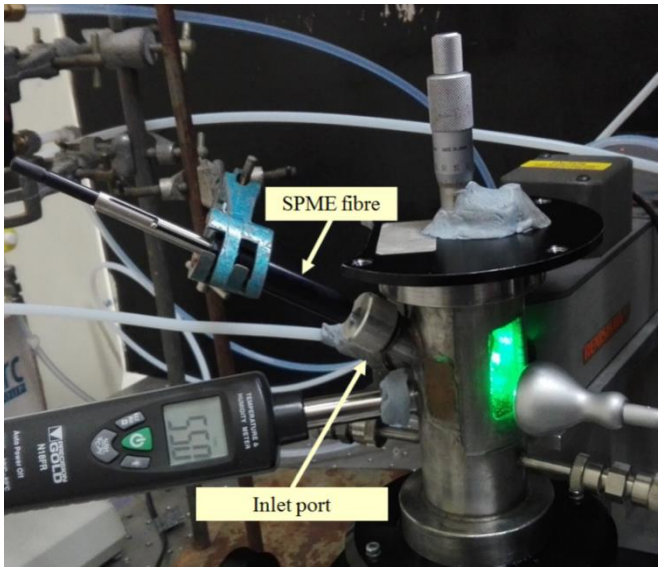

Figure 2.14. Picture of the stainless steel chamber showing the inserted SPME fibre to adsorb the products formed during an experiment of ozonolysis of a fatty acid.

- The fibre was removed from the chamber and transferred to the injection port of the GC-MS. The programme shown in Figure 2.15(b) was set to run the analysis of products of the ozonolysis of fatty acids. The high temperature in the injection port helped to desorb the analyte in a helium stream, transferring the analyte from the SPME fibre to the column to be separated in its components.

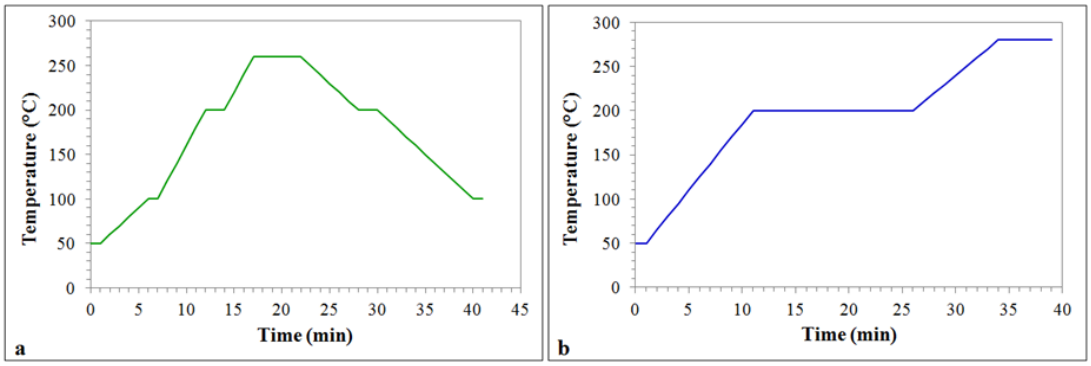

Figure 2.15 GC/MS methods applied to the SPME analysis of fatty acids: a) desorption method for cleaning of SPME fibre before the sample extraction; b) desorption method for separation and identification of the gas-phase products extracted from the reaction chamber.

2.4.7 PREPARATION OF MIXTURES OF FATTY ACIDS

A 1:1 mixture of oleic acid (OA) and sodium oleate (SO) was prepared and mixed with a seawater surrogate (NaCl); in this mixture, 3% corresponded to OA/SO and the remaining 97% was NaCl solution (10g/L).The procedure was previously described by Rastogi (2015), who used Eppendorf tubes to mix the components. A modification of the method has been used for the present study, by using 5 mL glass vials to prepare the mixture. The schematic of Figure 2.16 summarises the procedure followed here.

SO with a purity of ≥ 99% was purchased from Sigma-Aldrich, and analytical reagent grade NaCl was bought from Fisher Scientific. The vial was previously weighted, and

then approximately 20 µL of OA was added, with this amount it was possible to calculate the volume of NaCl; this step was followed by addition of the other components to the OA followed by stirring of the mixture. A previously calculated amount of SO was added to complete the ratio of 1:1 for OA/SO, and then the mixture was placed in a water bath in the sonicator at 50-55°C to homogenise it. The homogenisation was reached when all SO was completely dissolved and no solid SO visible. The mixture had a milky appearance, as shown in the picture of Figure 2.16.

The same procedure was followed to prepare a mixture of palmitoleic acid (PA) with SO and NaCl at same ratio PA/SO.

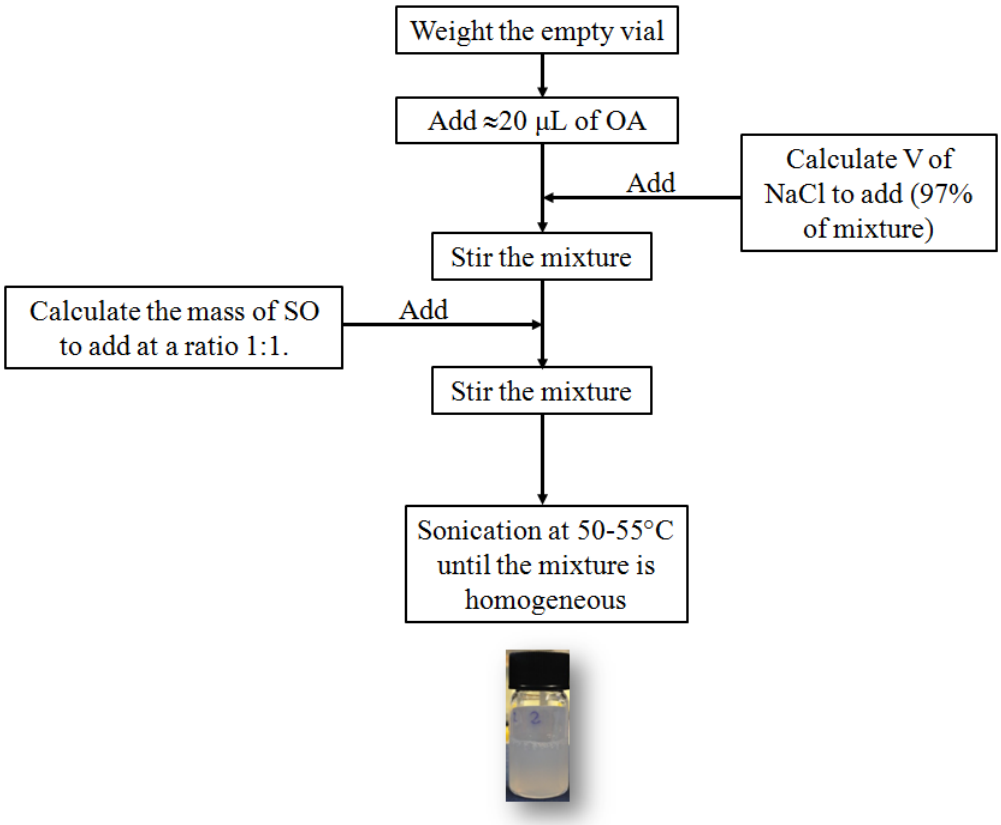

Figure 2.16. Procedure of preparation of the mixture OA/SO/NaCl.

CHAPTER 3

OZONOLYSIS OF INDIVIDUAL FATTY ACIDS

3.1 RAMAN SPECTRA OF FATTY ACIDS

Figure 3.1 shows the resultant Raman spectra that were obtained from single levitated droplets of pure unsaturated fatty acids before starting the reactions: oleic acid (OA), palmitoleic acid (PA) and linoleic acid (LA). Characteristic bands of the three fatty acids are listed in Table 3.1.

By examining the Raman spectra of oleic, palmitoleic and linoleic acid, it is possible to distinguish the similarities and differences in the bands. The three fatty acids are long-chain carboxylic acids having at least one double bond C=C; their structures are shown in Figure 3.2. Palmitoleic acid (PA) is a 16 carbon (ω-7) MUFA while oleic acid (OA) and linoleic acid (LA) are two carbon atoms longer than PA, monounsaturated (ω-9) and di-unsaturated (ω-6 and ω-9) fatty acids respectively. The structural differences of these three fatty acids can be distinguished in their Raman spectra, comparing the intensity of main three bands at ≈ 1280 cm^{-1} corresponding to the =C-H deformation mode, ≈ 1665 cm^{-1} due to the C=C stretching mode and ≈ 3020 cm^{-1} corresponding to =C-H stretching vibrations. These bands are more intense in the spectrum of linoleic acid due to a higher number of unsaturation and the length of carbon chain compared to oleic and palmitoleic acid. As the intensity of the band at ≈ 1455 cm^{-1} remains stable, this band is used as reference to calculate the ratio of Gaussian area under the curve in order to assess the kinetics of the reactions. The following sections describe the changes in the intensity of those peaks.

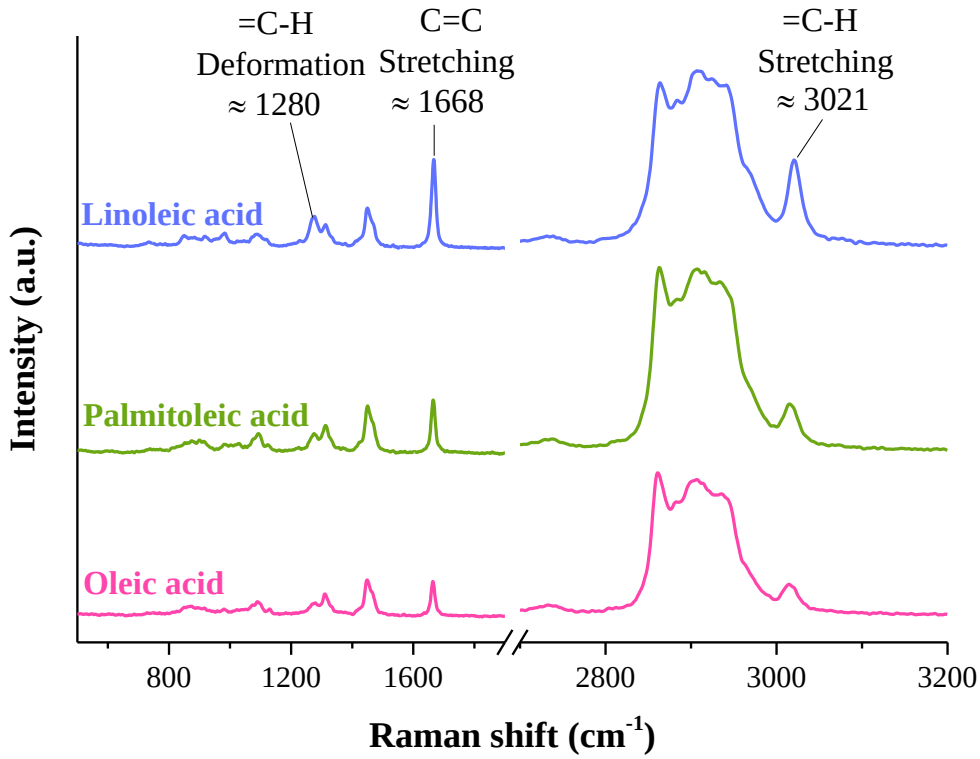

Figure 3.1 Raman spectra of unsaturated fatty acids: Oleic acid, palmitoleic acid, and linoleic acid.

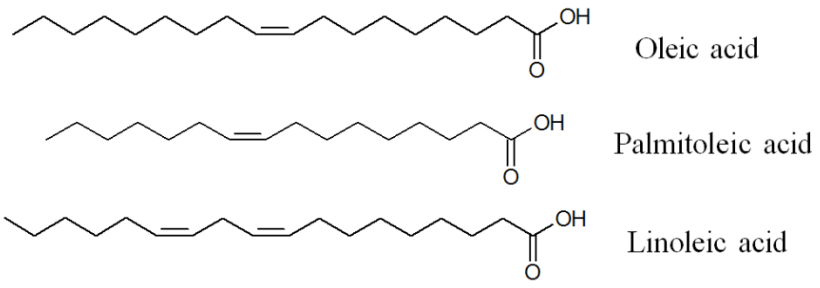

Figure 3.2 Structure of oleic, palmitoleic and linoleic acids

Table 3.1 Characteristic Raman bands found in the Raman spectra of the unsaturated fatty acids used in this study (Czamara et al., 2014, Socrates, 2004)

Position (cm^{-1})	**Functional group**	**Assignments**
800-950	O–O	Peroxides
1260-1275	HC=CH	CH Deformation
1312-1325	$-(CH_2)_n-$	Twisting CH_2 vibration
1443-1453	$-(CH_2)_n-$	CH_2 scissor
1664-1668	*C=C*	*cis*-C=C bond stretching
2860-2866	CH_3	Asymmetric stretching
2905-2915	CH_3	Symmetric stretching
3010-3025	cis-HC=CH	=C-H stretching

3.1.1 RAMAN SPECTRA OF OLEIC ACID

Oleic acid (*Cis*-9-octadecenoic acid) is an 18 C monounsaturated Ω-9 carboxylic acid, widely found in vegetable and animal fats and oils. In some vegetable oils, such as olive oil, oleic acid comprises the main long-chain unsaturated fatty acid.

The ozonolysis of oleic acid is usually the point of reference to assess the atmospheric reactions of fatty acids. This reaction follows a mechanism involving Criegee intermediates, to yield a variety of products, such as carboxylic acids and aldehydes. According to a comprehensive review by Zahardis and Petrucci (2007), the main four products formed from this reaction are nonanal, nonanoic acid, 9-oxononanoic acid and azelaic acid.

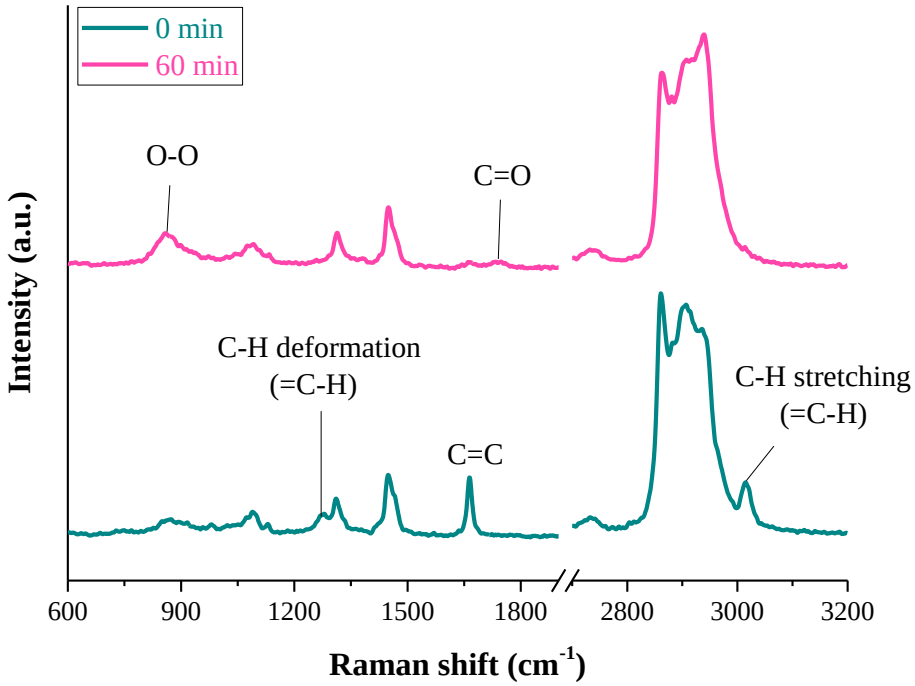

Figure 3.3 Raman spectra obtained from an ozonolysis experiment of a levitated droplet of oleic acid before starting the reaction (green line) and after one hour (pink line) of 40 ppm ozone exposure.

Evidence showed in the Raman spectra of Figure 3.3 obtained from the ozonolysis of a levitated droplet of oleic acid (diameter = 145 μm) suggest the formation of various oxygen-containing products, as the band at 864 cm^{-1} is intensified after 1 hour of exposition at 40 ppm ozone concentration (Compare Lee and Chan, 2007b). A considerable decrease in the intensity of the peaks at 1274, 1664 and 3016 cm^{-1} evidences the breaking of C=C, whereas the rise of a weak and broad peak at 1751 cm^{-1} suggests the formation of carbonyl groups. The intensity of the band at 1450 cm^{-1} remained constant, as the number of CH_2 groups over the reaction stayed constant. GC/MS analysis of products formed from this reaction will be detailed in Section 3.8, to complement the findings from Raman spectroscopy.

3.1.2 RAMAN SPECTRA OF PALMITOLEIC ACID

Palmitoleic acid is a 16 C monounsaturated Ω-7 carboxylic acid, also known as *Cis*-9-hexadecenoic acid. It is found in human adipose tissue (Gong et al., 2011). Vegetable sources such as *Roureopsis obliquifoliata* (Spencer and Kleiman, 1978), and *Macadamia ternifolia* seed oils (Bridge and Hilditch, 1950) comprise 32 and 20% of palmitoleic acid, respectively.

Figure 3.4 presents the resultant Raman spectra of a levitated droplet of palmitoleic acid (diameter = 175 μm) before and after 1 hour of O_3 exposure (40 ppm). It is evident in these spectra that there are many similarities between ozonolysis of PA and OA. The intensity of the peaks at 1274, 1664 and 3016 cm^{-1} dropped, indicating the cleavage of the carbon double bond, whereas the gradual increase on the band at 864 cm^{-1} indicates the formation of peroxides, and the broad peak at 1750 cm^{-1} emerged as a consequence of the formation of carbonyl groups. These results are consistent with the reported by Pryor et al. (1995) who confirmed the formation of a C7 aldehyde, but also C7 hydroxyperoxide and C7 Criegee ozonide from the ozonolysis of phospholipids containing palmitoleic acid; and also Spencer and Kleiman (1978) who stated that palmitoleic acid produced a seven-carbon aldehyde and a nine-carbon aldehyde-ester when reacted with ozone.

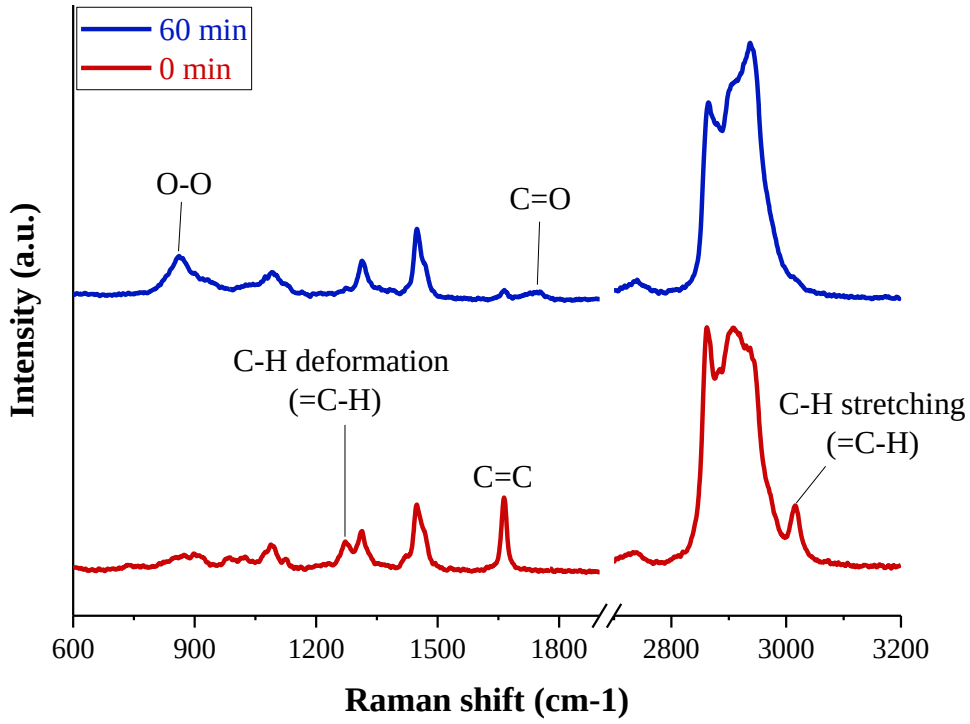

Figure 3.4 Raman spectra obtained from the ozonolysis of a levitated droplet of palmitoleic acid before starting the reaction (blue line) and after one hour (red line) of 40 ppm ozone exposure.

3.1.3 RAMAN SPECTRA OF LINOLEIC ACID

9-cis,12-cis -octadecadienoic acid, also known as linoleic acid, is a polyunsaturated Ω-6 and Ω-9 long-chain fatty acid, it is one of the essential fatty acids in mammalian diet and occurs naturally in plant glycosides.

The Raman spectra obtained from a levitated droplet of linoleic acid (diameter = 145

μm) before and after one hour of exposure to ozone at 40 ppm are shown in Figure 3.5. The intensity of the characteristic peaks of C=C at 3021, 1666 and 1274 cm^{-1} was clearly reduced after one hour of reaction, evidencing the consumption of C=C bonds, but when it is compared to its counterparts oleic and palmitoleic acids, the reduction in the intensity of the same bands is not as dramatic as in the spectra shown in Figure 3.3 and 3.4, evidencing the influence of the extra C=C in the oxidation of linoleic acid. Nevertheless, linoleic acid also yielded oxygen-containing products such as carbonyl and peroxides, which is seen by the increase in the corresponding bands at 1745 and 876 cm^{-1}, respectively. Moise and Rudich (2002) suggested an alternative pathway that involves rearrangements of the remaining double bond to produce more stable compounds due to the conjugation of C=C and C=O bonds. Section 3.8 will present the further analysis of products from the ozonolysis of linoleic acid at low and high RH.

Autoxidation of linoleic acid: Lee and Chan (2007a) pointed that the C=C bonds in linoleic acid are attacked by ozone in a very similar way as in oleic acid via Criegee intermediates, however they found evidence of a different mechanism occurring in the case of linoleic acid, especially at low ozone concentrations, when linoleic acid undergoes autoxidation, following a mechanism via free radicals and the formation of conjugated dienes. Thus in Figure 3.6 (a), it is observed an emerging, weak band at ≈1600 cm^{-1} corresponding to these species. In addition to this, the peak at 1660 cm^{-1} characteristic of C=C tended to increase when O_3 exposure time increased, it has been explained by the formation of a variety of products that keep the C=C; also there is evidence of the formation of carbonyl groups (which band at ≈1750 cm^{-1}). An experiment with LA exposed to oxygen (blank) was also conducted, and the increase of the ratio of Gaussian area of the peaks C=C/CH_2 (see Figure 3.12 and 3.20 with red dots

and black hexagons respectively representing the blank) was observed. Linoleic acid has shown a tendency to be oxidised at room temperature; this has been explained by Frenkel (1998) as the autoxidation of the fatty acid that is present in oils and tissue of animals and plants can react with O_2 to form radicals that contain two carbon-carbon double bonds. This reaction of autoxidation of UFA may explain the increasing peak and the appearance of peroxidic and C=C-C=C bands in the spectra taken during the experiment using only oxygen, and the increase of peaks at 1270 and 1663 cm^{-1}, indicating that C=C are formed, as shown in Figure 3.6 (b).

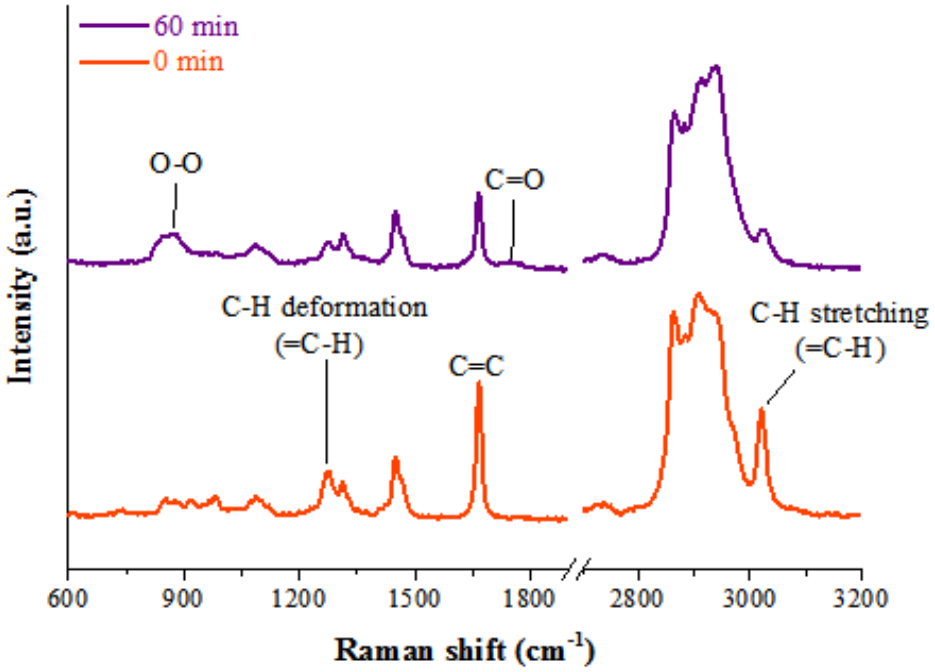

Figure 3.5 Raman spectra obtained from the ozonolysis of a levitated droplet of linoleic acid before starting the reaction (red line) and after one hour (purple line) of 40 ppm ozone exposure

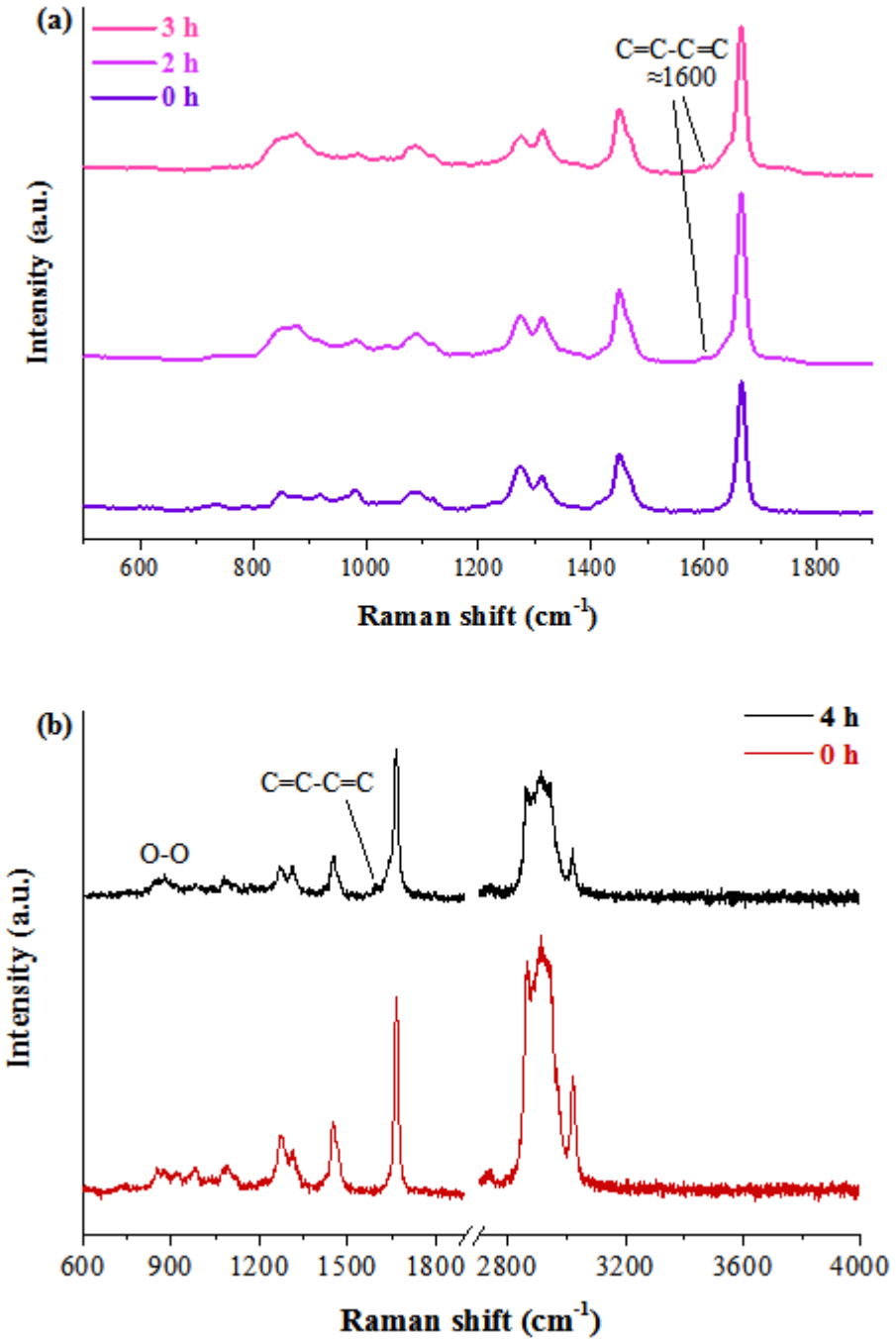

Figure 3.6 (a) Raman spectra obtained from the ozonolysis of a levitated droplet of linoleic acid before starting the reaction (blue line) and after two and three hours (purple and pink lines respectively) of 4 ppm ozone exposure. (b) Raman spectra of LA exposed to autoxidation with O_2 (blank), after 4 h a weak band at ≈ 1600 cm^{-1} emerged due to the formation of conjugated dienes.

3.2 REACTIVE UPTAKE

When a reaction is taking place, the reacting molecules start colliding, but these collisions need to be sufficiently reactive to ensure that bonds are breaking and new bonds are forming to yield new products. Depending on different conditions, such as the nature of reacting molecules, reaction phase, temperature or concentration, there is a probability of one of the molecules colliding with the other reactants. In gas phase reactions, such as the ozonolysis of fatty acids, the ozone molecule collides with the fatty acid molecule, either at the surface or in the bulk. The proportion of the number of collisions between both the gas molecule and the solid or liquid phase compound leading to a reaction is known as reactive uptake coefficient (Zeng et al., 2013; Smith et al., 2002) and is expressed for the ozonolysis of oleic acid as:

$$\frac{d[OA]}{dt} = -\gamma \left(\frac{P_{O_3}\bar{c}}{4RT}\right)\frac{S_A}{V} \qquad \text{Equation 3.1}$$

where γ is the probability of the reaction when one molecule of O_3 collides with a particle of OA, P_{O_3} is the partial pressure of ozone (in atm), $\bar{c}$ is the mean kinetic speed of ozone molecules in the gas phase (equivalent to 3.6 x 10^4 cm s^{-1}), [OA] is the oleic acid concentration, T is the temperature (298 K), R is the gas constant (0.082 atm L mol^{-1} K^{-1}), and S_A/V corresponds to Surface area/Volume ratio.

The reactive uptake coefficient has also been described as the reduction in the gas-phase particles, either at the surface or in the bulk of the particle. In their work, Worsnop et al. (2002) presented the resistor model to illustrate the chemical interaction between a gas and an aerosol particle, focussing on the gas uptake in the particle and the

transformations in the condensed phase. Based on this model, Smith et al. (2002), Hearn et al. (2005), Thornberry and Abbat (2004) and He et al. (2017) have calculated the ozone uptake coefficient for reactions of ozonolysis of fatty acids such as oleic, linoleic, and linolenic acids.

As the reaction can occur with gas interacting either at the surface or in the bulk, it should penetrate the particle. Given that the gas uptake is not constant over the reaction, it is necessary to have an extrapolation from the general decay of the reaction, thus, it has been established that the uptake coefficient can be limited by different processes, according to Smith et al. (2002) and Hearn et al. (2005), which is depending on the rate of diffusion of the ozone within the particle. The analysis of these cases helps to identify the operative case to calculate the uptake coefficient for the specific reaction. Table 3.2 summarises four limiting cases for the reaction of O_3 with fatty acids and the corresponding equations to calculate γ values for each reaction (Zahardis and Petrucci, 2007).

Table 3.2 Summary of limiting cases for the reaction of O_3 with oleic acid and other fatty acids used in this study (Zahardis and Petrucci, 2007). Analytical solutions of these equations are provided in detail in the original studies by Wornsop et al. (2002), Smith et al. (2002) and Hearn et al. (2005). The parameters in the equations are listed below.

Limiting case	**[OA]/ [OA]$_0$**	**γ**
Case 1: Diffusion of O_3 throughout the particle is fast, $l > r$	$e^{(-Hk2P_{O3}t)}$	$\frac{4HRTr\ k_2[OA]}{3\bar{c}}$
Case 2: Reaction of O_3 near the surface, limited diffusion, $l<r/20$	$\left(1 - \frac{3\ H\sqrt{Dk_2}\ P_{O3}t}{2r\sqrt{[OA]_0}}\right)^2$	$\frac{4HRT}{\bar{c}}\sqrt{Dk_2}\sqrt{[OA]}$
Case 3: Ozone reacts at the surface	$e^{\left(\frac{-3\delta^2 Hk_2^{surf} P_{O3}t}{r}\right)}$	$\frac{4HRT}{\bar{c}}\delta^2 k_2^{surf}[OA]$
Case 4: As [FA] is not constant across the particle, γ is limited by FA diffusion	$e^{\left(-\frac{12\ D_{[OA]}}{r^2}t\right)}$	$\frac{16D}{P_{O3}\ \bar{c}\ r}[OA]$

The Henry's Law coefficient of ozone is represented as H (0.48 M atm^{-1}) (Pfrang et al., 2011), r is the particle radius, δ is the depth of the surface layer, which is the penetration depth of O_3 in a self-assembled monolayer of the liquid (fatty acid), with an estimated value of ≈ 1 nm for oleic acid (Hearn et al., 2005), this parameter was reported by Shiraiwa et al. (2009) as 0.8 nm. The factor denoted as l is the reacto-diffuse length, which is the distance of diffusion of the ozone molecule throughout the particle before the reaction, and is calculated by:

$$l = \sqrt{\frac{D}{k_2[FA]}}$$ Equation 3.2

where D is the diffusion coefficient of ozone in oleic acid (1 x 10^{-5} cm^2 s^{-1}, Mendez et al., 2014), k_2 is the second order rate constant of the reaction (either bulk or surface, generally referred as k_2^{bulk} and k_2^{surf}, respectively), and [FA] is the concentration of the fatty acid.

In this study, reactive uptake coefficients were calculated for the reactions of ozone with oleic, palmitoleic and linoleic acids. From the plot of decay of the ratios of the Gaussian area for C=C/CH_2 a graph of $[FA]/[FA]_0$ as a function of $P_{O3}\,t$ was plotted, then plots of $\ln[FA]/[FA]_0$ and sqrt $[FA]/[FA]_0$ against $P_{O3}\,t$ were also obtained in order to determine the best fits, by taking the R^2 value of both exponential and quadratic fits. Figure 3.7 shows the plot of the decay of palmitoleic acid reacted as a function of ozone exposure (represented by P_{O3} t), with a droplet size of 155 μm and $[O_3]$ = 2 ppm. Fittings for this curve are exponential (dotted purple line) and quadratic (solid black line), with their respective R^2. From this plot it is inferred that the best fit is the quadratic, indicating that the reaction is taking place at the particle surface, thus case 2 is operative for this specific reaction (see Table 3.2).

In contrast, the decay profile shown in Figure 3.8 indicates that the best fit for the reaction of a droplet of palmitoleic acid (125 μm) with ozone at 40 ppm is exponential, leaving three possibilities to take into account, cases 1, 3 and 4. In order to decide which case is operative for this reaction, several aspects of the gas phase reaction should be considered for each case. In the study by Smith et al. (2005) Case 1 was described as fast diffusion of the ozone inside the particle, here the ozone concentration is constant

all over the particle and the rate of reactions is not affected by ozone diffusion. Given that the droplet size in this experiment was 125 μm, and also this case shows no dependence of the reaction rate on particle size, by taking into account that the authors of aforementioned study found that the value of the reacto-diffuse length (*l*) should be smaller compared to the size of the particle, this case was excluded from consideration, leaving case 3 and 4. These two cases show dependence on particle size, with case 4 having a square dependence on the radius (see equations in Table 3.2); thus case 4 cannot be considered as this experiment given the quadratic r dependence. Therefore, evidence from the decay profile suggests that this reaction occurred mostly at the surface. Similar analysis has been done for all experiments in order to calculate the uptake coefficients.

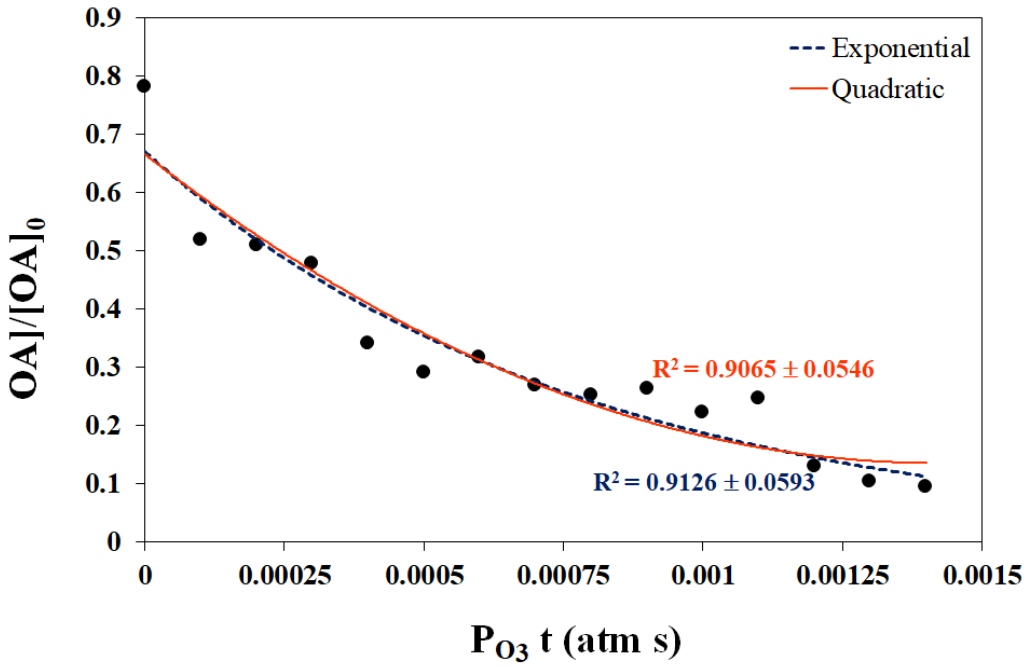

Figure 3.7 Reactive decay of the ratio $[OA]/[OA]_0$ obtained from ozonolysis of a levitated droplet (90 μm) of oleic acid at 20 ppm $[O_3]$. Trend lines are depicting quadratic fitting (---) and exponential fitting (---).

The following sections on this chapter will develop the kinetics of the ozonolysis of the unsaturated fatty acids, considering several factors that can affect the reaction: droplet size, ozone concentration, relative humidity and number of carbon double bonds.

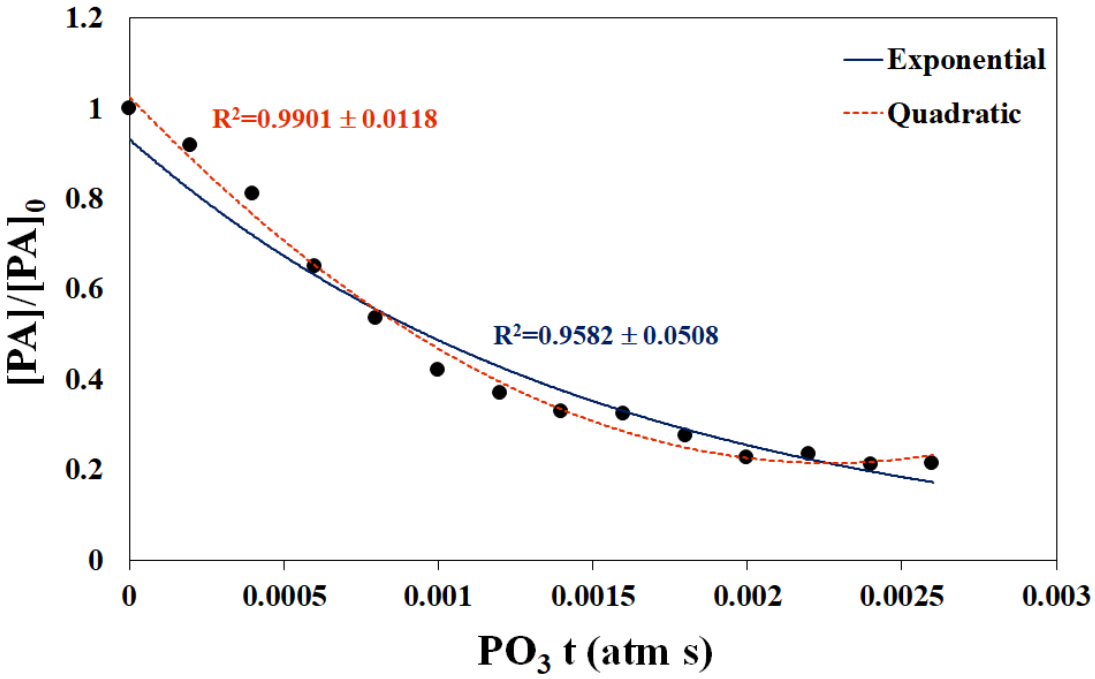

Figure 3.8 Reactive decay of the ratio $[PA]/[PA]_0$ obtained from ozonolysis of a levitated droplet (125 μm) of palmitoleic acid at 40 ppm $[O_3]$. Trend lines are depicting quadratic fitting (---) and exponential fitting (—).

3.3 EFFECT OF THE OZONE CONCENTRATION IN THE RATE OF REACTION OF OZONOLYSIS

Although atmospheric relevant ozone concentrations reported by Seinfeld and Pandis (2006) range from 20 to 40 ppb in rural areas and 100 to 400 ppb in urban areas, in this study the ozone concentrations were considerably higher than those ozone concentrations normally occurring in the atmosphere. These ozone concentrations were used in order to obtain sufficient experimental data in a short timescale, as the experimental conditions might retard the reactions at lower O_3 concentrations. In this section, the results of the ozonolysis of oleic, palmitoleic and linoleic acids as a function of [O_3] are presented, and the effect of different ozone concentrations in the reaction rate and obtained products are discussed and compared to previously reported studies.

3.3.1 OLEIC ACID

The ozonolysis of oleic acid was conducted at different ozone concentrations, ranging from 0.5 to 40 ppm. This section includes the results of experiments carried out at 2, 4, 12, 20, 32 and 40 ppm, and they are compared to the blank (see Figure 3.9).

The reaction was monitored by assessing the changes in the intensity of C=C (variable) with respect to CH_2 (constant). Thus, the plots in Figure 3.9 correspond to the changes in the ratio of the Gaussian area under curve of two Raman bands: C=C at ≈1664 cm^{-1} and CH_2 at ≈1445 cm^{-1}. These plots depict the effect of ozone concentration in the ozonolysis of levitated droplets of OA, which sizes were obtained randomly. They show a trend to accelerate the decay of the ratio of Gaussian area of those peaks when ozone

concentration is gradually increased. However, at higher [O_3] concentrations (over 12 ppm), the decay shows a very similar trend, thus these results are in agreement with the reported by Lee and Chan (2007b), who suggested that higher [O_3] exposure might not affect the mechanisms and products of this reaction significantly. Regarding the size of the droplet, its effect on the ozonolysis of oleic acid will be discussed in section 3.5 of this Chapter.

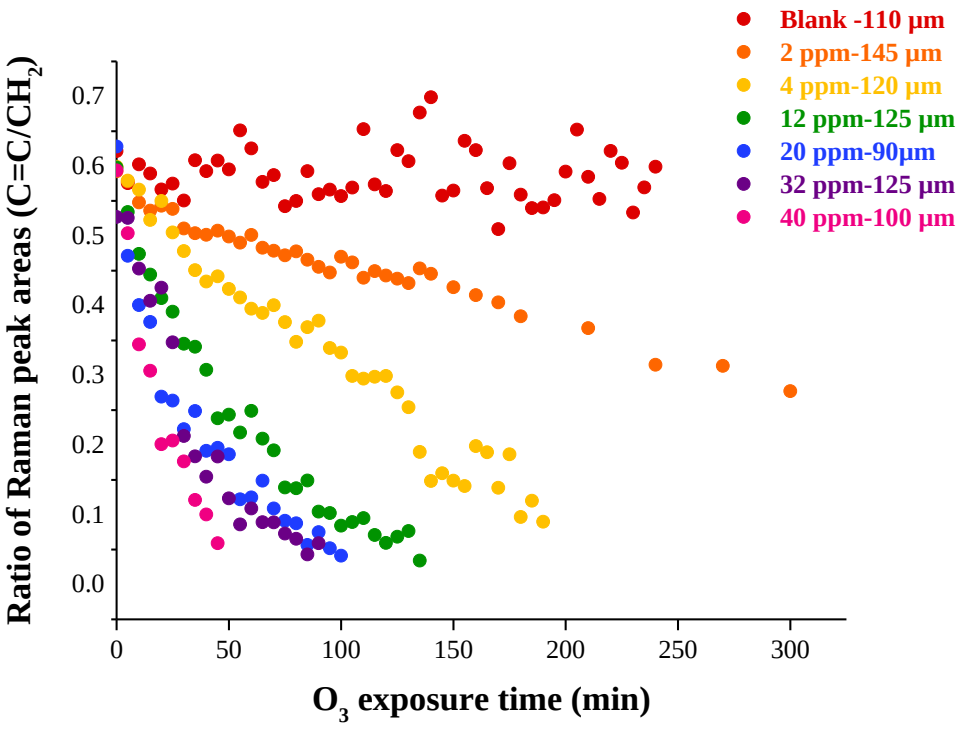

Figure 3.9 Effect of ozone concentration in the ozonolysis of various levitated droplets of oleic acid. Sizes of the droplets are given together with [O_3] in the legend.

3.3.2 PALMITOLEIC ACID

The reaction of ozonolysis of palmitoleic acid was carried out at same [O_3] as the oleic acid reaction. The decay in the ratios of Gaussian area under curve of Raman signatures at 1445 and 1666 cm^{-1} corresponding to CH_2 and C=C bonds, respectively obtained from the reaction of ozonolysis of palmitoleic acid at [O_3] of 2, 4, 12, 20, 32 and 40 ppm and exposure to O_2 (blank) are displayed in Figure 3.10. An incremental decay in these ratios is observed at ozone concentrations under 12 ppm, but at higher concentrations, the trend is comparable to that observed for ozonolysis of oleic acid.

Comparison between the rate of ozonolysis of OA and PA is shown in Figure 3.11, at concentrations of 2, 8 and 32 ppm. Linear regression was applied to all data sets, showing that the slopes corresponding to palmitoleic acid plots were 4.1, 2.1 and 1.3 times higher than the plots corresponding to oleic acid at 2, 8 and 32 ppm of ozone concentration, respectively, confirming the results previously reported by Weitkamp et al (2008), who stated that the same reaction of palmitoleic acid was faster than the ozonolysis of oleic acid.

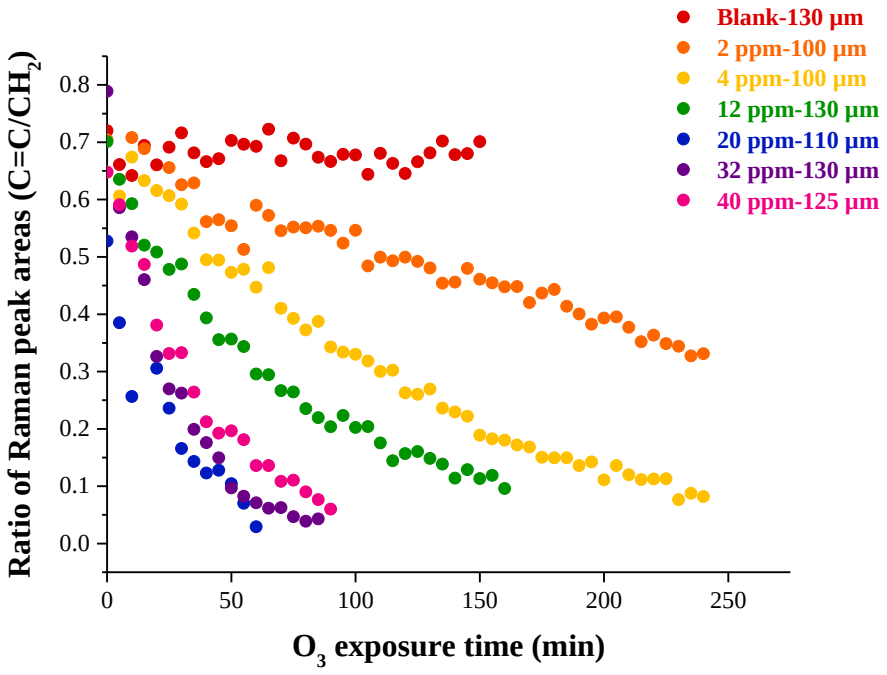

Figure 3.10 Effect of ozone concentration in the ozonolysis of various levitated droplets of palmitoleic acid. Sizes of the droplets are given together with [O_3] in the legend.

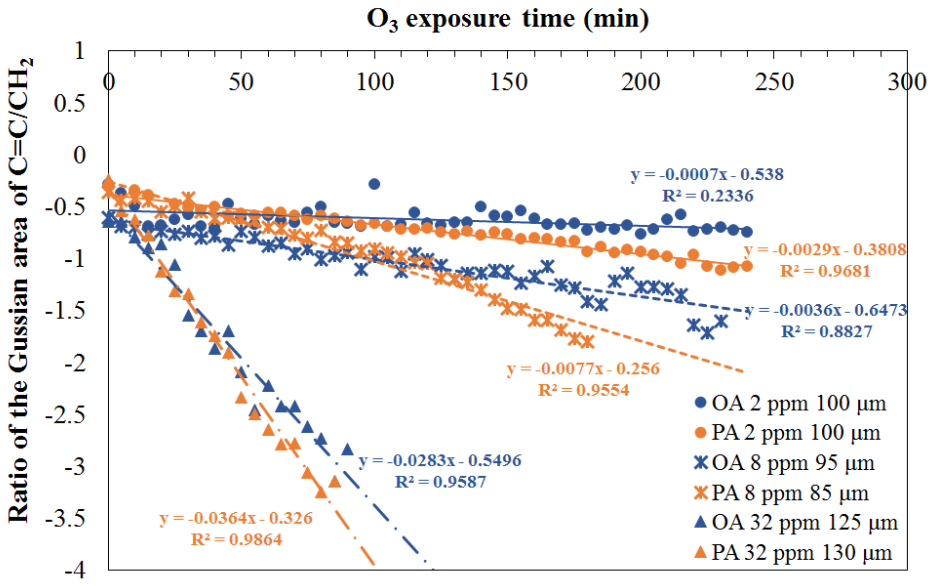

Figure 3.11 Comparison of the reactivity of oleic and palmitoleic acid at 2 ppm (●), 8 ppm (□), and 32 ppm (▲) [O_3].

3.3.3 LINOLEIC ACID

Figure 3.12 shows the effect of ozone concentration on the rate of reaction for ozonolysis of linoleic acid. The results of this reaction have proven that at low O_3 concentrations linoleic acid reacted completely different from oleic and palmitoleic acid. At $[O_3] < 4$ ppm, linoleic acid exhibits an increase in the ratio of Gaussian area of the peaks corresponding to C=C and CH_2, this behaviour has been explained by Lee and Chan (2007a) as the autoxidation of the fatty acids, which occurs in presence of oxygen only or even at low ozone concentration. On the contrary, at O_3 concentration higher than 12 ppm, a decay in the ratio of intensities mentioned, with a very similar pattern of reaction as oleic and palmitoleic acid.

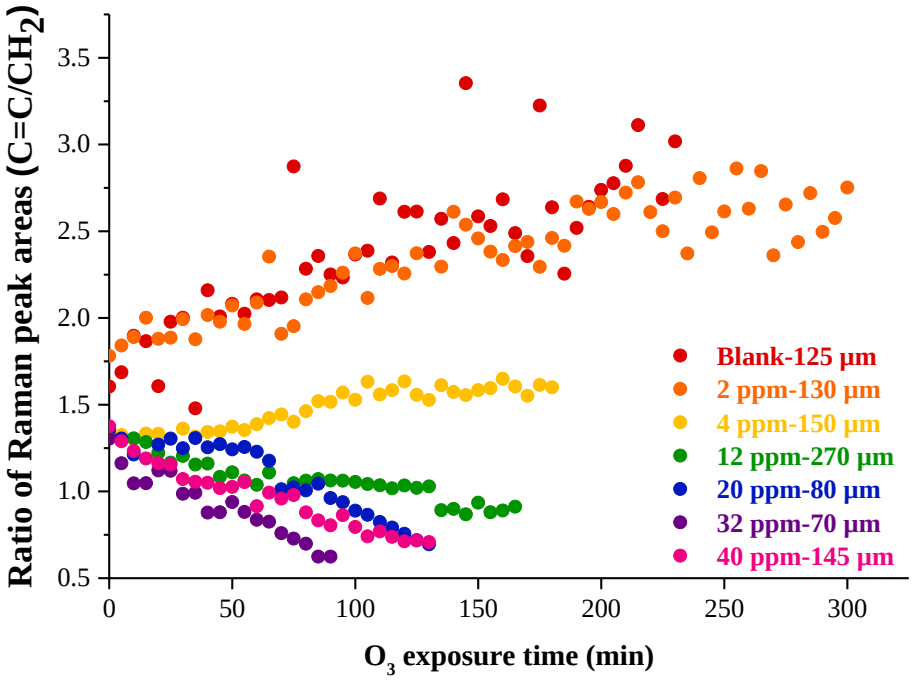

Figure 3.12 Effect of ozone concentration on the ozonolysis of various levitated droplets of linoleic acid. Sizes of the droplets are given together with $[O_3]$ in the legend.

In order to compare the relative reaction rate of linoleic acid versus oleic and palmitoleic acids, the results of experiments carried out at 8 ppm ozone concentration are presented in Figure 3.13. Linear regression was applied to calculate the slopes, finding that the reaction rate of linoleic acid was comparable to palmitoleic acid; however, it reacted faster than oleic acid. Some authors have reported that linoleic acid is expected to be more reactive than oleic acid (Lee and Chan, 2007a; Hearn and Smith, 2004) as the reactive uptake coefficient is augmented by the unsaturation degree of the molecule. From the results presented in Figure 3.13 it is possible to affirm that, for this specific reaction, linoleic and palmitoleic acid reacted faster than oleic acid. However, it is not possible to make this generalisation only based on these results. Therefore, the reactive uptake coefficients will be discussed in section 3.4.

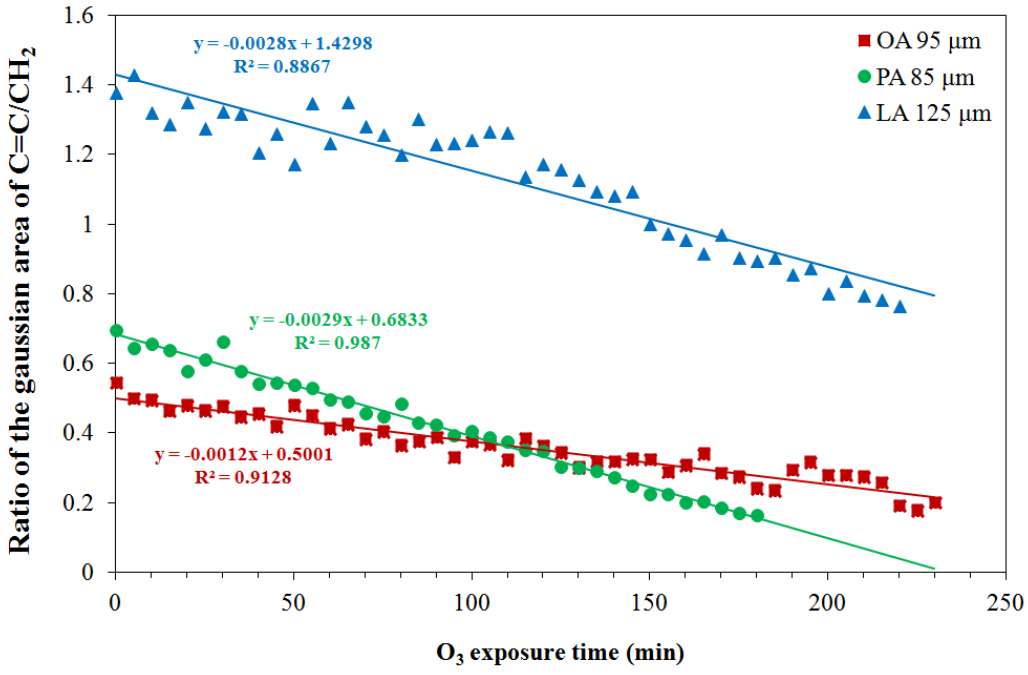

Figure 3.13 Comparison of the reactivity of oleic, palmitoleic and linoleic acid at 8 ppm ozone concentration.

3.4 EFFECT OF THE OZONE CONCENTRATION ON THE UPTAKE COEFFICIENT

This section will present and discuss the results of the effect of ozone concentration on the uptake coefficient for oleic, palmitoleic and linoleic acids, and compare with previously reported findings. Reactive uptake coefficients were obtained from the ozonolysis of oleic, palmitoleic and linoleic acids at different ozone concentrations, applying of limiting conditions listed in Table 3.2 to determine the operative case, as described in Section 3.2. Thus, the summary of reactive uptake coefficients calculated for various experiments at ozone concentrations ranging from 2 to 40 ppm is shown in Table 3.3. It is important to clarify that the reported uncertainty of these values was obtained as the average from a set of three experiments carried out at 40 ppm [O_3] for each fatty acid at low relative humidity.

It is clear that ozone concentration can affect the rate of reaction of ozone with oleic, palmitoleic and linoleic acids. Different authors have previously reported the effect of O_3 concentration on the uptake coefficient. In experiments of ozonolysis of oleic, linoleic and linolenic acid, He et al., (2017) explained that before the reaction starts, the ozone adsorbs onto the surface. With increasing O_3 concentration, more ozone molecules are around the particle until saturation. Thus the number of reactive sites will decrease, reducing the collision between the gas and the particle, therefore, a reduction in the value of γ is expected when the ozone concentration increases. Zeng (2013) stated similar conclusion for the ozonolysis of linoleic acid. The findings of these experiments are also in agreement with the results reported by He et al., (2017) who suggested a reduction of ozone collisions with the surface of the droplet when ozone saturates the

reactive sites because of an increment in the concentration. The γ was also calculated only for reactions at 40 ppm ozone exposure at the half-life (in red), this was the time when [FA] was the half of the initial concentration. The decreasing of the uptake coefficient throughout the reaction was observed, and this may be explained by the slight reduction of the droplet size, that reduces the surface area and the probability of collisions and hence the uptake coefficient, these results were consistent with the reported by He et al., (2017) who explained that the number of active sites decreases in smaller droplets, affecting the uptake coefficient.

Table 3.3 Comparison of calculated uptake coefficient values (γ) obtained from ozonolysis of droplets oleic acid (OA), palmitoleic acid (PA) and linoleic acid (LA). Figures in red correspond to γ at the half-life.

Fatty acid	$[O_3]$ ppm	Initial diameter (μm)	Total time of reaction (min)	Final diameter (μm)	γ
OA	2	145	300	140	$(2.40 \pm 0.13) \times 10^{-4}$
	4	120	190	115	$(1.71 \pm 0.13) \times 10^{-4}$
	12	125	135	115	$(6.14 \pm 1.28) \times 10^{-5}$
	20	90	100	85	$(1.80 \pm 1.28) \times 10^{-5}$
	32	125	90	115	$(4.23 \pm 1.28) \times 10^{-5}$
	40	105	60	105	$(3.78 \pm 1.28) \times 10^{-5}$
					$(9.03 \pm 9.19) \times 10^{-5}$
PA	2	100	240	100	$(1.95 \pm 0.30) \times 10^{-4}$
	4	100	240	115	$(6.83 \pm 3.03) \times 10^{-5}$
	12	130	160	120	$(4.43 \pm 3.03) \times 10^{-5}$
	20	105	60	100	$(7.93 \pm 3.03) \times 10^{-5}$
	32	130	85	130	$(2.00 \pm 3.03) \times 10^{-5}$
	40	125	65	125	$(5.00 \pm 3.03) \times 10^{-5}$
					$(1.38 \pm 2.20) \times 10^{-4}$
LA	2	135	300	135	$(3.52 \pm 0.07) \times 10^{-4}$
	4	155	180	155	$(9.12 \pm 0.72) \times 10^{-5}$
	12	270	165	270	$(9.35 \pm 0.72) \times 10^{-5}$
	20	80	130	75	$(2.84 \pm 0.72) \times 10^{-5}$
	32	70	90	70	$(2.07 \pm 0.72) \times 10^{-5}$
	40	107	150	107	$(2.46 \pm 0.72) \times 10^{-5}$
					$(3.90 \pm 2.61) \times 10^{-5}$

3.5 EFFECT OF THE SIZE OF THE DROPLET ON THE RATE OF REACTION OF OZONOLYSIS AND THE UPTAKE COEFFICIENT

Droplets of oleic, palmitoleic and linoleic acid of different sizes underwent ozonolysis at relative high [O_3] (32 ppm for experiments of OA and LA and 20 ppm for the ozonolysis of PA), and the results are displayed in Figure 3.14. The experiments were carried out at room temperature (298 K) and low RH (<10%). In order to determine the uptake coefficient for all these experiments, the analysis of limiting conditions was applied, following the limiting cases summarised by Zahardis and Petrucci (2007) based on the experimental uptake coefficient reported by Smith et al. (2002), and Worsnop et al (2002), considering the four study cases of ozone uptake by oleic acid previously mentioned in section 3.2; thus, the resultant uptake coefficient values of the current experiments are shown in Table 3.4.

As the times to complete reaction were variable, this table reports the estimated uptake coefficient at one hour of reaction and also at the end, which was the moment when the flow of ozone was stopped and the last Raman spectra registered. The calculated values reported in Table 3.4 indicate that γ increased when the size of the droplet increased both after one hour and at the end of the reaction. This behaviour was expected as a previous study by He et al. (2017) concluded that uptake coefficient might augment with increasing droplet diameter, due to larger droplets have more reactive sites on the surface compared to smaller droplets, easing the collisions that lead to ozonolysis of the fatty acid. It was also observed a decrease in γ when the reaction was finished, this might be due to the collisions of ozone with the particle surface that could decrease as a consequence of products formed at the surface that could have reduced the number of

reactive sites over the time of reaction; in addition, the droplet diameter was reduced, affecting the surface area and therefore the probability of collisions of ozone with the particle. These findings are consistent with the study above and they suggest that the assumption of a reaction either close to the surface of the droplet (case 2) or at the surface (case 3) is in accordance with the evidence.

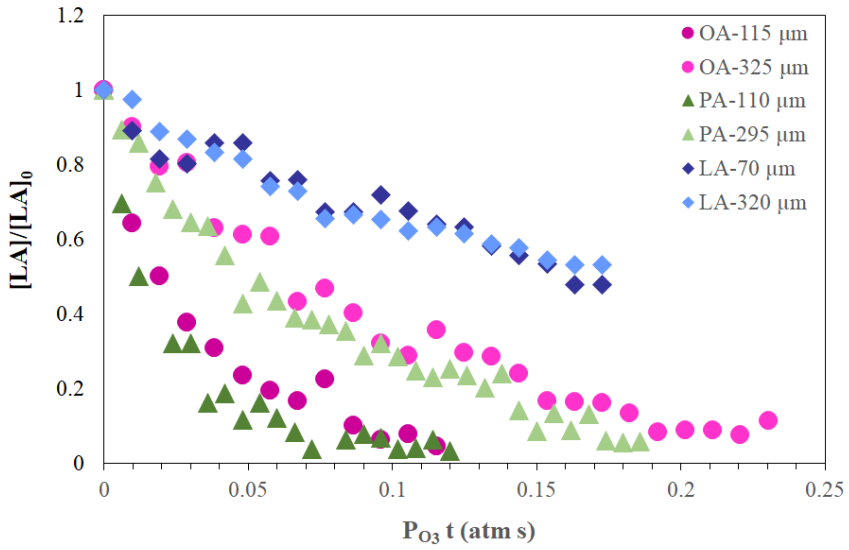

Figure 3.14 Comparison of result from ozonolysis of different droplet sizes of fatty acids at different ozone exposure time: Oleic acid at 32 ppm [O_3] (pink circles); Palmitoleic acid at 20 ppm [O_3] (green triangles); C) Linoleic acid at 32 ppm [O_3] (blue diamonds). Dark colours represent the small sizes of droplets, while light colours symbolize the large droplet diameters.

Table 3.4 Comparison of calculated uptake coefficient values (γ) obtained from ozonolysis of droplets of different sizes of three fatty acids: oleic acid (OA), palmitoleic acid (PA), and linoleic acid (LA).

Fatty acid	Initial diameter (μm)	Total time of reaction (min)	Final diameter (μm)	γ
OA	115	60	110	1.9×10^{-5}
	302.5	120	285	1.7×10^{-4}
PA	110	100	100	7.0×10^{-5}
	295	155	275	2.9×10^{-4}
LA	70	90	70	2.5×10^{-5}
	320	90	320	1.3×10^{-4}

It is clear that the droplet size affects the rate of fatty acid loss. Smith et al (2002) reported that the reactive uptake coefficients decreased as droplet size increased and thus they explained the results by assuming that the reaction is limited by oleic acid diffusion inside the particle with a more significant impact on larger particles, because these large particles must cover longer distances to diffuse to the reaction section to maintain a constant concentration of fatty acid through the particle. Likewise Hung and Tang (2010) reported that the fast consume of O_3 in the first stage of reaction in smaller droplets of oleic acid was probably due to higher total surface area of these droplets while in larger droplets O_3 was consumed at constant rate after 1 min of reaction although the concentration was notably lower compared to the initial value, thus this behaviour showed the significant effect of diffusion of ozone throughout the particle.

In a previous study in the group Rastogi (2015) reported the ozonolysis at 30 ppm [O_3] and RH <10% of two droplets of oleic acid with diameter 70 and 120 μm, it was found that the estimated uptake coefficient increased with the increasing size, from (2.16 ± 0.2) x 10^{-4} to 2.52 ± 0.3) x 10^{-4} however it was observed that droplets with smaller diameters reacted at higher rates than the bigger droplets after 1 hour of ozone exposure. This was explained by the faster diffusion of ozone in smaller droplets. In the research presented here, the most plausible explanation for a higher uptake coefficient when size increased might be the augmented surface area in larger droplets, with more reactive sites for ozone to react with the fatty acids.

3.6 EFFECT OF RELATIVE HUMIDITY ON THE RATE OF REACTION OF OZONOLYSIS

Water is present in the atmosphere, and the amount of water is measured as relative humidity (RH%). When organic aerosols are oxidised, they produce more compounds that might interact with the water depending on their hydrophilicity (Zhou et al. 2014). In the case of unsaturated organic compounds, it is known that the reaction follows the Criegee intermediate mechanism, and more specifically, for oleic acid this reaction produces four main compounds (Hearn and Smith, 2004; Katrib et al., 2004). However, under humid conditions, this reaction has been proven to yield additional products due to the secondary reactions with the water present in the system (Vesna et al. 2009). Also, it has been explained that pure water can decompose O_3 via a chain mechanism initiated by OH^- attack to form radicals that propagate the reaction (Staehelin and Hoigné, 1982, Bühler et al., 1984). This section will present the results of ozonolysis of oleic, palmitoleic and linoleic acids under dry and humid conditions, and the effect of relative humidity (RH) on the kinetics and products of these reactions will be discussed.

3.6.1 OLEIC ACID

Figure 3.15 (a) and (b) depict the Raman spectra obtained from the experiments carried out at 32 ppm [O_3], with RH of ≈15% and >60% to simulate dry and humid conditions respectively. In the first case, the exposure times were the initial (0 min) and final (75 min), whereas at high RH the exposure times are initial (0 min), intermediate (75 min to compare) and final (130 min). Droplet sizes were very similar, in order to compare the results and focus on the effect of relative humidity only. These spectra demonstrate that

RH can affect both the kinetics of the reaction and the products. A previous study by Vesna et al. (2008) reported that increased RH does not affect the growth factor of oleic acid since the mechanism of ozonolysis of this fatty acid undergoes an alternative pathway when Criegee intermediates (CIs) react with water forming smaller acids. The spectra in Figure 3.15 show that after 75 min, in both low and high RH the peak corresponding to double bond decreased, indicating that OA reacted with ozone, however at humid conditions the same peak is more visible compared to the spectrum of the same reaction at low RH. Likewise, the peaks at 1280 and 3020 cm^{-1} assigned to HC=CH deformation and CH_2 symmetric stretching respectively are still visible at high RH after 75 min of O_3 exposure, suggesting unreacted carbon-carbon double bond remaining. Vesna et al. (2009) also suggested that water affected ozonolysis as it might react with CIs to produce peroxides, and similarly, these CIs may react with other carbonyl compounds to form peroxidic polymers. This could explain the increased peak at 880 cm^{-1} appearing in the spectrum of ozonolysis of OA at high RH, corresponding to O−O stretching in peroxides. Then, after 130 min, the reaction carried out in humid conditions showed signs to be completed, as the C=C peak at ≈1664 cm^{-1} in the last spectrum (blue) has decreased to a minimum and the area of the peak associated to peroxides is augmented. In both cases, dry and humid conditions, the spectra suggest the formation of carbonyl compounds, with the rising of a weak band at ≈ 1750 cm^{-1} associated to C=O stretching.

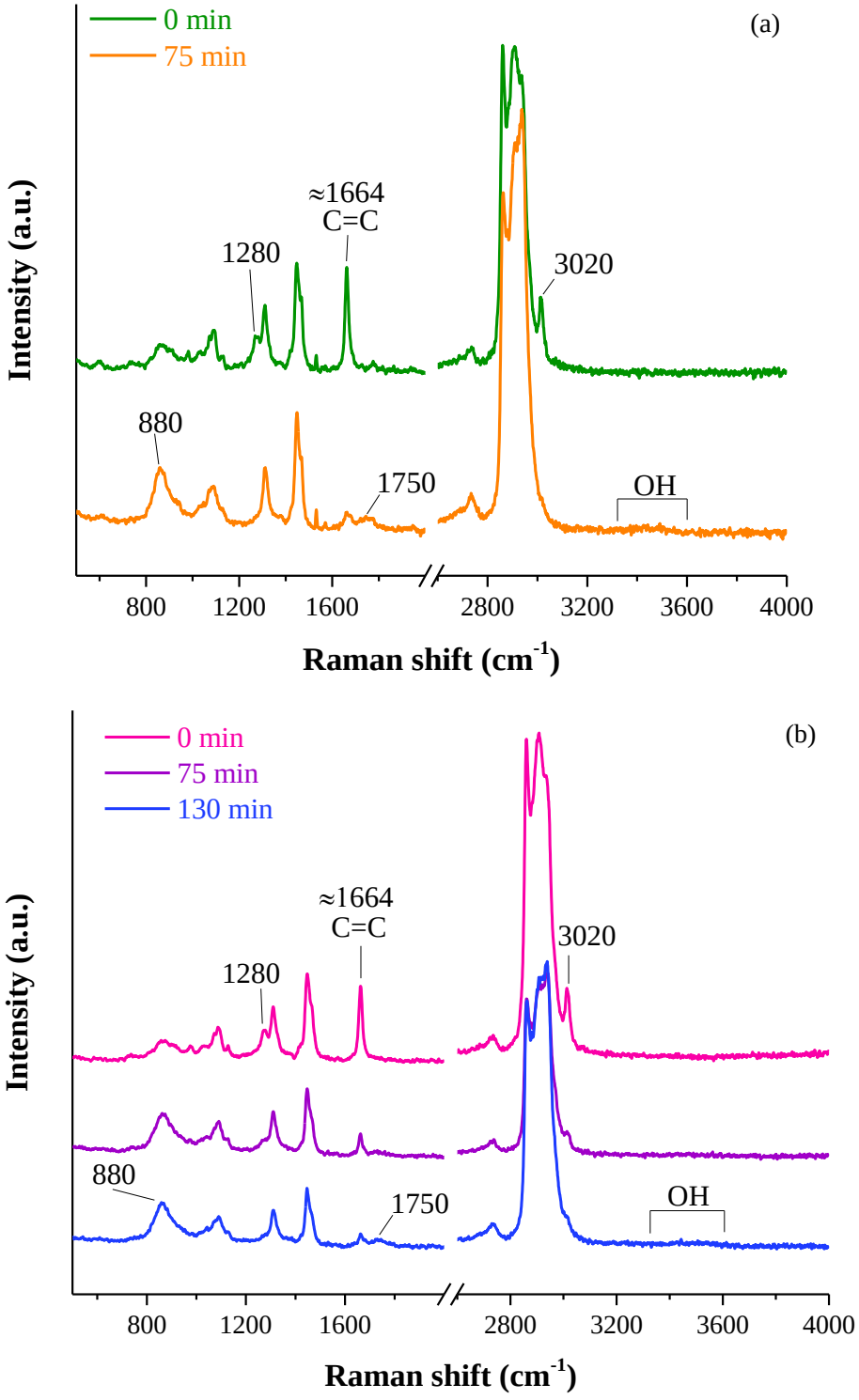

Figure 3.15 Raman spectra obtained from the ozonolysis of oleic acid under low (a) and high (b) RH conditions. The [O_3] was 32 ppm, and the diameter of levitated droplets were 140 μm (RH ≈15%) and 130 μm (RH > 60%).

Despite the evidence of incorporation of water to the droplet in the studies by Zeng et al (2013) and Asad et al (2004), for reactions of ozonolysis of linoleic acid and oleic acid respectively at high relative humidity and using FTIR to monitor the reactions, it is not completely clear in these experiments whether or not OA had incorporated water, except for the very weak peak at approximately 3500 cm^{-1} and normally related to intramolecular OH stretching in Raman spectra (Carey and Korenowski, 1998), which is hardly visible in the last spectrum (130 min) at high RH in Figure 3.14. This peak evidences the presence of OH^- from water and it is believed that this species could initiate the decomposition of ozone in water following the mechanism proposed by Stahelin and Hoigné (1982):

$$O_3 + OH^- \longrightarrow HO_2^- + O_2 \qquad \text{Equation 3.3}$$

And also HO_2^- may react with O_3,

$$O_3 + HO_2^- \longrightarrow OH\bullet + \bullet O_2 + O_2 \qquad \text{Equation 3.4}$$

Thus the concentration of O_3 may decrease causing the decay in the rate of reaction.

Figure 3.16 presents the plots obtained from the ozonolysis of oleic acid at different ozone concentrations (0.8 to 32 ppm) at a) low (<10%) and b) high (>50%) relative humidity. The sizes of levitated droplets are shown in the legend together with the ozone concentrations. For all reactions, the expected decay in the ratio of the Gaussian area of $C{=}C/CH_2$ peaks was obtained. By comparison of both (a) and (b) charts, a slight decay at lower ozone concentration is observed, but it is also evident that there is a

tendency to a gradual decay of the ratio when the concentration is augmented under dry conditions. In the plots at high RH (b), it is possible to distinguish a very similar trend when [O_3] increases, with considerable decay at the highest ozone concentration when compared to the reactions at O_3 concentrations lower than 2 ppm. Experiments were carried out using oxygen as a benchmark (grey stars) to contrast to the results of ozonolysis. The first interpolation was that at low RH the reactions are faster as the decays are considerably more noticeable in plots at low RH. However, previous evidence (He 2017; Zeng 2013; Lee 2012) suggested that the uptake of ozone slightly increased at higher RH for highly unsaturated species, such as linoleic, linolenic and arachidonic acid, with no dependence on RH in the case of oleic acid. This means that the expected results would be the decays of the ratios of Gaussian area at high RH to be steeper than the decays at low RH, but this was not the case for the results presented here. These findings can be explained by the decomposition of ozone in water may decrease the rate of reactions when [O_3] is to low, but when the concentration increased the saturation of gas is enough to be preserved, and it reacts with the fatty acid instead of water. This may also explain the constant intensity of the signal at 1663 cm^{-1} (C=C) throughout the reactions at [O_3] lower than 4 ppm.

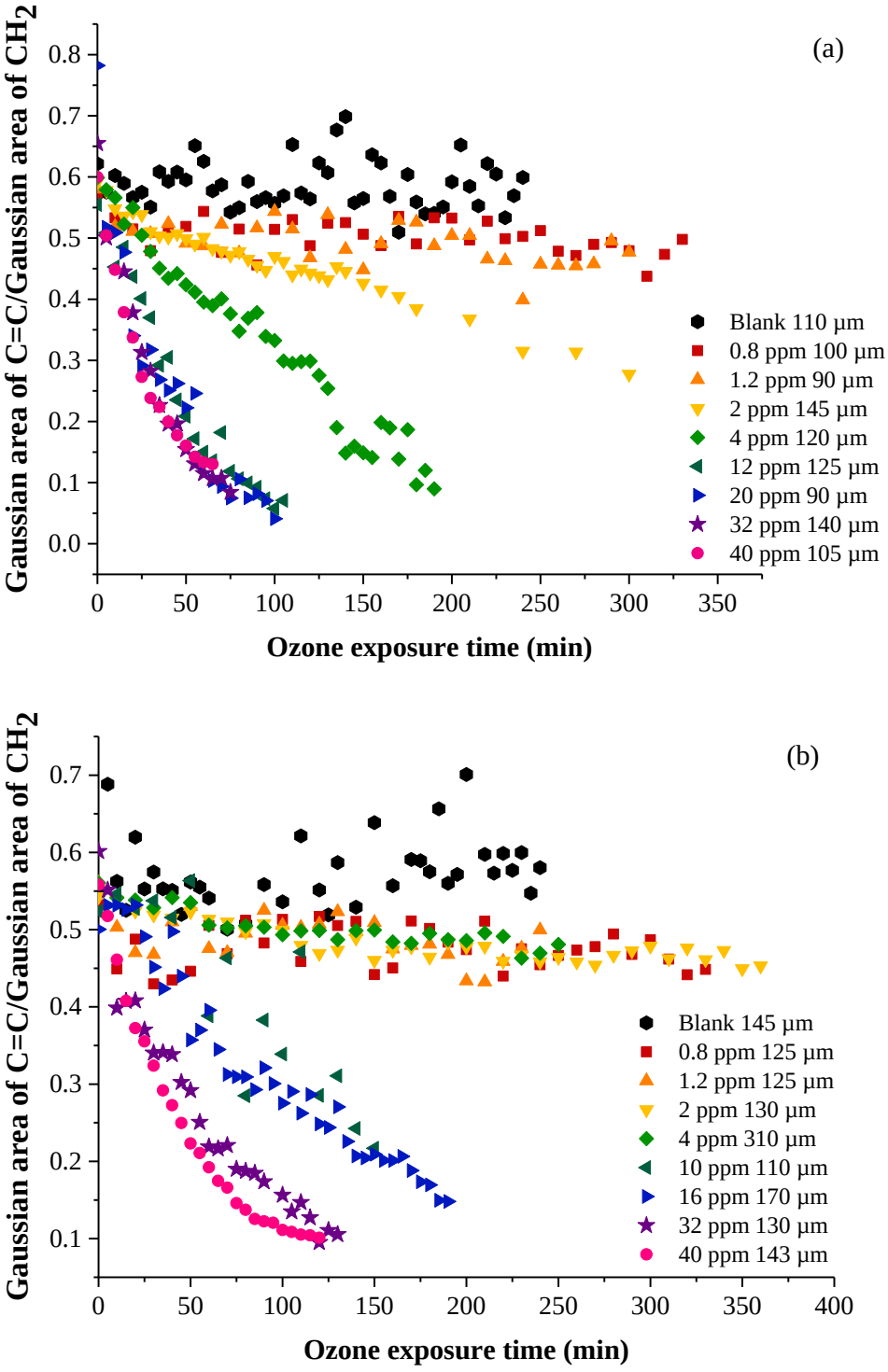

Figure 3.16 Decay of the ratio of Gaussian area of peaks C=C/CH_2 obtained from the ozonolysis of oleic acid at different ozone concentrations under (a) low and (b) high relative humidity. Sizes of the droplets are displayed in the legend together with [O_3].

3.6.2 PALMITOLEIC ACID

The Raman spectra obtained from the ozonolysis of palmitoleic acid at 32 ppm ozone concentration are shown in Figure 3.17. The reaction of ozonolysis of a droplet (140 μm in diameter) under low RH (Fig. 3.17 a) finished at the elapsed time of 85 min, while the ozonolysis of a droplet (diameter = 165 μm) at high RH (Fig. 3.17 b) was conducted for more than four hours. Both reactions showed many differences in the obtained spectra. At low RH the peaks located at 1270 and 1663 cm^{-1} corresponding to C=C deformation and C=C stretching respectively have decreased when the reaction finished. This feature is a clear indication of the cleavage of the carbon double bond. In addition, the peak at 3080 cm^{-1} corresponding to CH_2 stretching is not visible at the end of the reaction. An increase of the peak situated between 850 and 900 cm^{-1} characteristic of peroxides is noticeable, as well as the emerged peak at 1750 cm^{-1} due to carbonyl groups, confirming the formation of aldehydes.

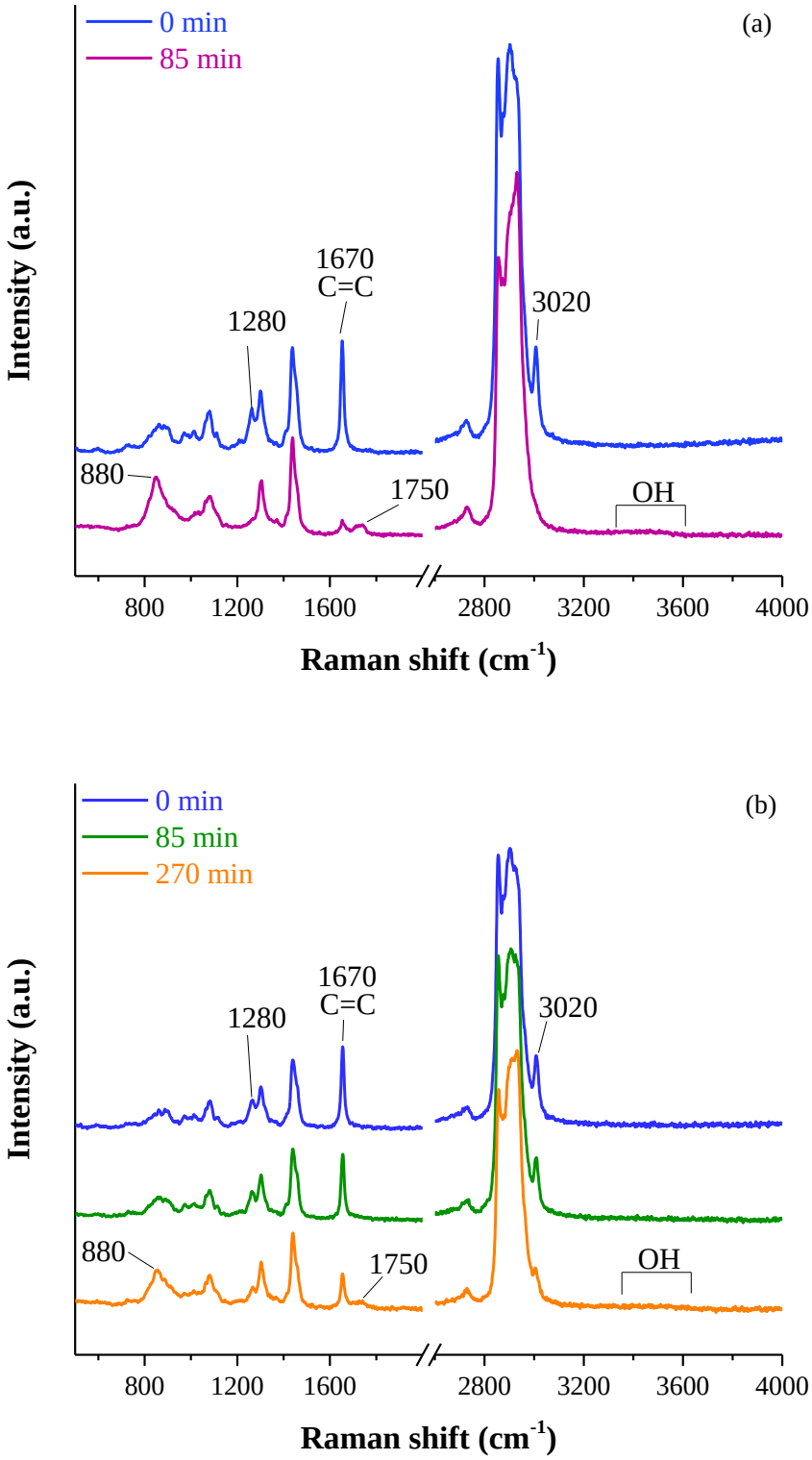

Figure 3.17 Raman spectra obtained from the ozonolysis of palmitoleic acid under low (a) and high (b) RH conditions. The [O_3] was 32 ppm, and the diameter of levitated droplets were 140 μm (RH <10 %) and 165 μm (RH > 60%).

In the case of Raman spectra obtained from the experiments at high RH, after 85 min the bands at 1270, 1663, 3080, and between 800 and 900 cm^{-1} remain with minimal changes in intensity, suggesting a slowdown in the rate of reaction in comparison with the same reaction under dry conditions. No emerging peak at 1750 cm^{-1} is observed. Significant changes in intensity are visible after four hours of ozone exposure, with RH over 70%. The decrease of the characteristic bands for C=C and CH_2 bonds and the slight rising of the typical peak of carbonyl compounds (1700-1750 cm^{-1}) is observed; also the intensity of the peroxide band increased when the experiment finished after 270 min.

The effect of the relative humidity in the decay of Gaussian area of the peaks C=C/CH_2 obtained from the ozonolysis of palmitoleic acid at ozone concentrations between 0.8 and 32 ppm is shown in Figure 3.18. Plots in (a) represent the experiments at low RH, while plots in (b) represent the experiments carried out at high RH. The gradual decay of the ratio when ozone concentration is augmented from 2 to 32 ppm is observed in (a). For lower concentrations (0.8, 1.2 and 2 ppm), the appearance of the plots indicates the reaction is occurring at very low rate. Plots in (b) show that palmitoleic acid experienced the ozonolysis apparently at a low rate compared to a higher ozone concentration. In both cases, the highest O_3 concentration (40 ppm) showed the fastest decay. As mentioned in the previous section, palmitoleic acid tends to be more reactive than oleic acid, thus the decays of the ratio of Gaussian peak areas are expected to be sharper for both set of experiments using PA (low and at high RH), but this was not the case, and one possible reason could be that bigger droplet sizes are affecting the decays, but also the decomposition of O_3 in water, as described in Equations 3.3 and 34.

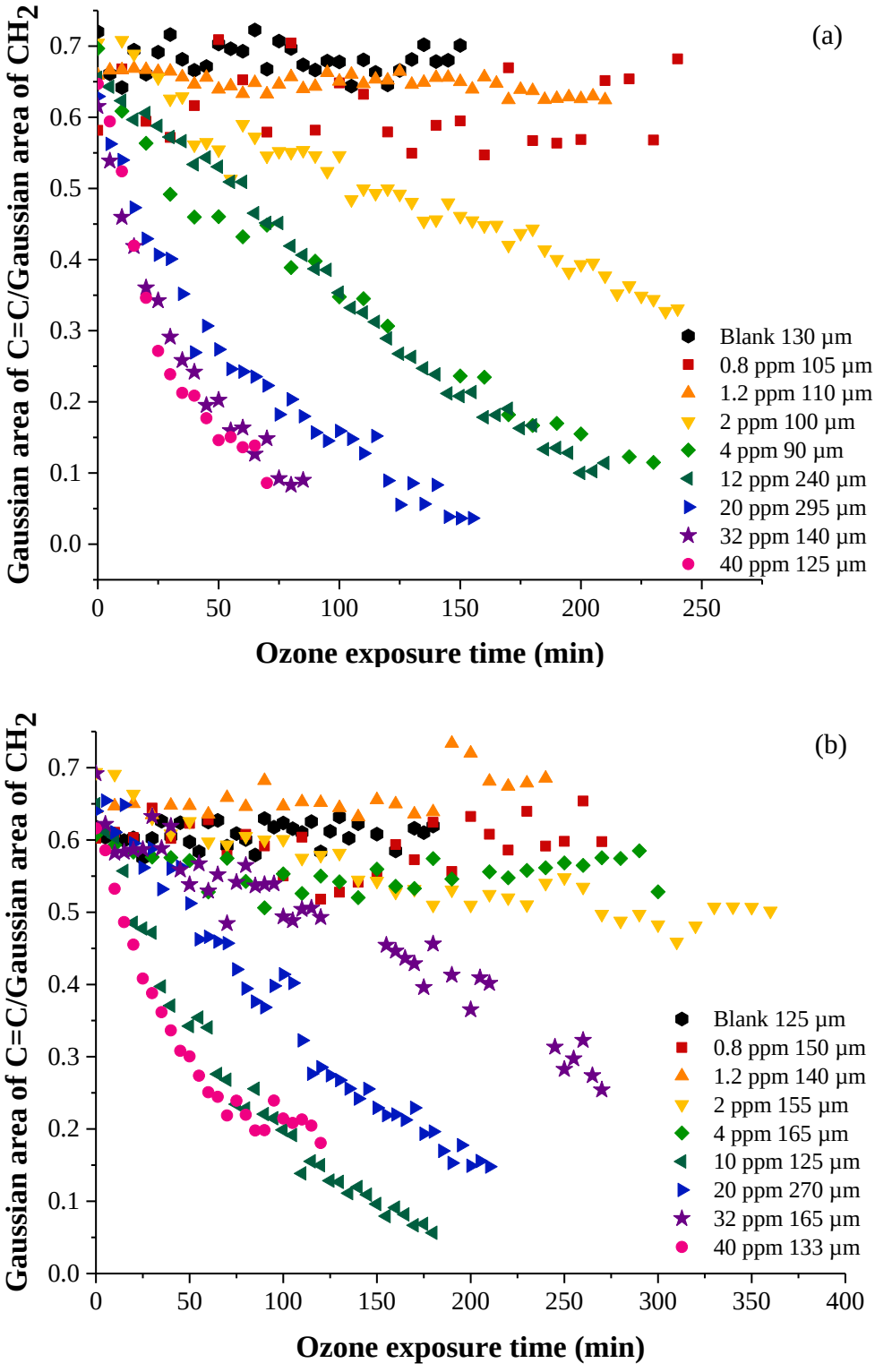

Figure 3.18 Decay of the ratio of Gaussian area of peaks C=C/CH_2 obtained from the ozonolysis of palmitoleic acid at different ozone concentrations under (a) low and (b) high relative humidity. Sizes of the droplets are displayed in the legend together with [O_3].

3.6.3 LINOLEIC ACID

The Raman spectra in Figure 3.19 correspond to the ozonolysis of linoleic acid at 40 ppm ozone concentration, for low (a) and high (a) relative humidity.

The spectra show changes in the characteristic bands. By inspection of the spectra at low RH, it is evident that after 60 min the bands at 1270, 1660 and 3080 cm^{-1} attributed to C=C have only insignificant changes in intensity. The reaction proceeded for more than four hours, and changes in the intensity of bands occurred slowly. For example, after 170 min the band at 1270 cm^{-1} scarcely reduced its intensity, although changes were noticeable after 270 min when the experiment was stopped. The peak at 3080 cm^{-1} has disappeared and the most representative band, at 1660 cm^{-1} was significantly reduced after 4hr 30 min, indicating the cleavage of C=C bonds. Formation of oxygen-containing groups caused the emerging of peaks at 850 and 1750 cm^{-1}, assigned to peroxides and carbonyl compounds, respectively.

The Raman spectra obtained from the experiment of ozonolysis of linoleic acid at 32 ppm and humid conditions showed that the reaction took place, but unlike the same reaction at low RH, the peak at 1663 cm^{-1} characteristic for the C=C bond maintained high intensity over the entire ozone exposure time. The reaction was stopped at 170 min, and few changes were observed: the loss of intensity of the peaks at 1270 and 3080 cm^{-1} indicate the breaking of the C=C bond, and the rising of the band characteristic for peroxides confirm that linoleic acid reacted with ozone. The appearance of a weak band around 1600 cm^{-1} indicates the formation of conjugated dienes, as stated by Lee and Chan (2007a). The peak that normally is located at 1750 cm^{-1} is still weak after 170 min

of reaction; this is an indication that the reaction follows a mechanism that involves the formation of different species apart from carbonyls. Zhou et al. (2014) found that the reaction of ozone with linoleic acid at the air/water interface yielded aldehydes such as hexanal, 3-nonenal and glyoxal, thus it is expected the emerging Raman signature of C=O located close to the high intensity band of C=C, as in the Raman spectra shown in Figure 3.19.

The ratios of Gaussian area calculated for the peaks $C=C/CH_2$ obtained from ozonolysis of linoleic acid at 40 ppm at low and high relative humidity was plotted, and the resultant charts are displayed in Figure 3.20. In most cases, the ratio increased due to the formation of products containing carbon-carbon double bonds, thus the peak at 1663 cm^{-1} increase. In various Raman spectra at different concentrations the bands located at 850, 1270, and 3080 cm^{-1} showed significant changes, this is an indication that linoleic acid reacted, but unlike oleic and palmitoleic acid, the reaction is probably following an alternative mechanism (autoxidation) leading to the formation of products that keep the double bond intact. These results were expected for ozonolysis of linoleic acid at concentrations lower than 4 ppm (Lee and Chan, 2007a); however, that was not the case. Only the reaction carried out at 32 ppm, and low RH showed a drop in the ratio of Gaussian area. It is possible to infer that both relative humidity and the size of droplet could affect the intensity of the carbon-carbon double bond peak. According to Zeng et al. (2013), given that the ozonolysis produces more hydrophilic compounds that can trap water, in addition to the fact that ozone is partially soluble in water, the residence time of ozone increase and therefore the uptake probability. This effect might favour the reaction to form more unsaturated species, thus the peak at 1663 cm^{-1} increases and therefore the ratios of the Gaussian areas. Also, species from water, such as OH^- ion and

HO_2 can destroy O_3 (Staehelin and Hoigné, 1982), this may alter the concentration and therefore decrease the rate of reaction.

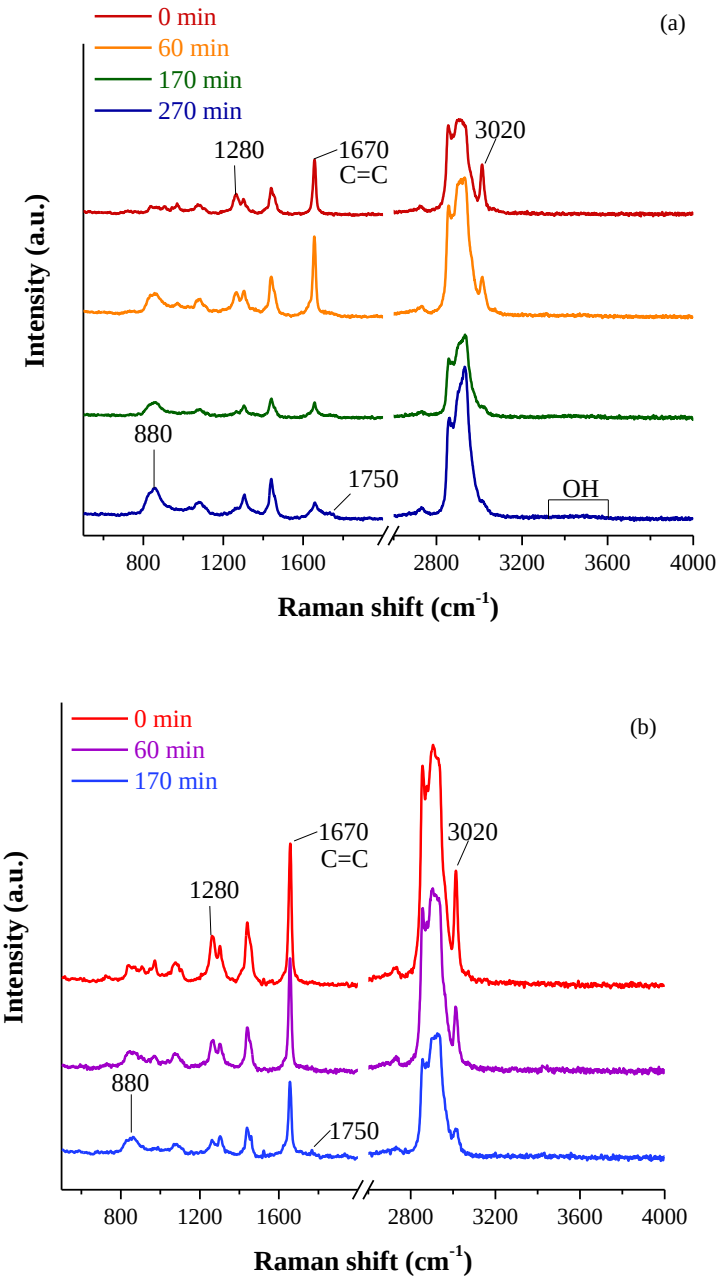

Figure 3.19 Raman spectra obtained from the ozonolysis of linoleic acid under low (a) and high (b) RH conditions. The $[O_3]$ was 32 ppm, and the diameter of levitated droplets were 115 μm (RH < 10 %) and 170 μm (RH > 70%).

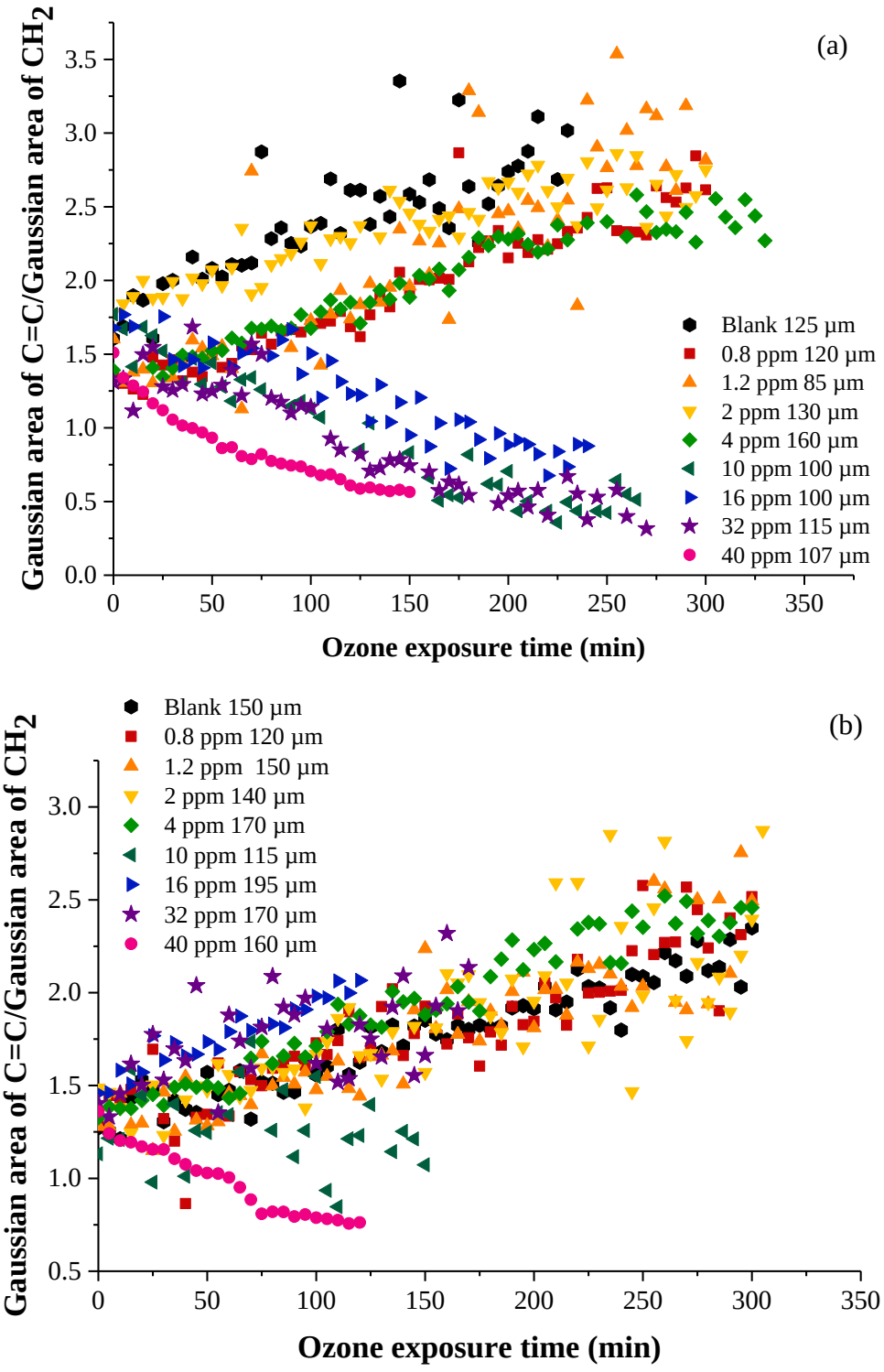

Figure 3.20 Decay of the ratios of Gaussian area of peaks C=C/CH_2 obtained from the ozonolysis of linoleic acid at different ozone concentrations under (a) low and (b) high relative humidity. Sizes of the droplets are included in the legend together with [O_3].

3.7 EFFECT OF RELATIVE HUMIDITY ON THE UPTAKE COEFFICIENT

Table 3.5 Comparison of calculated uptake coefficient values (γ) obtained from ozonolysis of droplets oleic acid (OA), palmitoleic acid (PA) and linoleic acid (LA) at low and high RH.

Fatty acid	RH%	$[O_3]$ ppm	Initial diameter (μm)	Total time of reaction (min)	Final diameter (μm)	γ
OA	<5	0.8	100	330	100	$(1.14 \pm 0.13) \times 10^{-4}$
	<5	1.2	100	300	100	$(1.12 \pm 0.13) \times 10^{-4}$
	<5	2	150	300	150	$(2.57 \pm 0.13) \times 10^{-4}$
	<5	4	120	190	115	$(1.71 \pm 0.13) \times 10^{-4}$
	≈10	32	140	75	135	$(3.52 \pm 1.28) \times 10^{-5}$
	53-66	0.8	125	330	125	$(1.69 \pm 0.36) \times 10^{-4}$
	56-68	1.2	130	240	130	$(1.14 \pm 0.36) \times 10^{-4}$
	50-69	2	130	360	125	$(6.52 \pm 3.59) \times 10^{-5}$
	68-71	4	300	250	300	$(9.75 \pm 3.59) \times 10^{-5}$
	55-65	32	130	130	125	$(2.18 \pm 3.59) \times 10^{-5}$
PA	<10	0.8	105	230	105	$(3.52 \pm 3.03) \times 10^{-5}$
	<10	1.2	115	210	115	$(6.22 \pm 3.03) \times 10^{-5}$
	<10	2	100	240	100	$(1.95 \pm 0.30) \times 10^{-4}$
	<15	4	100	230	95	$(8.10 \pm 3.03) \times 10^{-5}$
	<10	32	140	85	135	$(6.19 \pm 3.03) \times 10^{-5}$
	64-73	0.8	150	270	150	$(1.40 \pm 3.91) \times 10^{-5}$
	56-70	1.2	140	240	140	$(4.63 \pm 3.91) \times 10^{-5}$
	61-67	2	160	360	160	$(1.49 \pm 0.39) \times 10^{-4}$
	59-71	4	165	300	165	$(4.55 \pm 3.91) \times 10^{-5}$
	59-77	32	170	270	160	$(2.34 \pm 3.91) \times 10^{-5}$
LA	<5	0.8	120	300	120	$(1.27 \pm 0.72) \times 10^{-3}$
	<5	1.2	95	300	95	$(-6.30 \pm 0.07) \times 10^{-4}$*
	<5	2	120	300	118	$(2.87 \pm 0.07) \times 10^{-4}$
	<15	4	180	330	170	$(2.20 \pm 0.07) \times 10^{-4}$
	<15	32	125	240	115	$(1.80 \pm 0.72) \times 10^{-5}$
	58-69	0.8	125	300	125	1.41×10^{-3}
	67-69	1.2	160	300	155	-1.35×10^{-3}*
	57-70	2	150	305	150	-7.56×10^{-4}*
	57-73	4	170	300	170	3.37×10^{-4}
	68-75	32	170	170	170	-4.82×10^{-5}*

* Negative values of γ, due to the slopes of plots have positive values

Table 3.5 summarises the reactive uptake coefficient calculated for ozonolysis of oleic, palmitoleic and linoleic acid at ozone concentration ranging from 0.8 to 32 ppm and different relative humidity percentages. It is important to mention that the reported uncertainty of these values was obtained as the average from a set of three experiments carried out at 40 ppm [O_3] for each fatty acid at low relative humidity and only for OA and PA at RH higher than 60 %., it was not possible to carry out the same set of experiments with LA due to experimental limitations. The results of these experiments allowed the obtaining of γ at the half-life, the time when [FA] was the half of the initial concentration. Table 3.6 compares the values of uptake coefficient for each fatty acid in terms of RH and time of reaction (half-life and at the end of the reaction).

Table 3.6 Uptake coefficient obtained from the ozonolysis of droplets of OA, PA and LA exposed to 40 ppm ozone concentration and under dry and humid conditions. Two values of γ were calculated for each fatty acid: half-life and at the end of the experiment.

Fatty acid	**RH %**	**Particle radius (μm)**	**Half-life (min)**	**γ (half-life)**	**Total time of reaction (min)**	**γ (final)**
OA	< 15	105	22	$(9.03 \pm 9.19) \times 10^{-5}$	60	$(3.78 \pm 1.28) \times 10^{-5}$
	> 50	143	38	$(6.96 \pm 6.01) \times 10^{-5}$	110	$(2.88 \pm 3.59) \times 10^{-5}$
PA	< 15	125	20	$(1.38 \pm 2.20) \times 10^{-4}$	70	$(5.00 \pm 3.03) \times 10^{-5}$
	> 50	133	55	$(6.42 \pm 9.28) \times 10^{-5}$	110	$(3.18 \pm 3.91) \times 10^{-5}$
LA	< 20	107	85	$(3.90 \pm 2.61) \times 10^{-5}$	155	$(2.46 \pm 0.72) \times 10^{-5}$

By comparing the uptake coefficients in Table 3.5, some tendencies were identified in the reactive uptake coefficient depending on RH%. For example, OA showed a slight decrease at very low [O_3] when RH was augmented, then it increased at [O_3] higher than 2 ppm whereas palmitoleic acid experienced a fall in the value of uptake coefficient with increasing relative humidity.

In contrast, the uptake coefficient obtained from ozonolysis of linoleic acid raised with higher RH. It is worth to mention that the values marked with (*) indicate the obtained number was negative, given that operative case 3 was applied for these experiments, which is exponential, and the slopes of these curves were positive (see Figures 3.19 and 3.20). The discrepancies in the results for the other two fatty acids may be explained by the effect of the extra double bond C=C present in linoleic acid, as stated by He et al. (2017): the more unsaturation, the more dependence on relative humidity. Also, the study of ozonolysis of LA by Zeng et al. (2013) explained that uptake coefficient increased at higher RH due to LA can capture water molecules by forming hydrogen bonds, then this water can retain O_3 molecules to augment their residence times and therefore the probability of higher values of γ.

Concerning the values in Table 3.6, a comparison of the values of uptake coefficient of OA, PA and LA in terms of RH and time (half-life and at the end of the reaction). showed the tendency of γ to decrease throughout the reaction, also it was very clear that relative humidity affected the reaction of ozonolysis of oleic and palmitoleic acids, as the uptake coefficient was lower for experiments under humid conditions, although this may also be influenced by the particle size, because variations in size affect the reactive sites on the surface and have effects on values of uptake coefficient (He et al., 2017).

3.8 ANALYSIS OF PRODUCTS OF THE REACTION OF OZONOLYSIS OF FATTY ACIDS

Several changes were observed during the ozonolysis of fatty acids. Raman spectra showed the formation of products such as aldehydes and peroxides. Numerous studies have reported the possible formation of products from ozonolysis of fatty acids such as oleic and linoleic acid. The evidence suggested that products are peroxides, hydroperoxides, and polymers among others. They are formed via different pathways, for example in secondary processes when the products react with each other, also when products react with water, or even some of them undergo new reactions with ozone (Vesna et al., 2009; Moise and Rudich 2002; Ziemann 2005; Lee et al., 2012; Katrib et al. 2004; Zeng et al. 2013; Zhou et al., 2014).

This section will present the results of the analysis and identification of products using GC/MS and HS-SPME, and possible mechanisms are formulated from these findings.

3.8.1 OLEIC ACID

The mechanism of ozonolysis of oleic acid was shown in Figure 1.6 in Chapter 1; this reaction yields four main products: nonanal, nonanoic acid, azelaic acid and 9-oxononanoic acid, and also the secondary chemistry produces additional products such as octanoic acid, hydroperoxides and polymers (Hung, Katrib and Martin, 2005). As shown in the schematic of Figure 1.5 (Chapter 1), it is clear that ozonolysis of oleic acid might also produce dimeric peroxides, esters, lactones, and ozonides. Ziemann (2005) proposed a mechanism of the reaction of ozone with pure oleic acid that produces a

variety of high molecular weight compounds such as hydroperoxides, oligomers, and diperoxides, in addition to the known aldehydes and carboxylic acids. Similarly, Vesna et al. (2009) described the reaction of ozone with oleic acid as a sequence of three steps, that involves secondary reactions between the Criegee intermediate (CI) 1 or 2 and any of these compounds: 1) water, to produce hydroperoxides; 2) carboxylic acids or aldehydes formed in the first step to yield secondary ozonides or α-acyloxyalkyl hydroperoxides (AAHP); 3) reaction of two CI to form diperoxides, and 4) reaction of polymerization between AAHP and CI to produce high molecular weight compounds.

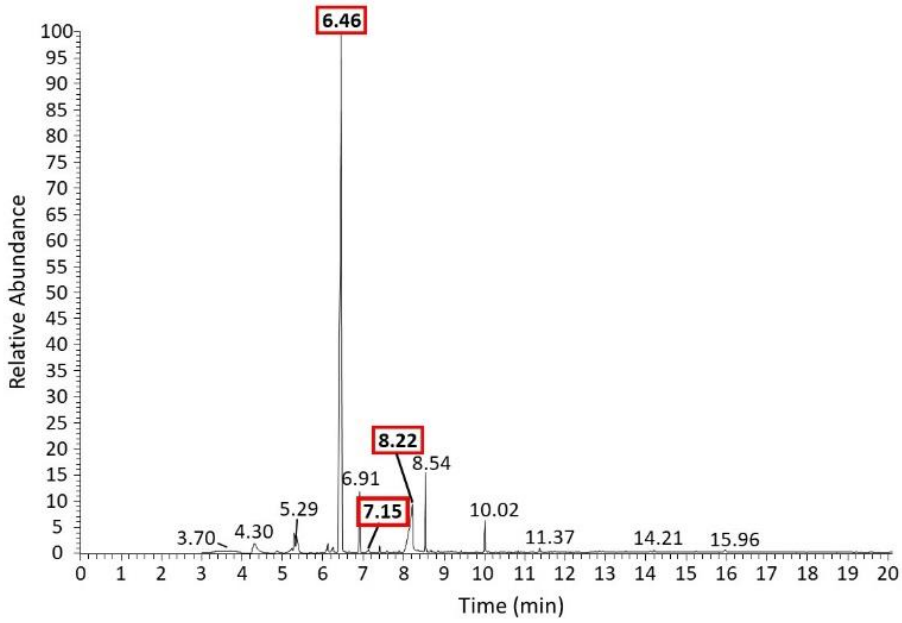

Figure 3.21 Chromatogram obtained from a levitated droplet of oleic acid exposed to 32 ppm O_3 concentration and low RH (<10%). The retention times of identified products are highlighted in red: 6.46, 7.15 and 8.22 corresponding to nonanal, octanoic acid and nonanoic acid respectively.

The analysis of products by GC/MS HS-SPME was carried out for the experiments of ozonolysis of oleic acid under dry and humid conditions and a high ozone concentration of 32 ppm. The chromatogram obtained from the ozonolysis of oleic acid at 32 ppm [O_3] and low RH (< 10%) is displayed in Figure 3.21, The retention times highlighted in red correspond to the compounds that were identified: 6.46 min corresponds to nonanal (MW 142), 7.15 min is due to octanoic acid (MW 144) and 8.22 min attributed to nonanoic acid (MW 158), their mass spectra are shown in Figure 3.22:. These mass spectra were compared to the reported MS by Rastogi (2015) and also the online spectral database (NIST Chemistry WebBook, NIST Standard Reference Database Number 69) in order to confirm they were nonanoic acid, nonanal and octanoic acid. Nonanoic acid (MW = 158) has peaks at *m/z* 129 and 115, from the loss of CH_2CH_3 and $CH_2CH_2CH_3$ fragments, whereas nonanal shows spectral peaks at *m*/z 125 and 114, from the loss of H_2O and C=O fragments, respectively. With respect to octanoic acid, the mass spectrum shows peaks at *m/z* 55, 73 and 115, they may be due to the loss of C_3H_7COO, C_5H_{11} and C_2H_5 fragments respectively. These compounds were also observed in the mass spectra of the reaction of oleic acid with ozone at 32 ppm and high RH. Azelaic and 9-oxononanoic acids were not observed, but spectra of high-molecular weight compounds were obtained; they probably are formed from secondary reactions, confirming the presence of peroxides that were detected by Raman spectroscopy (see Raman spectra in Figure 3.15).

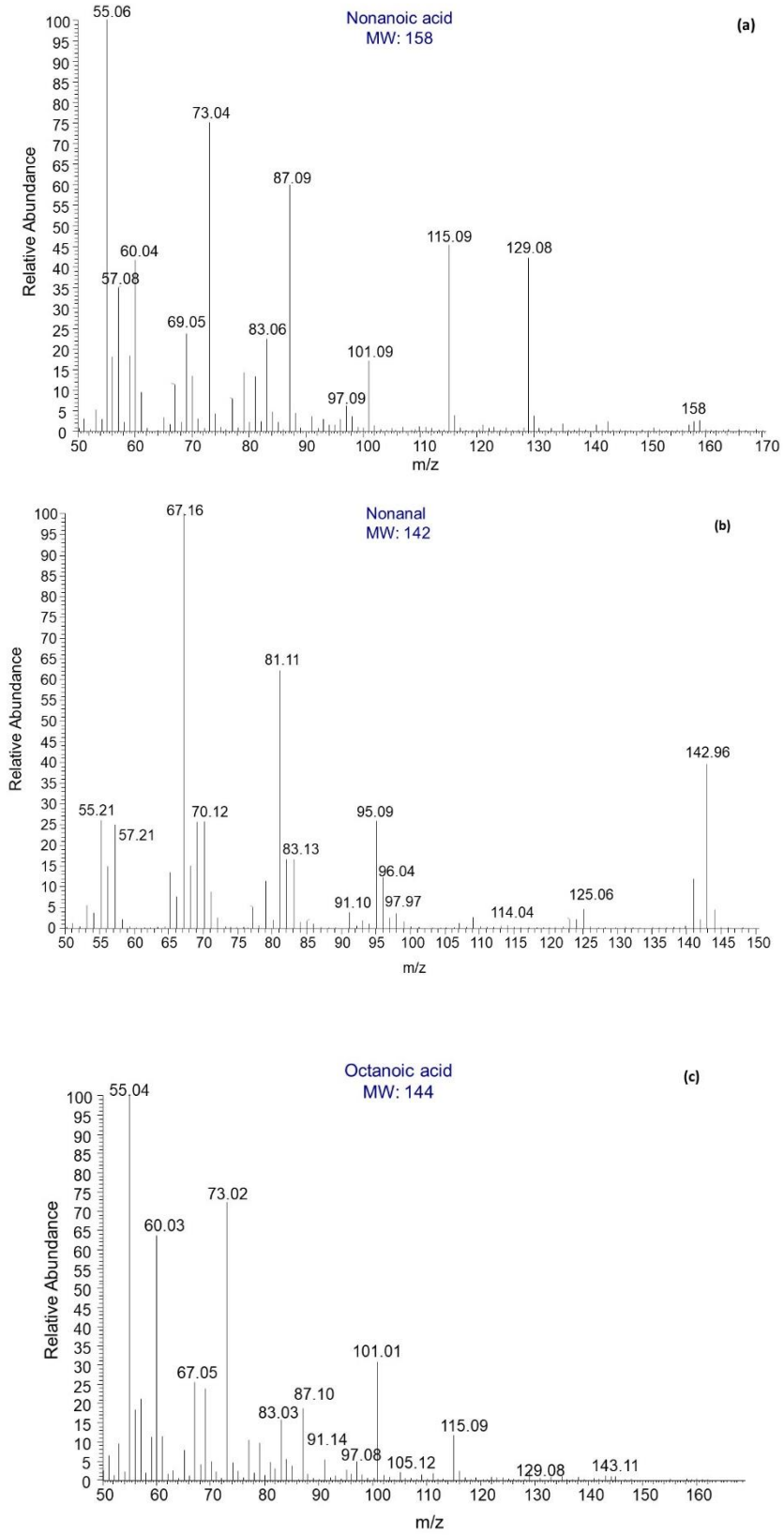

Figure 3.22 Mass spectra of a) nonanoic acid and b) nonanal and c) octanoic acid, obtained from the ozonolysis of oleic acid at 32 ppm and RH < 10%.

3.8.2 PALMITOLEIC ACID

According to Weitkamp et al. (2008), the ozonolysis of palmitoleic acid should produce azelaic acid. Spencer and Kleiman (1978) found two main products from the ozonolysis of palmitoleic acid: a seven-carbon aldehyde and nine-carbon aldehyde-ester, the former compound might correspond to heptanal, whereas the latter probably might be a derived from 9-oxononanoic acid.

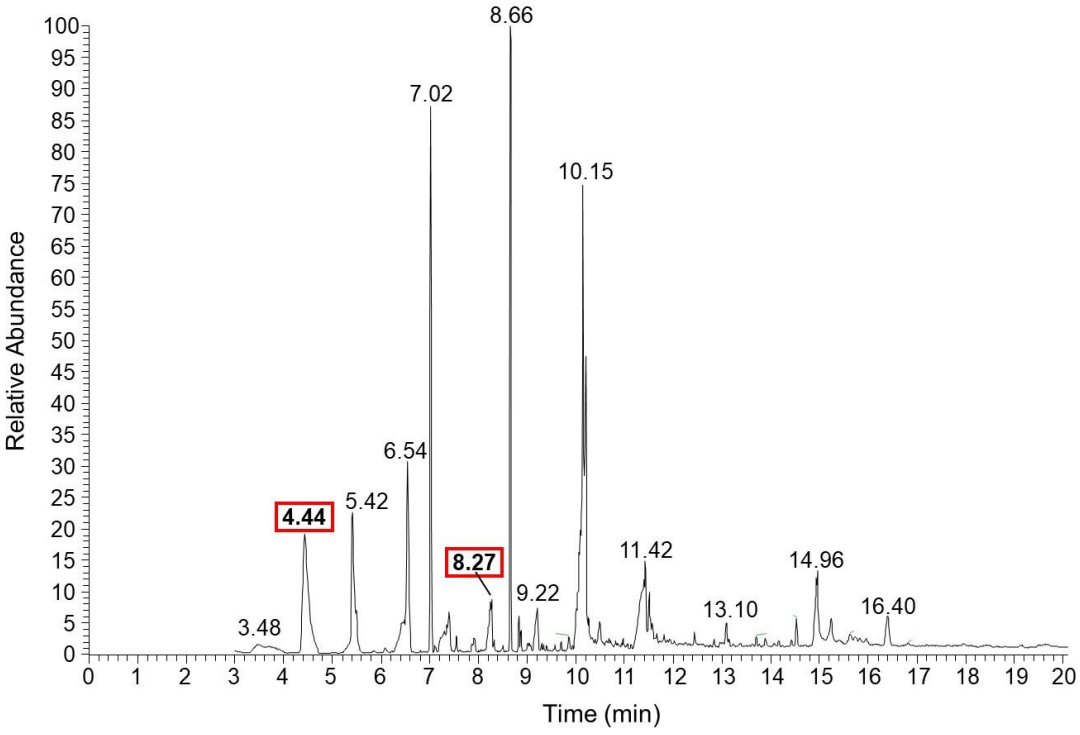

Figure 3.23 Chromatogram obtained from a levitated droplet of palmitoleic acid exposed to 32 ppm O_3 concentration and low RH (<10%). The retention times of identified products are highlighted in red: 4.44 and 8.27 corresponding to heptanal and nonanoic acid respectively.

The chromatogram obtained from the ozonolysis of palmitoleic acid at 32 ppm ozone concentration under dry conditions (< 10% RH) is shown in Figure 3.23. The retention times of two compounds are highlighted in red: 4.4 min assigned to heptanal and 8.27 min, apparently corresponding to nonanoic acid. Nonanoic acid is an expected product of the ozonolysis of OA. However the analysis of the mass spectra evidenced the presence of these two compounds after comparison of the MS obtained from this reaction to the MS reported by Rastogi (2015) for the same compound. The presence of that unexpected product might be explained by the isomerisation of the 9C Criegee intermediate (Ziemann, 2005; Hung and Ariya, 2007) formed when primary ozonide is decomposed into heptanal and ECI2 after PA underwent the cleavage shown in Figure 3.28 as "ac" (blue). The MS was also contrasted to the online spectral database (NIST Chemistry WebBook, NIST Standard Reference Database) confirming the formation of nonanoic acid as one of the products of this reaction. Figure 3.24 shows the mass spectra of nonanoic acid (a) and heptanal (b) obtained from the reaction of ozone with PA at 32 ppm and RH < 10. These compounds were also found in the mass spectra obtained from the reaction of ozonolysis at 32 ppm at high RH and 4 ppm at dry and humid conditions (RH < 10%). Moise and Rudich (2002) reported that azelaic and 9-oxononanoic acids were formed in condensed-phase; these two compounds are not easily volatilised and adsorbed into the SPME fibre. Therefore they were not identified by GC/MS. Evidence of high-molecular weight in the mass spectra confirmed the presence of peroxides, as shown in the Raman spectra reported in Figure 3.17.

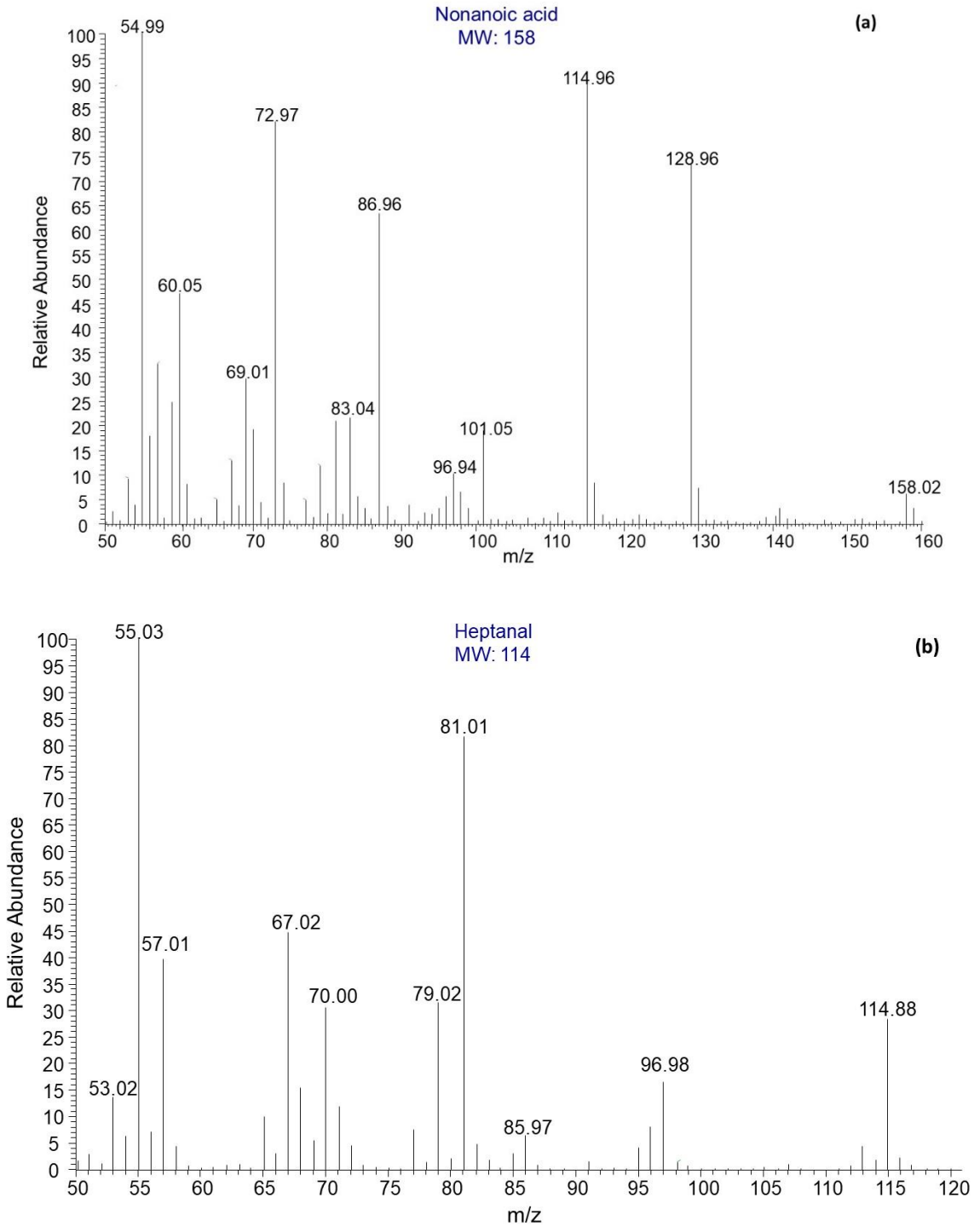

Figure 3.24 Mass spectra of a) nonanoic acid and b) heptanal, obtained from the reaction of ozone with PA at 32 ppm and RH < 10%.

3.8.3 LINOLEIC ACID

The ozonolysis of linoleic acid is expected to yield a variety of products, including saturated and unsaturated carboxylic acids and unsaturated aldehydes since this fatty acid has two carbon-carbon double bonds to react with ozone. Thus the unsaturated products might react with ozone to form more products, as stated by Zhou et al. (2014), who suggested a mechanism of reaction of 3-nonenal with ozone to form malondialdehyde and glyoxal at the air-water interface air/water at high humidity conditions. Moise and Rudich (2002) proposed the formation of 2-nonenal and 4-nonenal from isomerisation of 3-nonenal, and the formation of 1-hexenal, based on evidence from mass spectra of ozonolysis of linoleic acid, their pathway includes the formation of azelaic, 9-oxononanoic, 3-nonenoic and 3-dodecenedioic acids.

Figure 3.25 depicts the chromatogram obtained from the ozonolysis of linoleic acid exposed to 32 ppm O_3 concentration and low RH (<10%), the retention time of four products are highlighted in red: 3.56 min (hexanal), 5.71 min (hexanoic acid), 6.59 min ((*Z*)-non-3-enal) and 8.99 min ((*Z*)-non-3-enoic acid). These four compounds were identified by comparison of the mass spectra shown in Figure 3.26 to the spectral database (NIST Chemistry WebBook, NIST Standard Reference Database). They were present at the highest [O_3] and under dry conditions. However their presence was not evident in all cases, for example hexanal was also present at O_3 exposure of 4 ppm and low RH, whereas (*Z*)-non-3-enoic and (*Z*)-non-3-enal were not detected at 4 ppm [O_3] under high RH, and hexanoic acid was only detected when [O_3] was 40 and RH was <10%.

The expected products of the ozonolysis of linoleic acid are shown below in Figure 3.29 and Figure 3.30. These products are: a) saturated chain: hexanal, hexanoic acid, azelaic acid, and 9-oxononanoic acid; b) unsaturated chain: (*Z*)-non-3-enal (NA), (*Z*)-non-3-enoic acid (NEA), (9*Z*)-12-oxododec-9-enoic acid (ODDEA), and (*Z*)-dodec-3-enedioic acid (DDEA). Additional reactions might occur with ozone and the double bond of the unsaturated products mentioned in b) to form new products. Table 3.7 summarises the likely compounds from the second reaction of ozone with these unsaturated products and the sources of each product.

Table 3.7 Likely compounds formed from the second ozonolysis of unsaturated products during ozonolysis of linoleic acid.

Product name	**Source***	**MW**
Propanedioic acid	DDEA, NEA	104
9-oxononanoic acid	DDEA, ODDEA	172
3-oxopropanoic acid	DDEA, ODDEA, NA, NEA	88
Azelaic acid	DDEA, ODDEA	188
Malondialdehyde (MDA)	NA, ODDEA	72
Hexanal	NA, NEA	100
Hexanoic acid	NA, NEA	116

*Assigned abbreviations: (*Z*)-non-3-enal (NA), (*Z*)-non-3-enoic acid (NEA), (9*Z*)-12-oxododec-9-enoic acid (ODDEA), and (*Z*)-dodec-3-enedioic acid (DDEA).

These findings are in accordance with Zhou et al. (2014), who reported n-hexanal and 3-nonenal as main products of the reaction of ozone with LA monolayers, suggesting the possibility of decomposition of the primary ozonide to form these two compounds in the

gas phase. In humid conditions, some aldehydes and carboxylic acids formed are likely hydrophilic and tend to trap water molecules forming hydrogen bonds, then they stay in the condensed-phase, this may explain why they do not appear in the mass spectra of ozonolysis carried out at high RH. This might also be the case for azelaic and 9-oxononanoic acids; they are probably staying in the condensed phase, and therefore were not detected in the mass spectra obtained. Spectral evidence showed peaks of high molecular weight compounds, probably due to the formation of peroxides, ozonides and hydroperoxides, confirming the results of the Raman spectra shown in Figure 3.5.

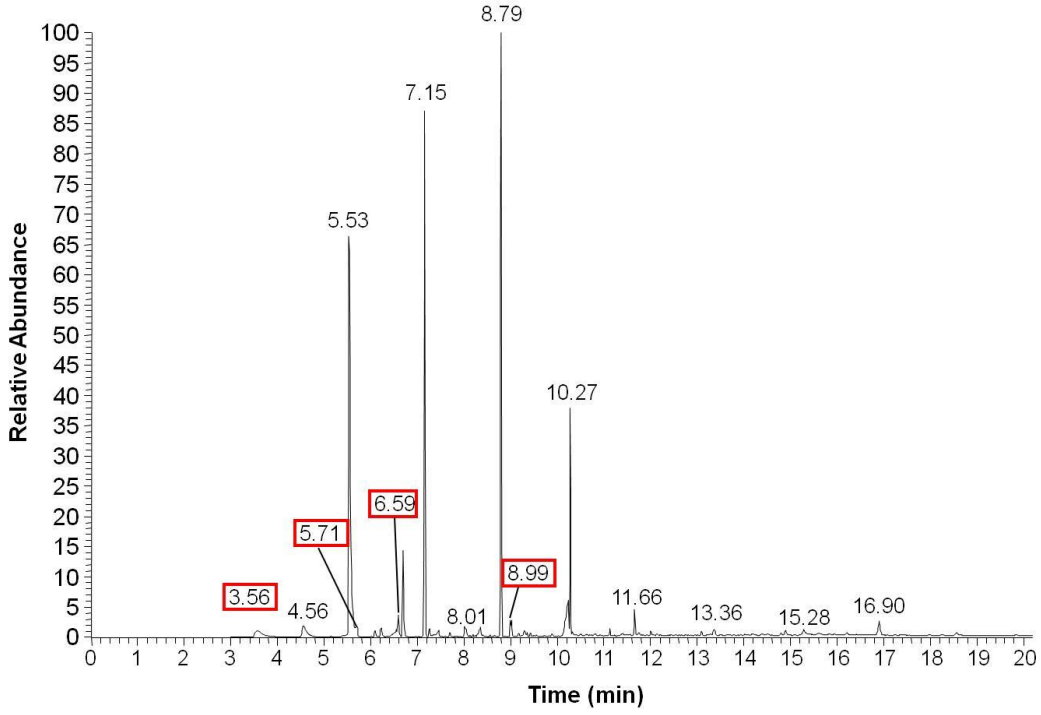

Figure 3.25 Chromatogram obtained from a levitated droplet of linoleic acid exposed to 32 ppm O_3 concentration and low RH (<10%). The retention times of identified products are highlighted in red: 3.56, 5.71, 6.59 and 8.99 corresponding to hexanal, hexanoic acid, *(Z)*-non-3-enal and non-3-enoic acid respectively.

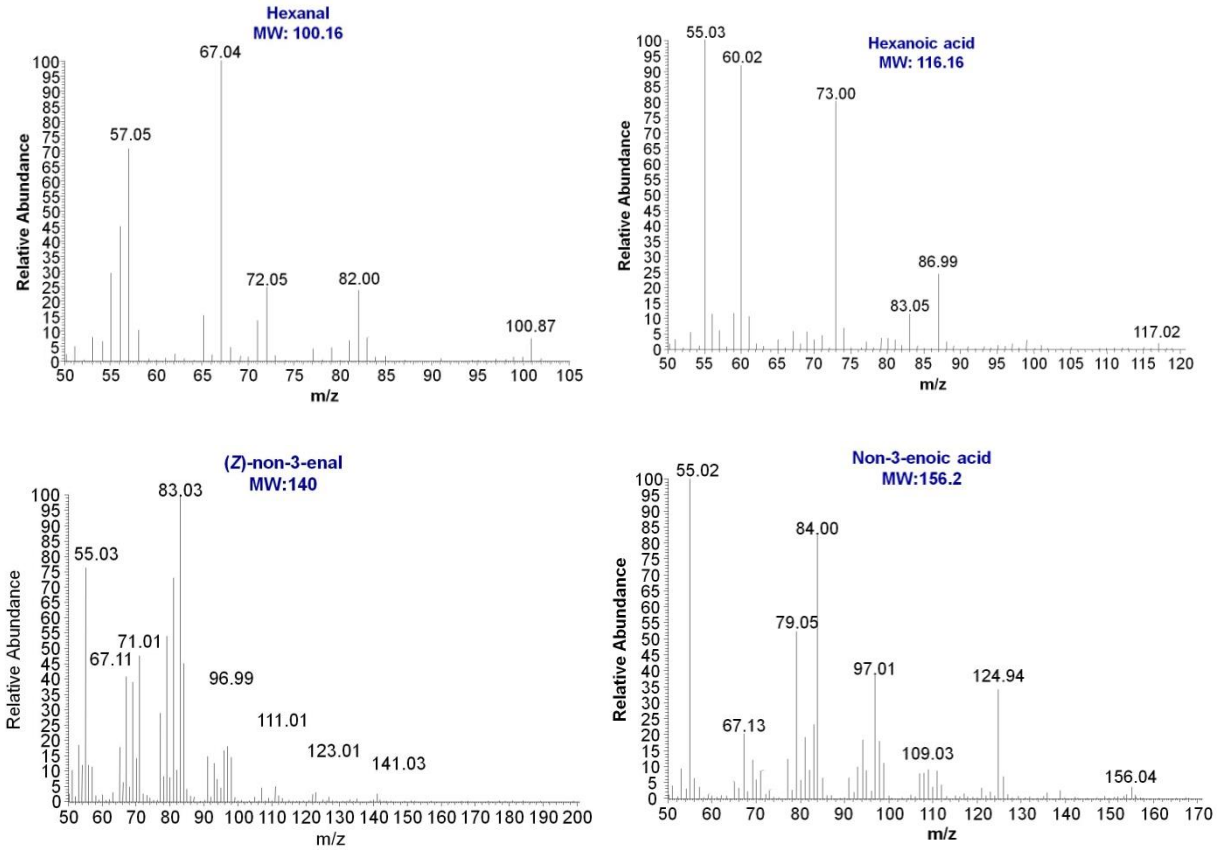

Figure 3.26 Mass spectra obtained from the ozonolysis of LA at 32 ppm O_3 concentrations and low RH (<10%).

3.9 DISCUSSION

3.9.1 RAMAN SPECTRA OF FATTY ACIDS

Raman spectra obtained from ozonolysis of OA and PA showed the decrease of the peak corresponding to carbon-carbon double bond. LA showed a different behaviour depending on the concentration of ozone. It was observed an increase of the Raman signature of C=C at low O_3 concentrations; this suggested the formation of compounds containing double bonds. This finding was consistent with the reported by Lee and Chan (2007a), who attributed the results to the autoxidation of linoleic acid at low O_3 concentrations, and it is believed that the reaction may follow an alternative mechanism with the formation of a diradical from the reaction of ozone with the double bond, as suggested by Lee and Chan (2007a) and Pryor (1994). It was also observed the formation of a small band at ≈1600 cm^{-1} during the ozonolysis of LA, confirming the presence of conjugated structures, such as dienes (Lee and Chan, 2007a). However, ozonolysis of LA at O_3 concentrations over 12 ppm also showed the reduction of the band attributed to C=C, and it was verified that this FA is more reactive that oleic acid due to the additional C=C, in agreement with the reported by Lee and Chan (2007a) and Hearn and Smith (2004).

3.9.2 REACTIVE UPTAKE COEFFICIENT

It was reported that reactive uptake of ozone might be affected by ozone concentration, particle size, RH and the number of double bonds (He et al., 2017). The results of uptake coefficient obtained in this study showed an evident dependence in size, but not constant tendencies at low and high RH. He et al. (2017) reported no RH dependence

for the reaction of ozone with OA, but an insignificant RH dependence for the ozonolysis of LA. It was also observed that the uptake coefficient tended to decrease over the time for oleic and palmitoleic acid, probably due to a reduction of active sites because of the reduction in size. On the contrary, the uptake coefficient of LA increased over the time, and this may be due to LA is polyunsaturated, with one extra reactive site to react with ozone. These results are in accordance with the reported by Moise and Rudich (2002) who observed that reactivity is related to the number of unsaturated bonds, this structural difference between OA and LA may lead to higher availability of the double bonds present on LA. Weitkamp reported 30% higher reactivity of PA compared to OA. In this study, PA showed a faster rate of decay when compared to OA. Although a higher uptake coefficient of O_3 was expected for the ozonolysis of PA when compared to OA, the calculated values were lower. However, the uptake coefficient indicates that more O_3 molecules have been adsorbed on the surface, which causes the saturation of the reactive sites; with this saturation, the reaction remains invariable until reactive sites are available (Zeng, 2013). From the evidence of this study and taking into account that ozone diffusion probably occurred either near or at the surface, structural effects of the reactants in addition to the surface area of the droplet of the fatty acids and increasing O_3 concentrations may affect the uptake coefficient of ozone on PA. Nevertheless, results from this study suggests that high uptake coefficient values will not guarantee faster reactions.

Tables 3.8 and 3.9 summarise the comparison of the γ values calculated in this study for OA and LA under dry and humid conditions to the ozone uptake coefficient reported in previous studies. Given the little information concerning to palmitoleic acid in the literature, the calculated values for this fatty acid were unable to be compared here.

Under dry conditions, two studies used very similar techniques or conditions, for example the ozone uptake coefficient obtained of the ozonolysis of a 120 μm droplet of oleic acid at 30 ppm [O_3] by Rastogi (2015) was appreciably higher than the reported here using the same method and technique and very similar [O_3] and particle size. The majority of previously reported studies show ozone uptake coefficient values in the order of 10^{-3} and 10^{-4}, which is considerably higher than the γ obtained in this study. Many factors may explain these differences, for example, the particles used in the majority of these studies were significantly smaller than the droplets used here, and also the high ozone concentrations applied in the experiments reported here probably caused lower uptake coefficient values. Likewise, the values of uptake coefficient obtained from ozonolysis of droplet of LA at 4 and 40 ppm ozone concentration and low RH were also lower than the γ reported by He et al (2017) and Zeng et al (2013), probably due to the different experimental conditions (droplet size and [O_3]).

Under humid conditions (see Table 3.9), the uptake coefficient calculated from experiments of ozonolysis of OA and LA were close to the values founded in the literature. For example in a study of the reaction of OA and O_3 conducted by Al-Kindi et al. (2016) using aerosol flow tube with smaller droplets and similar [O_3] and RH the uptake coefficients were similar to the values presented here. For the case of LA, the uptake coefficients calculated here were compared to the work by Zeng et al. (2013) and also Thornberry and Abbatt (2004), finding some discrepancies that may be attributed to the different experimental conditions used for these workers.

Table 3.8 Comparison to other studies of uptake coefficients from ozonolysis of OA and LA under dry conditions.

		This study	Rastogi (2015)	He et al (2017)	Zeng et al (2013)	Mendez et al (2014)
	Method and detection technique	**Acoustic levitation combined with Raman microscopy**	**Acoustic levitation combined with Raman microscopy**	**Gas-flow system combined with micro-FTIR**	**Flow reactor coupled to ATR- FTIR(1)**	**Aerosol flow tube**
Oleic acid	Particle diameter (μm)	Two droplets. Particle diameter: 125	120	50-200	N/A	0.15
	$[O_3]$ (molecules/cm^3)	2.96 x 10^{14} and 7.78 x 10^{14}	7.88 x 10^{14}	Increases from 1,25 x 10^{14} to 1.00 x10^{15}		6.16 x 10^{11}- 2.71 x 10^{13}
	Temperature (K)	298	» 298	298		295 (± 2)
	Uptake coefficient	(6.14±1.28) x 10^{-5} and (4.23±1.28) x 10^{-5}	2.52 x 10^{-4}	Decreases from 2.06 x 10^{-3} to 1.32 x 10^{-3}		(1.0 ± 0.2) x 10^{-3}
	Identified Products	Nonanal, nonanoic acid	Nonanal, nonanoic acid, 9-oxononanoic acid, azelaic acid, octanoic acid	N/A		Nonanoic acid, azelaic acid, 9-oxononanoic acid
Linoleic acid	Particle diameter (μm)	Two droplets. Particle diameter: 155 and 150	N/A	50-200	Film thickness = 0.2	N/A
	$[O_3]$ (molecules/cm^3)	9.85 x 10^{13} and 9.85 x 10^{14}		Increases from 1,25 x 10^{14} to 1.00 x10^{15}	Increase from 6.16 x 10^{12} to 8.62 x 10^{12}	
	Temperature (K)	298		298	293	
	Uptake coefficient	9.0 x 10^{-5} and 2.3 x 10^{-5}		Increases from 2.18 x 10^{-3} to 1.47 x 10^{-3}	(5.08 ± 0.44) x 10^{-4} to (3.48 ± 0.18) x 10^{-4}	
	Identified Products	Hexanal, hexanoic acid, non-3- enoic acid, (Z)-non-3-enal		N/A	N/A	

(1) Attenuated total reflection FT infrared spectroscopy.

Table 3.8 (Continued). Comparison to other studies of uptake coefficients from ozonolysis of OA and LA under dry conditions.

		Hung and Tang (2010)	Nash et al. (2006)	Hearn and Smith (2004)	Morris et al. (2004)	Thornberry and Abbatt (2004)
	Method and detection technique	**ATR-FTIR**	**Flow tube reactor coupled to Single-particle MS**	**Aerosol flow tube coupled to aerosol CIMS(2)**	**Aerosol flow tube**	**Coated-wall flow tube coupled to CIMS**
Oleic acid	Particle diameter (μm)	≈ 10	2	0.8 (average)	0.2-.06	Not specified
	$[O_3]$ (molecules/cm^3)	1.11×10^{13}	5.9×10^{14}	$(2\text{-}3) \times 10^{15}$	2.46×10^{15}	9.85×10^{15}
	Temperature (K)	25	Not specified	Not specified	Not specified	298
	Uptake coefficient	$3.43 \pm 11.4 \times 10^{-4}$	$3.4 (\pm 0.3) \times 10^{-4}$	$(7.5 \pm 1.2) \times 10^{-4}$	$(1.6 \pm 0.2) \times 10^{-3}$	$(8.01 \pm 0.3) \times 10^{-4}$
	Identified Products	N/A	N/A	Nonanal, 9-oxononanoic acid, nonanoic acid, azelaic acid	N/A	Nonanal
Linoleic acid	Particle diameter (μm)	N/A	N/A	0.8 (average)	N/A	Not specified
	$[O_3]$ (molecules/cm^3)			$(2\text{-}3) \times 10^{15}$		9.85×10^{15}
	Temperature (K)			Not specified		298
	Uptake coefficient			$(1.1 \pm 0.2) \times 10^{-5}$		$(1.33 \pm 0.3) \times 10^{-3}$
	Identified Products			Hexanal, hexanoic acid, nonenal, 9-oxononanic acid, azelaic acid		Nonenal, hexanal

(2) Chemical ionization mass spectrometry.

Table 3.8 (Continued). Comparison to other studies of uptake coefficients from ozonolysis of OA and LA under dry conditions.

		Moise and Rudich (2002)	**Smith et al. (2002)**
	Method and detection technique	**Cylindrical rotating wall flow reactor coupled to MS**	**Aerosol flow tube coupled to a Single - particle MS**
Oleic acid	Particle diameter (μm)	Not specified	0.68-2.45
	$[O_3]$ (molecules/cm^3)	8×10^9 - 2×10^{11}	1.48×10^{14} - 2.46×10^{15}
	Temperature (K)	286-291	Not specified
	Uptake coefficient	$(8.3 \pm 0.2) \times 10^{-4}$	$5.8\text{-}9.8 \times 10^{-3}$
	Identified Products	Azelaic acid	Nonanoic acid, 9-oxononanoic acid
Linoleic acid	Particle diameter (μm)	Not specified	N/A
	$[O_3]$ (molecules/cm^3)	8×10^9 - 2×10^{11}	
	Temperature (K)	274-265	
	Uptake coefficient	$(1.2 \pm 0.2) \times 10^{-3}$	
	Identified Products	2-nonenal, 4-nonenal, hexanal	

Table 3.9 Comparison to other studies of uptake coefficients from ozonolysis of OA and LA under humid conditions.

		This study	Al-Kindi et al (2016)	Zeng et al (2013)	Vesna et al (2009)	Thornberry and Abbatt (2004)
	Method and detection technique	**Acoustic levitation combined with Raman microscopy**	**Aerosol flow tube coupled to SMPS(1) and ATOFMS(2)**	**Flow reactor coupled to ATR- FTIR(3)**	**Aerosol flow reactor combined with GC-MS**	**Coated-wall flow tube coupled to CIMS(4)**
Oleic acid	Particle diameter (μm)	Two droplets. 130	0.015-0.667	N/A	Geometric mean diameter = 7.8×10^{-2}	N/A
	$[O_3]$ (molecules/cm^3)	2.96×10^{13} and 7.88×10^{14}	4.93×10^{14}		1.23×10^{13}	
	Temperature (K)	298	298		298	
	RH%	50 - 70	65.0 ± 0.2		65	
	Uptake coefficient	1.1×10^{-4} and 2.2×10^{-5}	$2.40 \pm 0.3 \times 10^{-4}$		» 10^{-4}	
	Identified Products	N/A	9-oxononanoic acid, nonanal, nonanoic acid, azelaic acid		Nonanal, nonanoic acid, 9-oxononanoic acid, azelaic acid	
Linoleic acid	Particle diameter (μm)	Two droplets. 70	N/A	Film thickness = 0.2	N/A	Not specified
	$[O_3]$ (molecules/cm^3)	9.85×10^{13} and 7.88×10^{14}		6.16×10^{12}		9.85×10^{15}
	Temperature (K)	298		293		263
	RH%	57 - 75		From 0 to 55		55
	Uptake coefficient	3.4×10^{-4} and 4.8×10^{-5}		$(5.08 \pm 0.44) \times 10^{-4}$ - $(9.52 \pm 1.21) \times 10^{-4}$		$(1.20 \pm 0.06) \times 10^{-3}$
	Identified Products	N/A		N/A		Nonenal, hexanal

(1) Scanning mobility particle sizer. (2) Aerosol time-of-flight mass spectrometer. (3) Attenuated total reflection FT infrared spectroscopy. (4) Chemical ionization mass spectrometry.

3.9.3 PRODUCTS OF THE OZONOLYSIS OF FATTY ACIDS

It is known that the reaction of ozone with olefins generates oxygen-containing compounds, such as aldehydes and ketones (Wade, 2013) but also peroxides (Criegee, 1975). In the case of fatty acids, it is expected that carbonyl compounds and carboxylic acids will be formed. Pryor et al. (1995) stated that the presence of water leads to form two moles of aldehyde and one mole of hydrogen peroxide.

From ozonolysis of OA, C9 aldehydes and C9 carboxylic acids, such as nonanal, azelaic acid, nonanoic acid and 9-oxononanoic acid are the main expected products; but this reaction can also yield more products from secondary reactions. Hung et al., (2005) proposed a mechanism of formation of octanoic acid, CO_2 and azelaic acid from the isomerization of one of the Criegee intermediates, this reaction is shown in the Figure 3.27. Ziemann (2005) and Lee and Chan (2007b) stated that the ozonolysis of OA also produces peroxidic products and Vesna (2009) suggested a mechanism of ozonolysis of OA at high RH, with the formation of hydroperoxides, peroxides and polymeric products. Although products were not quantified, the mass spectra provided the evidence to confirm the bands appearing in the Raman spectra, corresponding to carbonyl compounds, peroxides and the cleavage of the double bond to form these products. Mass spectra of the products of the ozonolysis of OA showed the presence of nonanoic acid and nonanal. There was no evidence of azelaic and 9-oxononanoic acid, as they probably are present in the condensed-phase. The formation of high molecular weight compounds such as peroxides was also confirmed under dry and humid conditions, being AAHP identified in the MS. These results are in agreement with the reported in the previous studies and demonstrated that the products of ozonolysis of OA were mainly aldehydes and peroxides.

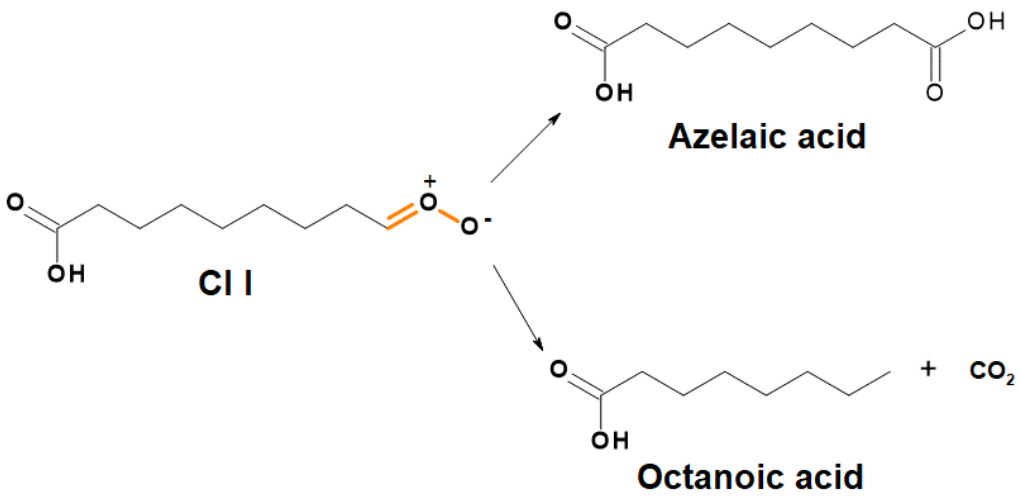

Fig. 3.27 Proposed mechanism of conversion of the Criegee intermediate I into azelaic and octanoic acids by isomerisation (from the mechanism shown in Fig. 1.6).

Similarly, the ozonolysis of PA has been reported to yield C7 and C9 carbonyl compounds and carboxylic acids, such as heptanal and azelaic acid (Spencer and Kleiman, 1978; Weitkamp et al., 2008). However, to the best of author's knowledge, the mechanism of ozonolysis of PA via Criegee intermediate has not been reported yet. It is known that this carboxylic acid reacts with ozone to form carboxylic acids and aldehydes following a Criegee intermediate mechanism, the mechanism shown in Figure 3.28 is proposed to explain the reaction of ozonolysis, based on Criegee (1975), obtaining products such as heptanoic acid, heptanal, and also azelaic and 9-oxononanoic acid, and also products of secondary reactions, such as the isomerisation of the Criegge intermediate ECI 2 to form nonanoic acid (Ziemann, 2005;, Hung and Ariya, 2009). The MS obtained from ozonolysis of PA showed the presence of heptanal and nonanoic acid, also it is presumed that high molecular weight compounds should be formed from

the ozonolysis of palmitoleic acid, similar to the products obtained from ozonolysis of OA, but they were not included in the mechanism shown in Figure 3.28. Thus, the MS confirmed two of the expected products and the results showed in the Raman spectra of ozonolysis of PA that contained characteristic bands of carbonyls and peroxides.

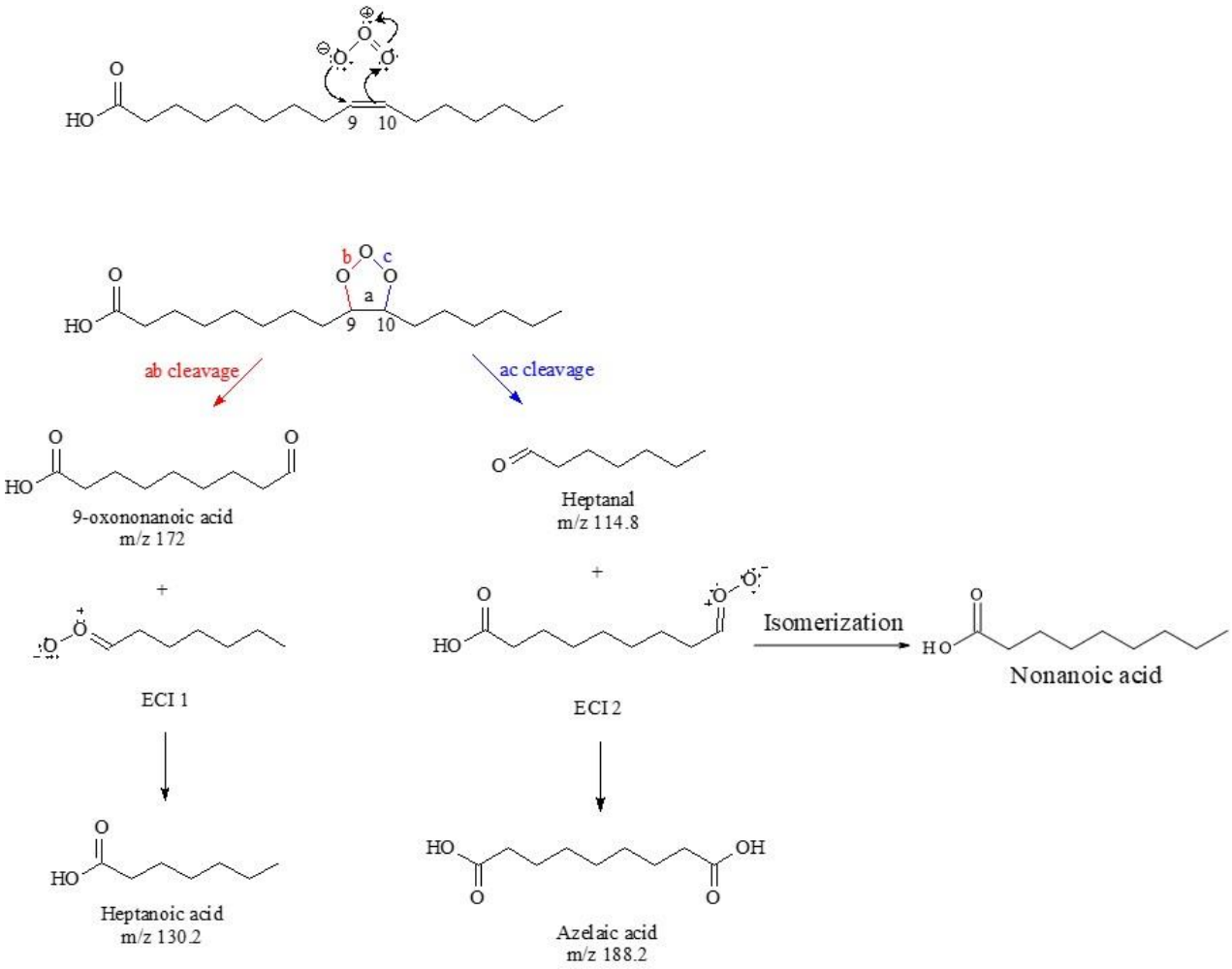

Figure 3.28 Proposed mechanisms of ozonolysis of PA, based on Criegee (1975), Hung & Ariya (2007) and Ziemann (2005)

LA has been reported to produce C9 and C6 aldehydes, C9 and C6 carboxylic acids, peroxides, hydroperoxides, but unlike OA and PA, the products may contain C=C, and this generates C9, C6 and C3 oxygen-containing secondary products (Moise and Rudich, 2002; Zhou et al., 2014). Lee and Chan reported the formation of conjugated dienes and peroxidic products of autoxidation. Raman spectra obtained from ozonolysis of LA showed carbonyls, conjugated dienes, and peroxidic compounds were possibly formed during the reaction. Mass spectra obtained from the ozonolysis of LA confirmed some of the expected products: hexanal, hexanoic acid, *(Z)*-non-3-enal and *(Z)*-non-3-enoic acid were formed. The presence of high molecular weight products such as peroxidic compounds was confirmed by MS (m/z = 355).

Following the mechanism stated by Criegee (1975) for ozonolysis of an unsaturated compound, the reaction of ozone with LA may form the products proposed in the schemes of Figures 3.29 and Figure 3.30. The former corresponds to the reaction between O_3 and the C_{12}-C_{13} double bond, whereas the latter illustrates the cleavage of the C_9-C_{10} double bond.

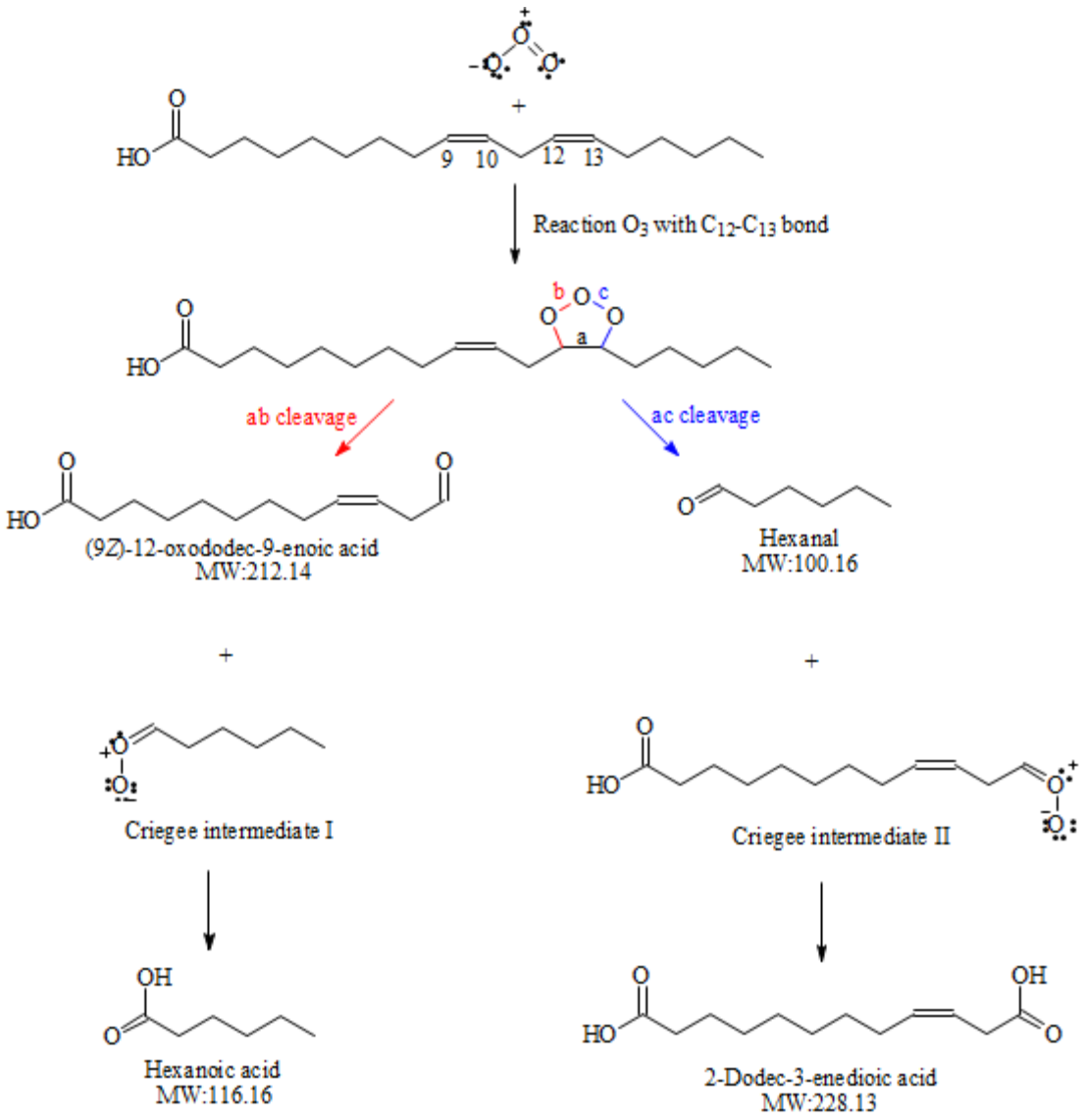

Figure 3.29 Proposed mechanism of reaction of ozone with the C_{12}-C_{13} double bond of linoleic acid, based on Criegee (1975).

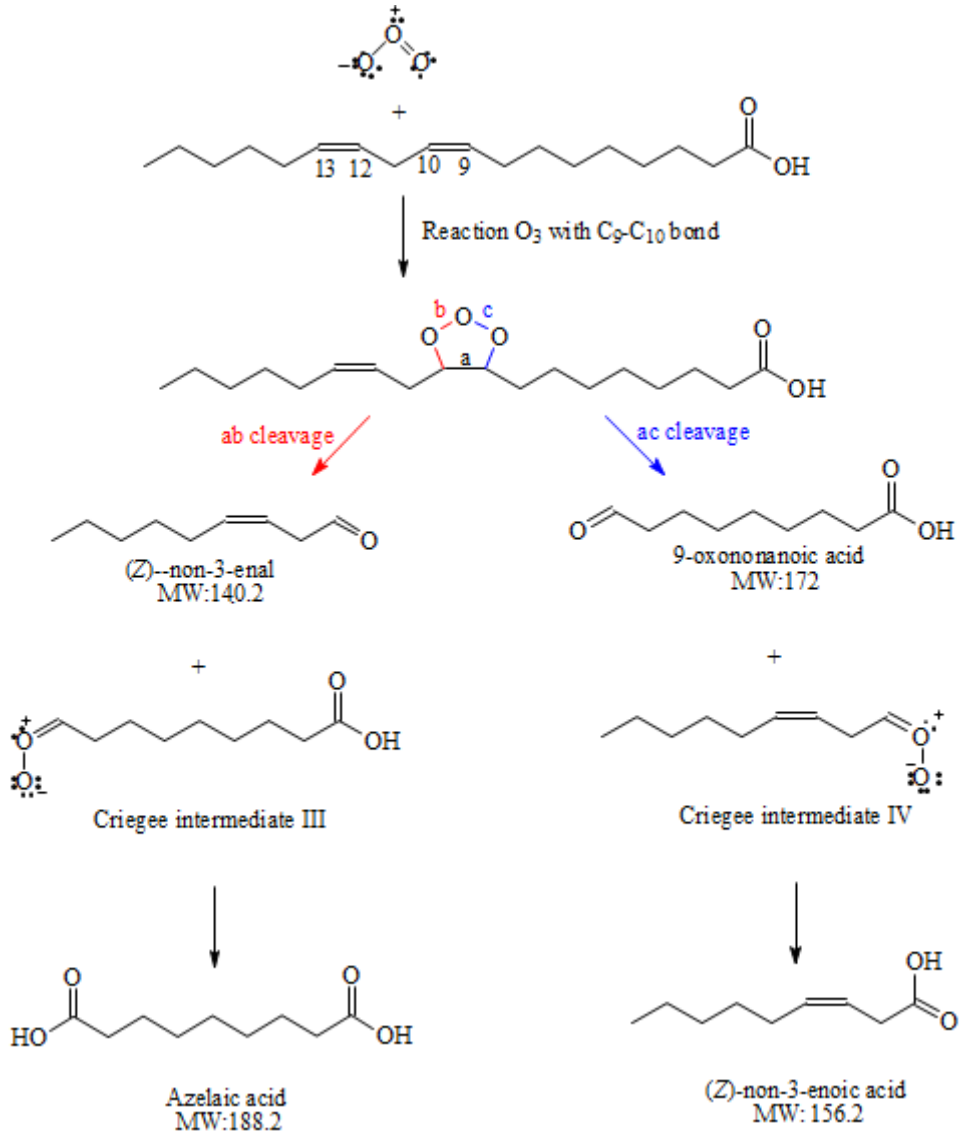

Figure 3.30 Proposed mechanism of reaction of ozone with the C_9-C_{10} double bond of linoleic acid, based on Criegee (1975).

CHAPTER 4

OZONOLYSIS OF SELF ASSEMBLED MIXTURES OF FATTY ACIDS

Surfactants (surface active agent) are amphiphilic molecules that usually consist of two differentiated parts, a polar head group which is joined to a non-polar chain (Tiddy, 1980). It has been estimated that at least 10% of the organic fraction of atmospheric aerosols is composed of surfactants (Nájera, 2007; Latif and Brimblecombe, 2004). The impact of these surfactants on the physical and chemical properties of atmospheric aerosols is still poorly understood. They can act in several ways for instance, at the air/liquid interface as surface films of atmospheric particles and form organic aggregates in aqueous solution. Thus they affect the absorption properties of water and gases among other effects (Nájera, 2007). The formation of organic films at the surface can influence the mass transfer of water through the droplet surface as well as the gas-phase content and the properties of bulk solution and therefore the chemical behaviour (Davies et al., 2012).

Previous studies have reported the hygroscopic growth of atmospheric aerosols by using Raman microscopy to assess the effect of absorption or loss of water content in size, changes of phase, morphology, products of reaction, and reactivity of levitated droplets, as Raman spectroscopy is a very sensitive technique to identify phase changes and molecular interactions in levitated droplets (Lee et al., 2008). Sodium oleate (SO) is the salt of oleic acid, these two compounds are commonly selected as proxies in atmospheric studies, given their ubiquity and atmospheric relevance (Nájera, 2007).

This Chapter will present the results of the reaction of ozone with droplets of self-assembled mixtures containing fatty acid (either oleic or palmitoleic acid), sodium oleate and NaCl solution that were prepared as described in Section 2.4.7 as proxy for atmospheric aerosols.

4.1 RAMAN SPECTRA OF MIXTURES OF FATTY ACIDS

The mixture droplet exists in self-assembled planes (Pfrang et al., 2017), a lamellar system that is highly viscous (see Figure 4.1). In these conditions, it is crucial to maintaining high humid conditions, in order to ensure the adequate humidity and avoid the water evaporation and therefore the solidification of the droplet (Seddon et al., 2016). Thus, in most of the experiments carried out in this study, RH was kept over 50%. Sodium oleate is known to exhibit micellization and coagelization at critical temperatures, and Raman spectra can detect these phase transitions (Wong and Mantsch, 1983). Figure 4.2, 4.3 and 4.4 show the Raman spectra obtained from the reaction of O_3 with droplets of a mixture of oleic acid with SO and NaCl at ozone concentration of 32, 20 and 4 ppm respectively. It is known that Raman spectroscopy is highly sensitive to the intramolecular forces, such as hydrogen bonds, helping to elucidate the multiple interactions of water with ions and molecules in the aerosol particle (Lee et al. 2008, Carey and Korenowski, 1998). Therefore, the high intensity bands corresponding to OH stretching vibration, located at ≈ 3450 cm^{-1} in Figure 4.2 and 4.3 are present due to the effect of high RH (in this case, >75%) in the deliquescence of the droplet of mixture, as water can have different types of intramolecular interactions (ion-dipole forces and hydrogen bonds) with NaCl and with other water molecules and ions present in the dissolution (Carey and Korenowski, 1998,

Sun 2012).

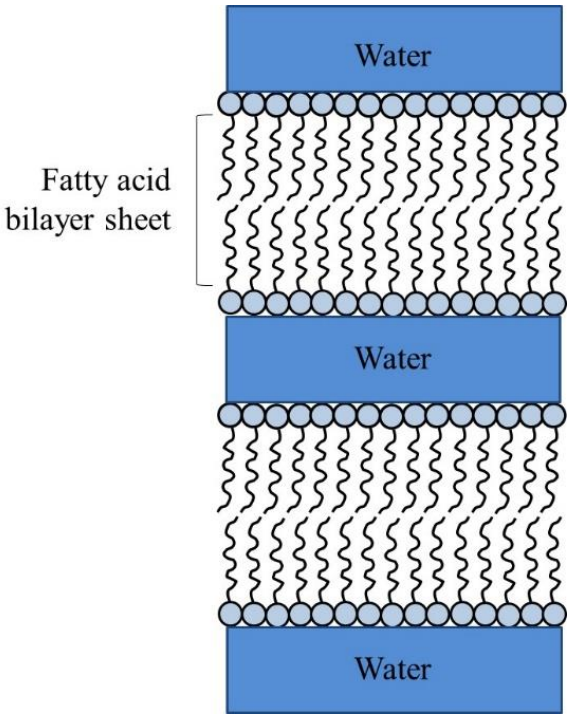

Figure 4.1 Model of the self-assembled layers. Bilayers of fatty acids are stacked forming a lamellar phase with the polar heads of FA attaching the water.

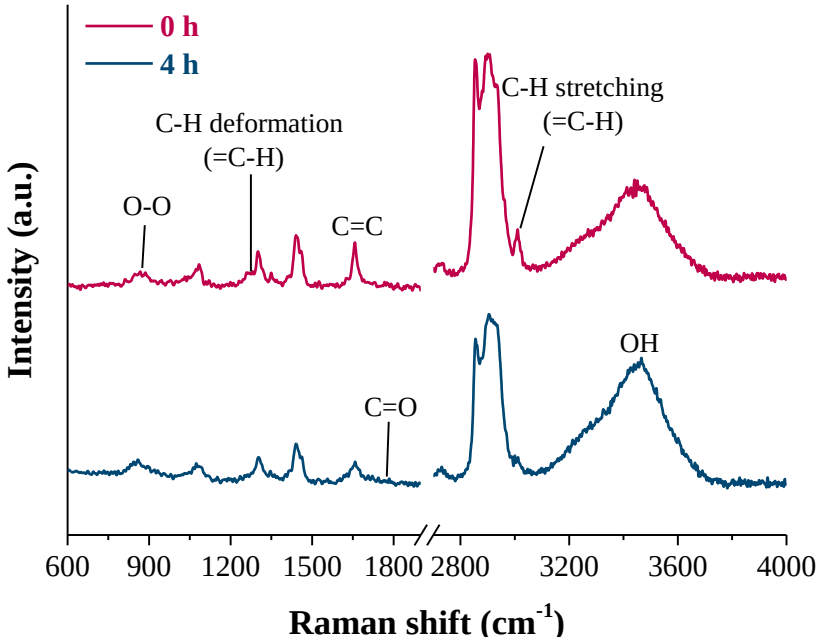

Figure 4.2 Raman spectra obtained from the reaction of O_3 with a mixture droplet of oleic acid, SO and NaCl 32 ppm O_3 (d = 125 μm) and a RH between 80 and 86%.

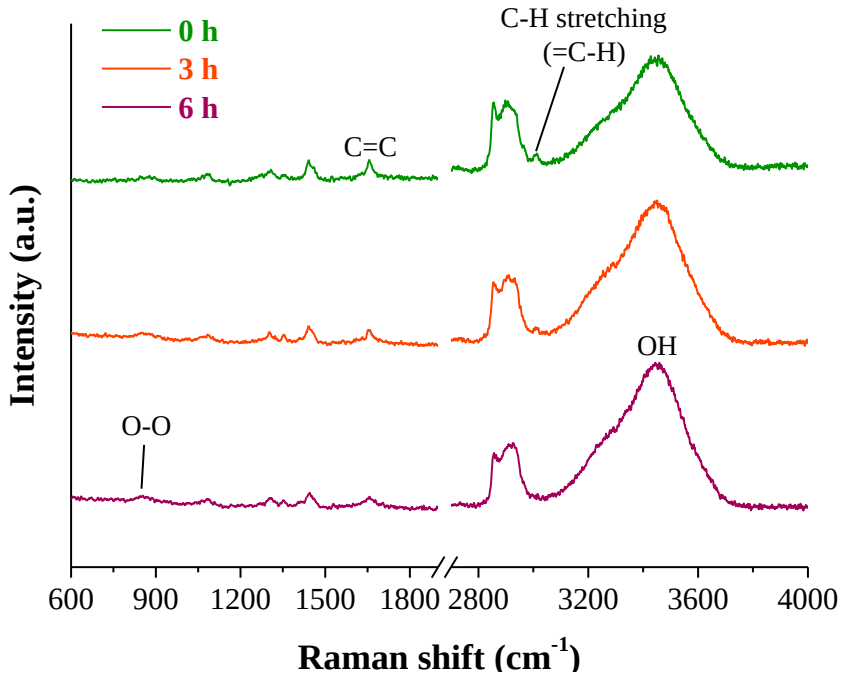

Figure 4.3 Raman spectra for the reaction of a mixture droplet of oleic acid, SO and NaCl (d = 255 μm) with O_3 at a concentration of 20 ppm and RH in the range of 76 to 80%.

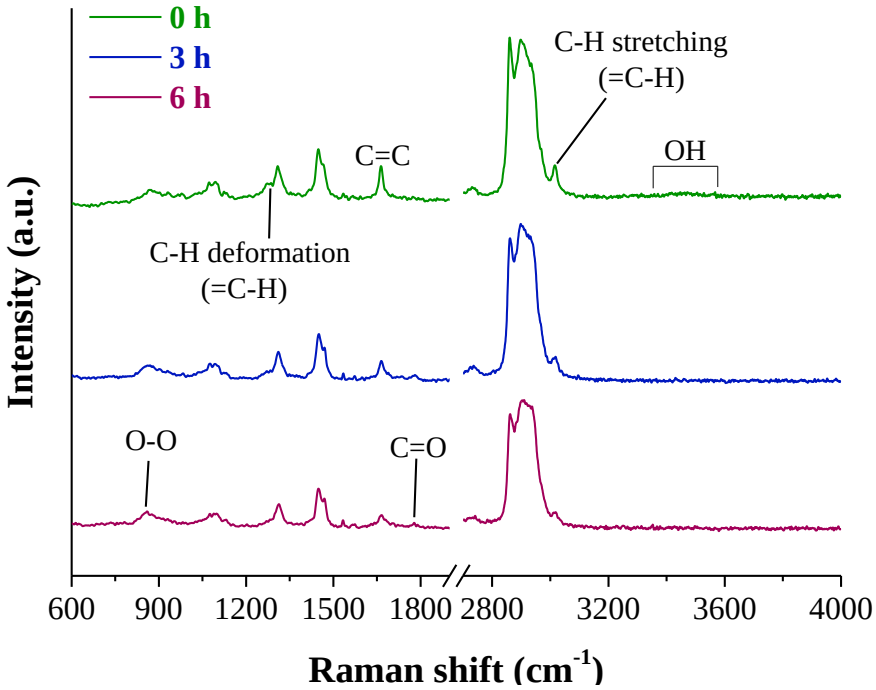

Figure 4.4 Raman spectra obtained from the reaction of a levitated mixture droplet of oleic acid, SO and NaCl (d = 130 μm) with O_3 at 4 ppm and RH around 50 %.

The pictures in Figure 4.5 show the levitated droplets in the experiments of ozonolysis of droplets of mixture carried out at (a) 32 and (b) 4 ppm ozone concentration. Once the droplets were levitated they tended to shrink and change the size, as a consequence of the reduction in water content, in some cases the appearance of the droplet indicated that it was not solidified, as seen in Figure 4.5 (a) when the relative humidity remained at high values. Additionally, changes in size were observed during the reaction. These observations confirm the Raman band at ≈ 3450 cm^{-1} shown in Figure 4.2, corresponding to the different stretching OH vibrations of water (Sun, 2009). Also, the presence of NaCl intensifies the band at 3450 cm^{-1}, this may be due to the concentration of salt increased with the evaporation of water. At moderate values of RH (≈ 50%), the droplets tended to lose a significant mass of water, and then they undergo phase transformations, before the ozone exposure started, as can be seen in Figure 4.5 (b). In this case the O_3 exposure concentration was 4 ppm, and changes in size during the reaction were not observed. The Raman spectra in Figure 4.4 showed the low content of water, with absence of the characteristic high-intensity band at ≈ 3450 cm^{-1} in the spectra taken after 3 and 6 hours of ozone exposure, only the spectrum taken before starting the reaction showed a very small band in that region, confirming the visual appearance of a liquid at these three different times. Despite the evident reduced water content, it was observed that the reaction of oleic acid with ozone (4 ppm) proceeded and products such as aldehydes, and peroxides were formed while the characteristic bands of C=C at 3080, 1663 and 1272 cm^{-1} were reduced. Same observations in the intensity of bands in Raman spectra obtained at 20 and 32 ppm [O_3] indicate that ozonolysis of OA also occurred.

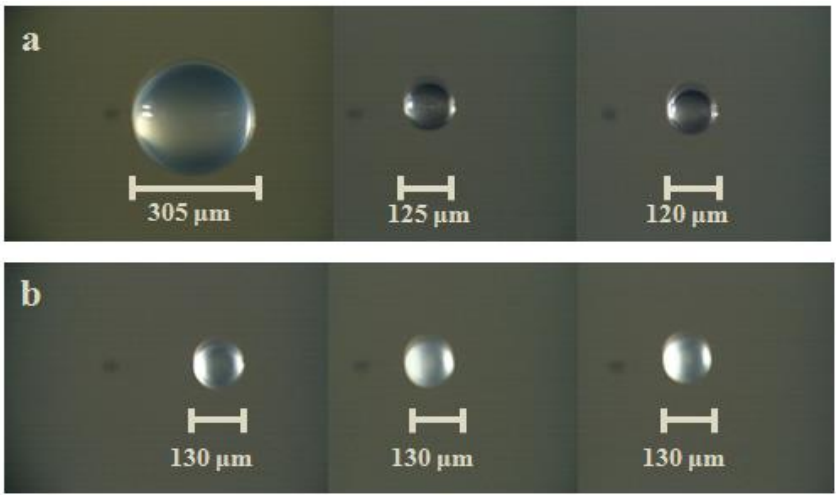

Figure 4.5 Levitated droplets of the mixture OA-SO-NaCl reacting at (a) 32 ppm [O_3], and (b) 4 ppm [O_3]. In the upper photo row (a), the first picture shows the droplet few seconds after levitation, and then its size was rapidly reduced. The lower photo row (b) shows the that the droplet was remarkably reduced in size after levitation to some extent that first photo was not captured, this droplet had significant loss of water content and showing visually observable phase change.

The Raman spectra in Figures 4.6 and 4.7 correspond to reactions of O_3 with droplets of a mixture of PA-SO and NaCl at 32 ppm and 4 ppm ozone concentration respectively. These spectra show the loss of water content of droplets; however, the pictures taken few seconds after levitation reveal that phase transformation was not observed in the case of the droplet reacting at 4 ppm. On the contrary, the droplet exposed to 32 ppm [O_3] tended to become highly viscous, but probably during the reaction the hydrophilic compounds formed retained water molecules, then the deliquescence of this droplet was recovered, evidence of this is shown in the spectra in Figure 4.6 with an emerging band at 3450 cm^{-1} corresponding to the stretching vibrations of water. As can be seen in the spectra in Figure 4.6, reactions of ozone with C=C present in the molecules of palmitoleic acid took place, as the intensity of peaks at 3080, 1663 and 1272 cm^{-1} was

reduced, and the characteristic peak of aldehydes at 1750 cm^{-1} slightly emerged. It worth mentioning that water also shows bands at 1645 cm^{-1}, corresponding to OH bending, this may explain the broadening at the bottom of the band, which caused some difficulties during the deconvolution of the peak corresponding to C=C that is overlapped with OH bending band. The spectra in Figure 4.7 show that some water was retained into the core of the droplet, and the reaction proceeded at a very slow rate.

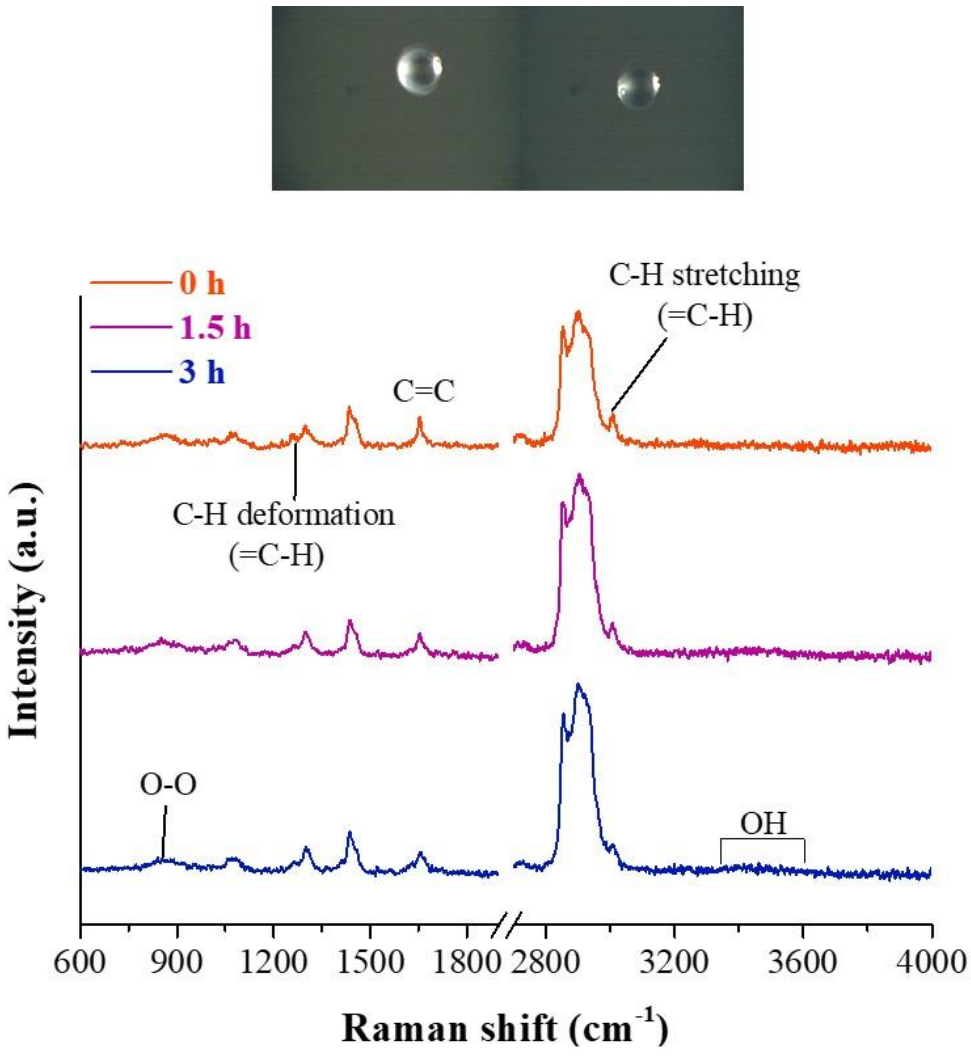

Figure 4.6 Raman spectra obtained from the reaction of levitated droplets (d=140 μm). of a mixture of palmitoleic acid, SO and NaCl with ozone at 32 ppm and humid conditions (RH 63-71%)

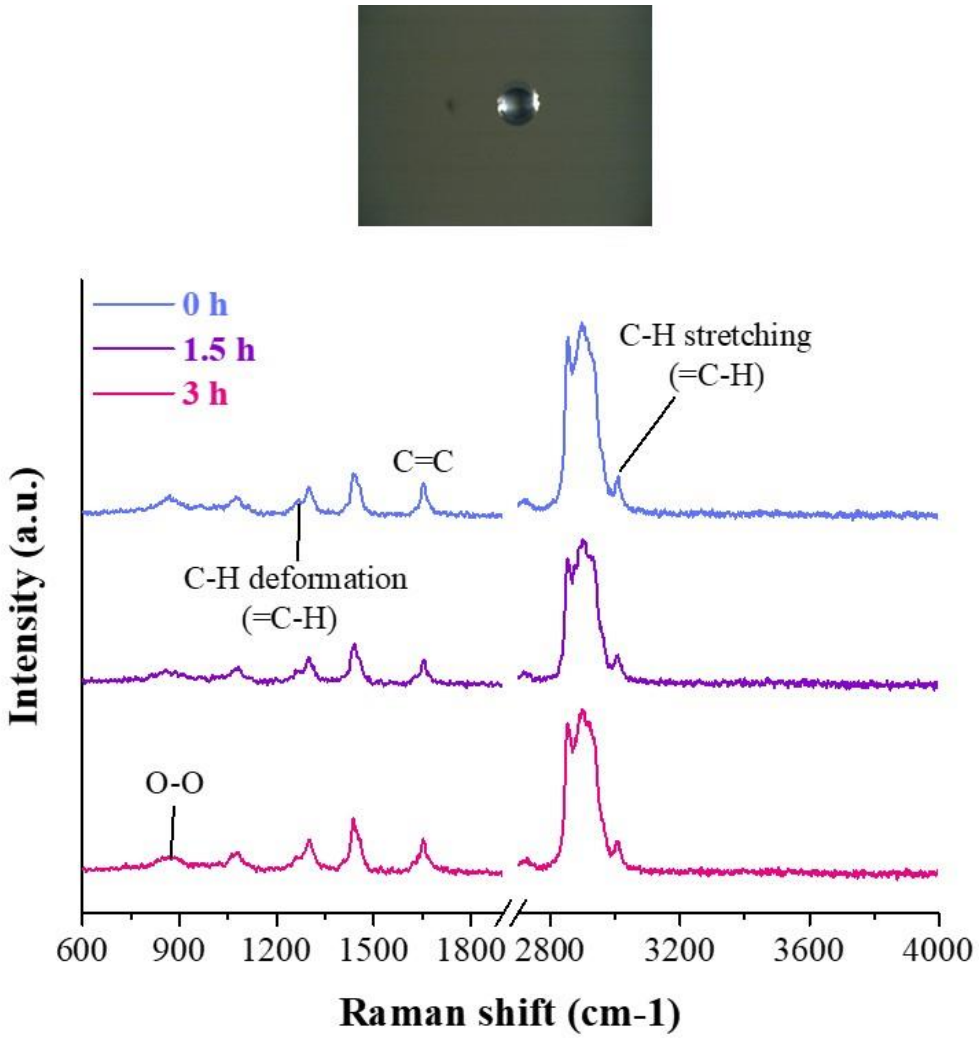

Figure 4.7 Raman spectra obtained from the reaction of levitated droplets (d=115 μm). of a mixture of palmitoleic acid, SO and NaCl with ozone at 4 ppm and humid conditions (RH 65-67%)

4.2 REACTIVITY OF MIXTURES OF FATTY ACIDS.

The chemical reactivity of the self-assembled mixtures of oleic and palmitoleic acid is compared to the reactivity of the pure fatty acids. The diameter of levitated droplets of oleic acid and its mixture was 125 μm, while the diameter of droplets of palmitoleic acid and its mixture was 140 μm. The decay of the ratio of Gaussian area of $C=C/CH_2$ peaks for oleic acid, and mixture OA-SO-NaCl is shown in Figure 4.8 (a), whereas Figure 4.8 (b) corresponds to the decay for palmitoleic acid and the mixture PA-SO-NaCl.

Pure fatty acids showed a faster decay of C=C band, whereas this band showed slower decay in the spectra of self-assembled mixtures. Slopes obtained from plots indicate that pure OA reactivity is 11 times higher compared to the corresponding mixture, whereas pure PA is eight times more reactive than its mixture. These results suggest that self-assembly occurring in these mixtures diminishes the rate of reaction of ozonolysis of fatty acids.

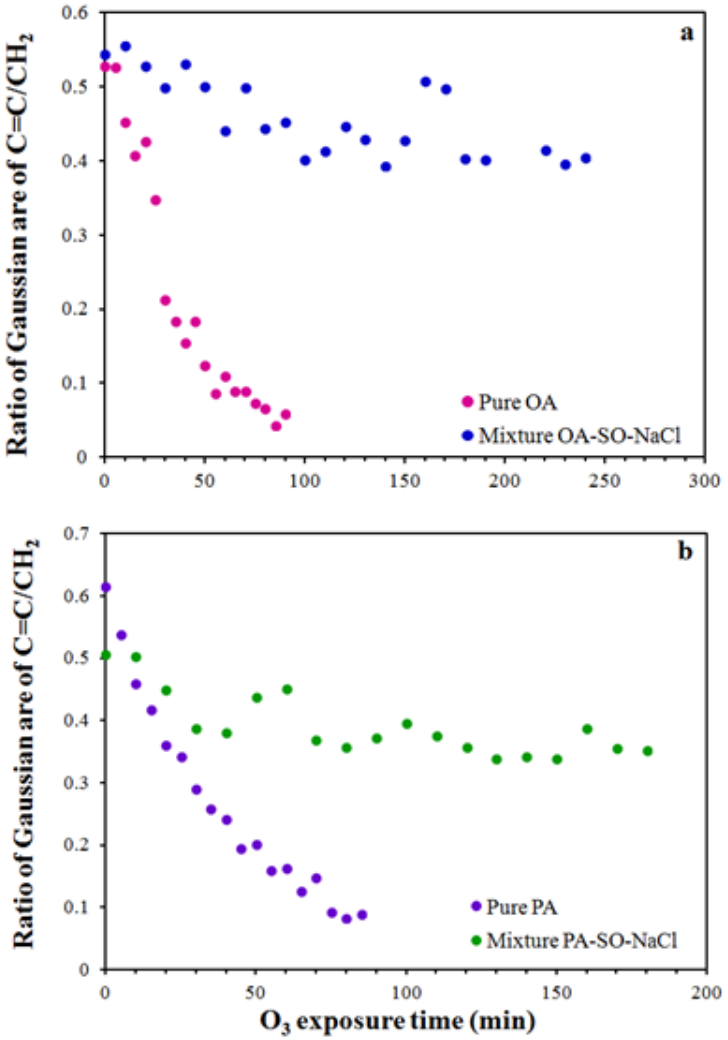

Figure 4.8 Comparison of reactivities of pure oleic (a) and palmitoleic acids (b) and its internal mixtures at 32 ppm ozone concentration. The levitated droplets of OA and mixture OA-SO-NaCl were 125 μm in diameter, while levitated droplets of PA and mixture PA-SO-NaCl were 140 μm in diameter.

Uptake coefficients of these reactions were calculated following the procedure described in Section 3.2 of Chapter 3, the data obtained for each experiment were plotted, and in all cases it was found that the best fit was quadratic, therefore based on Table 3.2, it was inferred that Case 2 was operative for all the results presented here. The resultant uptake coefficients are shown in Table 4.1. As can be seen, γ was affected by the droplet size, O_3 concentration and nature of carboxylic acid. Given that with a greater surface area and lower content of ozone molecules, the droplet might capture more ozone at the surface, leading to a higher uptake. For the case of the mixture OA-SO-NaCl, it is observed the increasing of uptake coefficient with the increasing [O_3]. Figure 4.9 depicts the decay in the ratio of Gaussian area of the peaks C=C/CH_2 of levitated droplets of the mixture OA-SO-NaCl reacting with ozone at 4, 20 and 32 ppm, the maximal decay occurred at 4 ppm [O_3], which corresponds to the highest value of γ, whereas the minimal decay was obtained at 20 ppm [O_3], it may be attributed to the size of the droplet levitated for this experiment. Likewise, the mixture PA-SO-NaCl showed the similar tendency to reduce the value of γ with higher ozone concentrations. However, the reactivity of this mixture was augmented when [O_3] increased, as shown in Figure 4.10. Due to unfavourable experimental conditions, sets of three or more experiments for each mixture at different [O_3] were unable to be repeated. Therefore the values of uptake coefficient reported in Table 4.1 and linear fits in Figures 4.9 and 4.10 do not include the uncertainty.

Table 4.1 Comparison of calculated uptake coefficient values (γ) obtained from ozonolysis of droplets of pure OA and PA at low RH (10%) and mixtures of 3% fatty acid (OA or PA) with SO (1:1 ratio FA/SO) and 97% of a solution of NaCl (10g/mL).

Mixture	**Initial diameter (μm)**	**$[O_3]$ ppm**	**Total time of reaction (min)**	**Final diameter (μm)**	**γ**
OA-SO-NaCl	130	4	300	125	1.52×10^{-6}
	255	20	360	240	3.59×10^{-7}
	125	32	240	110	9.76×10^{-8}
Pure OA	125	32	90	115	$(1.37 \pm 3.59) \times 10^{-5}$
PA-SO-NaCl	115	4	180	115	1.52×10^{-6}
	140	32	180	140	2.68×10^{-7}
Pure PA	140	32	85	135	$(6.19 \pm 3.91) \times 10^{-5}$

The calculated values of γ obtained from ozonolysis of droplet mixtures at 32 ppm $[O_3]$ are compared to the values obtained from experiments carried out at low RH using pure oleic and palmitoleic acids at same ozone concentration and same droplet diameter. As expected, pure fatty acids exhibit faster decay and higher ozone uptake coefficient, as sodium oleate can form micelles, providing a film at the surface of the droplet, making adsorption of ozone more difficult and therefore reducing the uptake coefficient values. Also the presence of water in the ozonolysis of self-assembled mixtures may contribute to the decomposition of ozone in water, affecting the rate of reaction and uptake coefficient of ozone. Table 4.2 summarises the comparison of the uptake coefficient obtained from the ozonolysis of mixture OA-SO-NaCl at 7.88×10^{14} molecules/cm^3 (32 ppm) to the values obtained in previous studies. Rastogi (2015) reported values of γ in the order of 10^{-5} at 6.89 and 9.85×10^{14} molecules/cm^3 $[O_3]$ and RH% < 10 for droplets

of OA-SO-NaCl mixture in a range size from 107 to 170 μm, the discrepancies may be due to the experiments reported here were carried out under humid conditions that may cause the decomposition of ozone in water. The γ reported by Nájera et al. (2015) for droplets which size were 2.8-2.9 μm reacting with ozone at concentrations ranging from 9.61 to 41.6 x 10^{14} molecules/cm^3 and RH >90% was higher than the uptake coefficient calculated here and this may be attributed to the significant difference in particle size between both experiments. For the case of the mixture PA-SO-NaCl, there was no previous report in the literature to compare to the results of this study.

Table 4.2 Comparison of reactive uptake coefficient obtained from ozonolysis of the self-assembled mixture of OA-SO-NaCl

	This study	**Rastogi (2015)**	**Nájera et al. (2015)**
Method and detection technique	**Acoustic levitation combined with Raman microscopy**	**Acoustic levitation combined with Raman microscopy**	**Aerosol flow tube coupled to FTIR**
Particle diameter (μm)	125	107-112 and 90- 170	2.8-2.9
$[O_3]$ (molecules/cm^3)	7.88 x 10^{14}	6.89 and 9.85 x 10^{14}	(9.61-41.6) x 10^{14}
Temperature (K)	≈ 298	≈ 298	292-295
RH%	> 50	<10	91-95
Uptake coefficient	9.8 x 10^{-8}	(3.1 – 1.2) x 10^{-5} and (2.9 – 1.9) x 10^{-5}	(1.7 – 0.7) × 10^{-6}

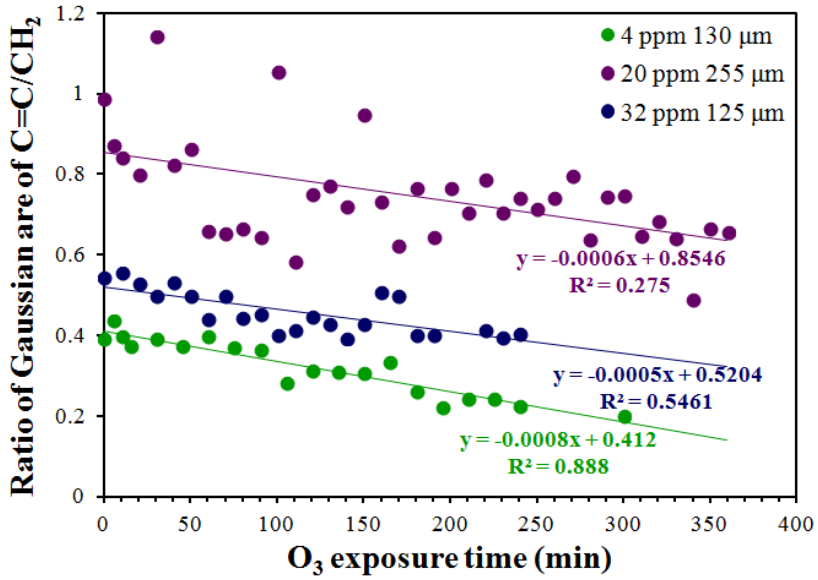

Figure 4.9 Decay of the ratio of Gaussian area of the peaks C=C/CH_2 obtained from the ozonolysis of the mixture OA-SO-NaCl at three different ozone concentrations. Trendline and equations are shown.

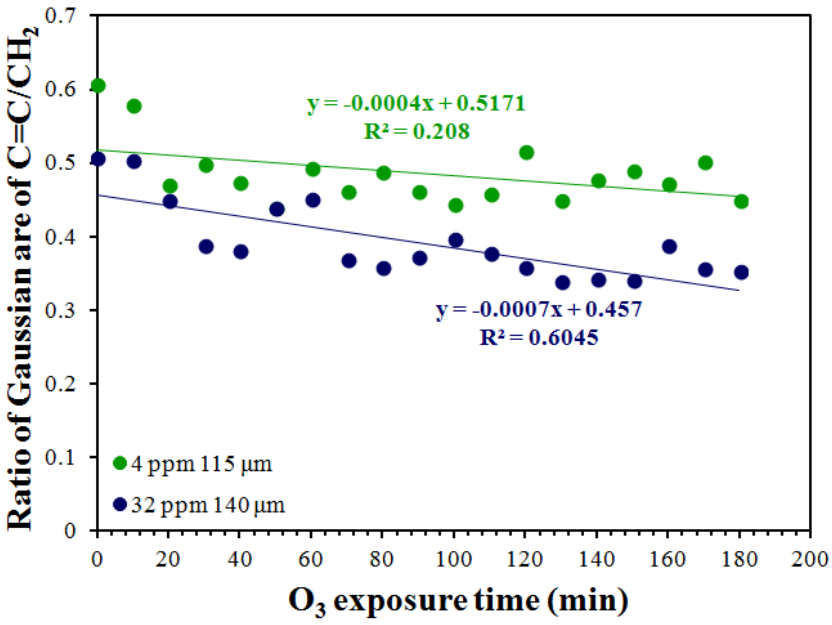

Figure 4.10 Decay of the ratio of Gaussian area of the peaks C=C/CH_2 obtained from the ozonolysis of the mixture PA-SO-NaCl at two different ozone concentrations. Trendline and equations are shown.

CHAPTER 5

CONCLUSIONS AND FUTURE WORK

5.1 CONCLUSIONS

The chemical oxidation of atmospheric aerosols has become relevant in these days. Many studies have focused on heterogeneous reactions of unsaturated organic acids in the gas phase. The study presented here was focussed on the ozonolysis of three prevalent UFAs in urban environments, this reaction has shown to occur at the surface of the droplet, which affects the kinetics of the particles. The formation of products from these reactions and the chemical nature of the aerosol may alter the reactivity of the surface. Most of the products are highly oxygenated and hydrophilic and, due to their low volatility, they may have an effect on the CCN and growth factor of the aerosol, mainly under humid conditions.

Experiments using acoustic levitation linked to Raman microscopy to carry out the ozonolysis of levitated proxies of atmospheric aerosols were conducted to study the ozonolysis of the three prevalent long-chain unsaturated fatty acids in the organic aerosol fraction: oleic acid, linoleic acid and palmitoleic acid. They were oxidised by ozone at different concentrations. It was observed that the rate reaction depended on several factors, such as the number of C=C, size of the droplet, the concentration of O_3, relative humidity and the presence of surfactants.

The size of droplet has shown to have an effect on the rate of reaction of the studied fatty acids. The uptake coefficient of ozone was also affected, this was explained by the effect of the surface area on the uptake of the gas molecule (O_3), the larger the droplet, the greater surface area, therefore higher probability of ozone uptake. It was also observed the effect of ozone concentration in the rate of reaction, as faster reactions occurred with increasing ozone concentration.

Linoleic and palmitoleic acids showed more reactivity compared to oleic acid. Likewise, linoleic acid showed a tendency to undergo autoxidation due to reaction with oxygen or low O_3 concentration. The plots of linoleic acid showed an increase in the ratio of Gaussian area, indicating the formation of unsaturated products. This was confirmed by MS analysis and Raman spectroscopy.

Reactions of O_3 with fatty acids at high relative humidity were compared to reactions carried out at low relative humidity. The effect of the RH in the rate decay was identified. However it was not clear if there is an effect of RH on the uptake coefficient, especially for the ozonolysis of oleic and palmitoleic acid. On the contrary, the uptake coefficient of linoleic acid showed a slight dependence in RH.

Self-assembled internal mixtures were prepared using oleic and palmitoleic acid mixed with sodium oleate and NaCl (10g/mL). This mixture was used to levitate droplets that reacted with ozone at different concentrations. Relative humidity was maintained high and constant, in some cases it was possible to identify the phase transformation, from a deliquesced droplet to a highly viscous phase. The uptake coefficients from ozonolysis

of pure oleic and palmitoleic acid was compared with the uptake coefficient obtained from the mixtures, noticing a reduction of the γ when mixtures were used, this indicates that the presence of surfactants affected the properties of droplet, as phase change may limit the uptake and diffusion of ozone at the surface, because of these particles may exist as self-assembled structures.

A mechanism of ozonolysis of palmitoleic and linoleic acids was proposed, following the mechanism stated by Criegee. Some of the volatile products were verified by mass spectra, confirming the Raman signatures that indicated they were formed.

5.2 FUTURE WORK:

Many ideas of experimental work emerged during this research, but they were left for the future due to limited time, or they need to be strategically planned in order to obtain successful results.

1. Previous studies reported electrodynamic balance (EDB) and Raman spectroscopy to assess the phase transformation of aerosols (Lee et al., 2008), and the role of the relative humidity in the ozonolysis of levitated droplets of carboxylic acids, including oleic acid and maleic acid was studied using mass spectra (Lee et al., 2012). Initially in this research maleic acid was used as the first proxy for aerosol, but experimental difficulties arose at that moment due to the levitated droplets were unstable and underwent phase transformation, making difficult to carry out successful experiments, leading to obtaining poor quality results that were not reported here. New proxies were selected, starting with oleic and linoleic acid, then palmitoleic acid completed the scenario of this

research. Although the intention was to come back to the experimental work using maleic acid, the experiments using this compound were finally discarded due to lack of time. Future research could explore in detail the reaction of ozonolysis of maleic acid using the experimental techniques presented in this thesis, planning the experimental work with this compound and taking into account the phase transformation it undergoes.

2. Linoleic acid has demonstrated to form gas-phase aldehydes when forming sea surface microlayers (Zhou et al., 2014). Some of those aldehydes are produced from the direct reaction of LA with O_3 and contain one carbon-carbon double bond. Thus they can react with ozone producing new compounds. In this thesis the ozonolysis of self-assembled mixtures of PA and OA with SO and NaCl was reported, but the ozonolysis of mixture using LA was not carried out, as LA can be easily oxidised even at room temperature, and the process to prepare the mixture involves using temperature above 25° C. This reaction shows promising results if is carried out to a mixture of LA with its sodium salt and brine, but the procedure to prepare this mixture should be reconsidered and modified to avoid the oxidation of LA. The use of synchrotron radiation to elucidate the structure of the self-assembled mixture of LA may also be considered as part of the further experimental work. The comparison of the two systems, LA and OA self-assembled mixtures might be relevant to understand the structural arrangements recently reported by Pfrang et al. (2017), as these two fatty acids 18C but they differ in the number of C=C.

3. Arachidonic acid and linolenic acid have been found in the atmosphere in

minimal amounts. Arachidonic acid was considered to be one of the proxies for reactions with ozone in this research, but time limitations did not allow to use it. Previous work using EDB (Lee et al., 2012) showed the effect of humid conditions in the ozonolysis of arachidonic acid, whereas Raman spectroscopy and EDB showed the high reactivity of linolenic acid (Lee and Chan 2007a), although this fatty acid was not taken into consideration to carry out experiments. Therefore, It will be important that future research investigates the influence of the number of C=C in the reactivity of UFA under dry and humid conditions, and compare the findings with the results presented in this thesis.

4. Ozonolysis of oleic, palmitoleic and linoleic acids at different pressure and variable temperatures would provide a better insight of this reaction for comparison with the results of this study.

5. One intended experiment in this study was the analysis of emission from food cooking in a simulated environment. Due to limitation of time, this experiment was not carried out. Reports from studies using a different kind of meat have shown the composition of the organic aerosol fractions present in environments nearby restaurants and kitchens (Mohr et al., 2009; Robinson, 2006). It would be relevant to explore the impact of indoor cooking emissions, using different types of oils, food and cooking styles in order to assess the potential impact of the aerosols in health, and also estimate the further reactions they may undergo and products that are released in indoor and outdoor environments.

APPENDIX

A. Publications:

From the results reported in this thesis, some publications have been planned to be published soon. The approaches for these publications will be:

1. Elucidation of the structural composition of droplets of mixtures of OA and PA with SO and NaCl (self-assembled mixtures) using small angle x-ray scattering (SAXS) and Raman spectroscopy (Experimental work carried out in the synchrotron science facility in Diamond Light Source).

2. The influence of ozone concentrations, relative humidity, droplet size and nature of fatty acids in the ozone uptake coefficients.

3. Raman spectroscopy applied to the study of fatty acids as proxies for atmospheric aerosols.

B. List of attended conferences:

Posters were presented in three conferences:

Conference Atmospheric chemistry in the Anthropocene, Faraday Discussion, RSC. York, UK, 22-24 May April 2017.

Department of Chemistry

University of Reading

THE EFFECT OF RELATIVE HUMIDITY ON THE OZONOLYSIS OF ACOUSTICALLY LEVITATED PROXIES FOR ATMOSPHERIC AEROSOLS

Edna Cabrera | Sukhpreet Talewar| Christian Pfrang

INTRODUCTION

The presence of water may affect the reaction of ozonolysis of fatty acids, since it is believed that both, the carboxylic acid and its reaction products may retain water at the surface, increasing the residence time of dissolved ozone at the surface[1] and therefore slow down the reaction. This study intends to assess the impact of relative humidity on the reaction of ozone with a range of unsaturated fatty acids.

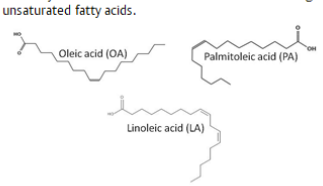

OBJECTIVE

This study evaluates the influence of relative humidity on the ozonolysis of acoustically levitated droplets of oleic acid (OA), linoleic acid (LA) and palmitoleic (PA) acid by optical and Raman microscopy at ozone concentrations ranging from 0.5 to 40 ppm and relative humidities (RH) ranging from 0 to 80%.

EXPERIMENTAL METHOD

Figure 1 displays the experimental set-up.

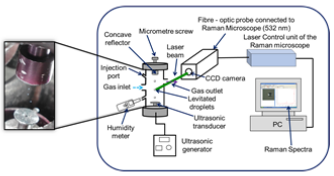

Figure 1. Experimental set-up for Raman acoustic levitation.

Instrumentation and experimental conditions:

- The Renishaw inVia Raman microscope is interfaced to an acoustic levitator via a fibre-optic probe (excitation wavelength: 532 nm)
- The ultrasonic levitator is contained in a custom-built environmental chamber
- The O_2 flow rate was 145 mL min^{-1}
- Ozone was produced by using a UV lamp producing O_3 concentrations ranging 0.5 to 40 ppm
- Raman spectra were obtained at intervals of 5 to 10 min
- Raman spectra were collected in the range from 100 to 4000 cm^{-1}
- RH was controlled by balancing dry and wet flows of oxygen.
- Relative humidity was measured in close proximity to the levitated droplet throughout the experiment by using a humidity meter
- Droplets are levitated by using a µL syringe inserted into the injection port. The gases produced during the reaction are collected by means of headspace solid-phase microextraction fibre (HS-SPME) inserted into the same port.

RESULTS

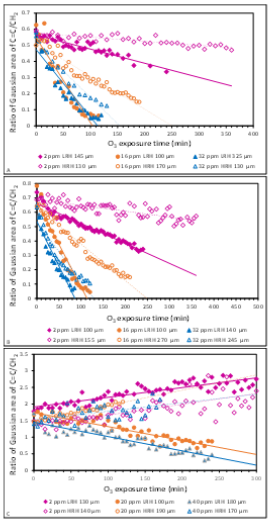

Figure 2. Effect of RH in the ozonolysis of various levitated droplets of: A) oleic acid (OA), B) palmitoleic acid (PA), and C) linoleic acid (LA), at ozone concentrations of 2, 16 and 32 ppm. Droplet diameters are given in the legend together with [O_3]. Low RH (LRH) ranged from 0 to 15%, and High RH (HRH) ranged from 60 to 75%.

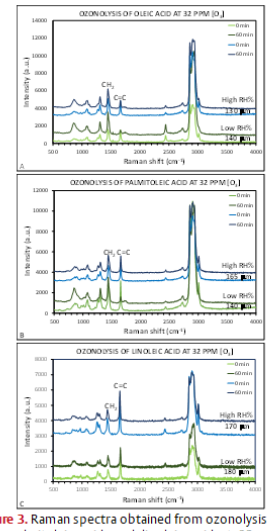

Figure 3. Raman spectra obtained from ozonolysis of : oleic acid, palmitoleic acid, and linoleic acid at 32 ppm [O_3] before start the reaction and after 1 hour. A decay in the intensity of the peak corresponding to the double bond C=C (≈1665 cm^{-1}) can be observed. The CH_2 peak (≈1450 cm^{-1}) remains constant. Diameters of the droplets are stated.

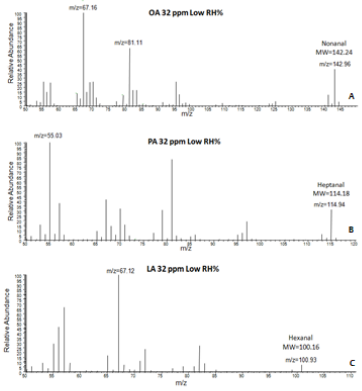

Figure 4. Mass spectra of A) oleic acid, B) palmitoleic acid, and C) linoleic acid taken from the reactions of ozonolysis at 32 ppm at low RH%. Some expected products were identified in all cases.

FINDINGS AND FUTURE WORK

- Ozonolysis of oleic acid and palmitoleic acid occurred a higher rate than that of linoleic acid at all studied ozone concentrations. Linoleic acid showed a different pattern in the decay the ratio C=C/CH_2 at low [O_3]. This result was consistent with literature[1] and can be explained by the two double bonds present in LA.
- Evidence from Raman spectra suggested the formation of carbonyl compounds (≈1750 cm^{-1}) and peroxides (800-900 cm^{-1}). Aldehydes were identified in the mass spectra.
- Ozonolysis of fatty acids is affected by changes in RH. It was observed that the higher RH the slower the reactive decay, especially at lower ozone concentrations. The slower decay of the ratio C=C/CH_2 could be caused by the formation of hydrophilic products that can retain water and therefore increase the residence time of ozone in the layers[5]. However more evidence is still required to confirm the mechanism.
- Further analysis of MS data is in process, as well as the discussion of the influence of the RH on the uptake coefficient.

REFERENCES

1. Lee, A. K. Y. and Chan, C. K. *J. Phys. Chem. A.*, 2007, **111**, 6285-6295.
2. Spencer, G.F. and Kleiman, R. *J. Am. Oil Chem. Soc.*, 1978, **55** (10), 689.
3. Thornberry, T., and Abbatt, J.P. *Phys. Chem. Chem. Phys*, 2004, **6**, 84-93.
4. Zahardis, J. and Petrucci, G.A. *Atmos. Chem. Phys.*, 2007, **7**,1237-1274.
5. Zeng, G., Holladay, S., Langlois, D., Zhang, Y. and Liu Y. *J. Phys. Chem. A.*, 2013, **117**, 1963-1974.

Acknowledgements
- E. Cabrera-Martinez acknowledges financial support from the Department of Science, Technology and Innovation – Colciencias. Colombia.

Contact information
- Department of Chemistry, University of Reading, Whiteknights, RG6 6AH
- Email: e.r.cabreramartinez@student.reading.ac.uk

Department of Chemistry

University of Reading

STUDY OF THE EFFECT OF RELATIVE HUMIDITY IN THE OZONOLYSIS OF ULTRASONICALLY LEVITATED DROPLETS CONTAINING UNSATURATED FATTY ACIDS

Edna R. Cabrera-Martinez | Christian Pfrang

Introduction

It is known that meat cooking is one of the most important sources of atmospheric organic aerosols in urban environments. There are three main long chained unsaturated fatty acids that contribute considerably to the aerosol fraction: :oleic acid (OA), linoleic acid (LA) and palmitoleic acid (PA). The products of ozonolysis of these carboxylic acids might have an impact on climate, health and life on Earth.

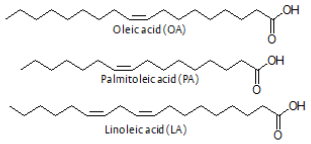

Objective

In the present work, the ozonolysis of acoustically levitated droplets of the three fatty acids has been analyzed by optical and Raman microscopy at ozone concentrations ranging from 2 to 40 ppm and low and relative humidity (RH) ranging from 0 to 70%.

Experimental Methods

- Renishaw inVia Raman microscope was linked to a fibre-optic probe (excitation wavelength: 532 nm) (see scheme 1).
- Ultrasonic levitator was contained in a custom-built environmental chamber
- O_2 flow rate was 145 mL min^{-1}
- O_3 is produced by using a UV lamp. O_3 concentrations ranging 2 to 40 ppm
- Raman spectra were obtained at intervals of 5 min
- Raman shift ranged from 100 to 3200 cm^{-1} (in some cases to 4000 cm^{-1})

Details of the experimental set-up for the Raman acoustic levitation of fatty acids droplets are displayed in the scheme in Figure 1.

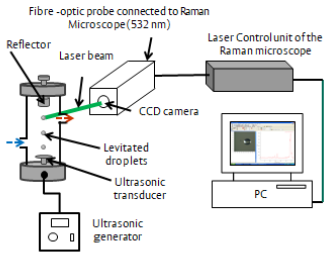

Figure 1. Experimental set-up for Raman acoustic levitation.

Results

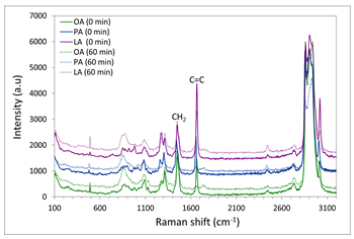

Figure 2. Raman spectra obtained from ozonolysis of : Oleic acid (diameter: 145 µm) , Palmitoleic acid (diameter: 160 µm), and Linoleic acid (diameter: 145µm), at 40 ppm ozone concentration. A decay in the intensity of the peak corresponding to double bond C=C (≈1665 cm^{-1}) can be observed. The CH_2 peak (≈1450 cm^{-1}) remains constant.

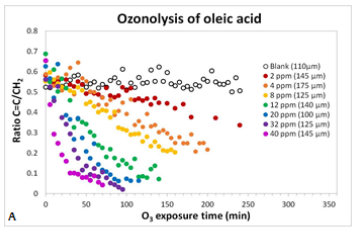

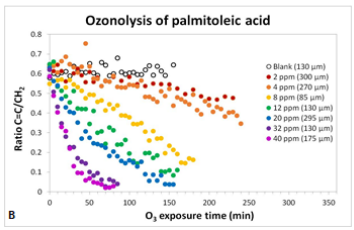

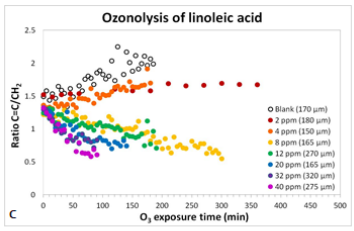

Figure 3. Ozonolysis of various levitated droplets of: A) Oleic acid, B) Palmitoleic acid, and C) Linoleic acid, at ozone concentrations ranging from 2 to 40 ppm (droplet diameters are given in the legend together with [O_3]).

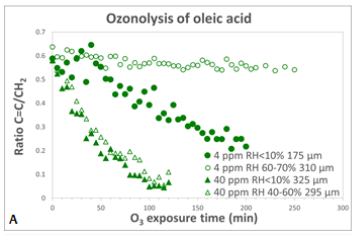

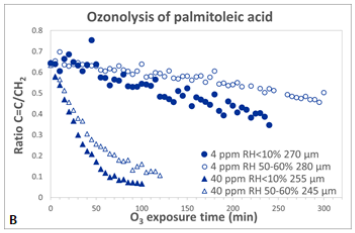

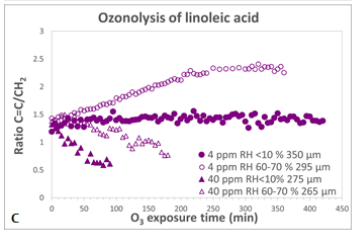

Figure 4. Effect of RH in the ozonolysis of various levitated droplets of: A) Oleic acid, B) Palmitoleic acid, and C) Linoleic acid, at ozone concentrations of 4 (●) and 40 (▲) ppm. Droplet diameters are given in the legend together with [O_3].

Conclusions and Future Work

In this study, it was found that ozonolysis of OA and PA occurs a higher rate than that of LA, at all studied ozone concentrations. LA showed at the lowest O_3 concentrations and in the blank that the ratio C=C/C-H increases. This result was consistent with literature [1] and can be explained by the two double bonds present in LA.

Also it was found that, the higher RH the slower the decay of ratio C=C/CH_2. It can be explained by the formation of H_2O layers in the surface of the droplet due to the new formed hydrophilic products retain water, increasing the residence time of ozone in the layers and hindering its reaction with the fatty acid [5]. Immediate work will be carried out in order to verify how higher RH affect the reaction of ozonolysis of carboxylic acids.

Upcoming experimental work is focused on the analysis of the products formed during the reactions, by means of GC-MS and Solid Phase Micro-Extraction (SPME).

References

1. Lee, A. K. Y. and Chan, C. K. *J. Phys. Chem. A.*, 2007, **111**, 6285-6295.
2. Pfrang, C., Shiraiwa, M. and Pöschl, U. *Atmos. Chem. Phys.*, 2011, **11**(14), 7343- 7354.
3. Spencer, G.F. and Kleiman, R. *J. Am. Oil Chem. Soc.*, 1978, **55**(10), 689.
4. Zahardis, J. and Petrucci, G.A. *Atmos. Chem. Phys.*, 2007, **7**,1237-1274.
5. Zeng, G., Holladay, S., Langlois, D., Zhang, Y. and Liu Y. *J. Phys. Chem. A.*, 2013, **117**, 1963-1974.

Acknowledgements

- E. Cabrera-Martinez acknowledges financial support from the Department of Science, Technology and Innovation -Colciencias. Colombia..
- Support for development of the acoustic levitator was provided by NERC (NE/G000883/1) and the Royal Society (2007/R2).

Contact information

- Department of Chemistry, University of Reading, Whiteknights, RG6 6AH
- Email: e.r.cabreramartinez@student.reading.ac.uk

Conference: Chemistry in the Urban Atmosphere, Faraday Discussion, RSC. London, UK, 6-8 April 2016. Poster prize was awarded.

Department of Chemistry

University of Reading

OZONOLYSIS OF ULTRASONICALLY LEVITATED DROPLETS CONTAINING UNSATURATED CARBOXYLIC ACIDS

Edna R. Cabrera-Martinez | Harry J. Ancill | Kunal Rastogi | Christian Pfrang

Introduction

Carboxylic acids are present in the atmosphere as key contributors to secondary organic aerosol formation. It is known that meat cooking is an important source of atmospheric organic compounds, such as oleic acid (OA), linoleic acid (LA) and palmitoleic acid (PA), that contribute considerably to the aerosol fraction as a result of the ozonolysis that they undergo, which yields a series of products that may impact on climate and human health.

Objective

In the present work, the ozonolysis of acoustically levitated droplets of the three fatty acids has been analyzed by optical and Raman microscopy at ozone concentrations ranging from 2 to 40 ppm.

Experimental Methods

- Renishaw inVia Raman microscope was linked to a fibre-optic probe (excitation wavelength: 532 nm)
- Ultrasonic levitator was contained in a custom-built environmental chamber
- O_2 flow rate was 145 mL min^{-1}
- A UV lamp was used to produce O_3 at concentrations ranging 2 to 40 ppm
- Raman spectra were obtained at intervals of 5 min
- Raman shift ranged from 100 to 3200 cm^{-1}
- Reagents: Pure oleic acid, palmitoleic acid, and linoleic acid.

Details of the experimental set-up for the Raman acoustic levitation of fatty acids droplets are displayed in Scheme 1.

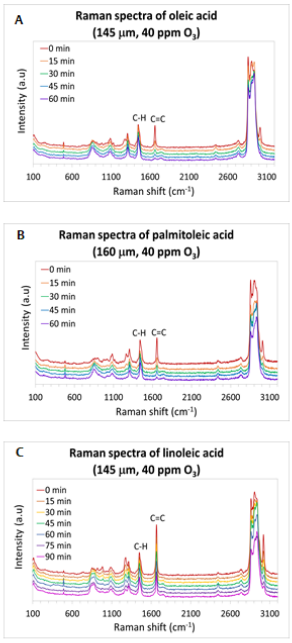

Figure 2. Raman spectra obtained from ozonolysis of: A) Oleic acid (diameter: 145 µm), B) Palmitoleic acid (diameter: 160 µm), and C) Linoleic acid (diameter: 145µm), at 40 ppm ozone concentration. A decay in the intensity of the peak corresponding to double bond C=C (≈1665 cm^{-1}) can be observed. The C-H peak (≈1450 cm^{-1}) remains constant.

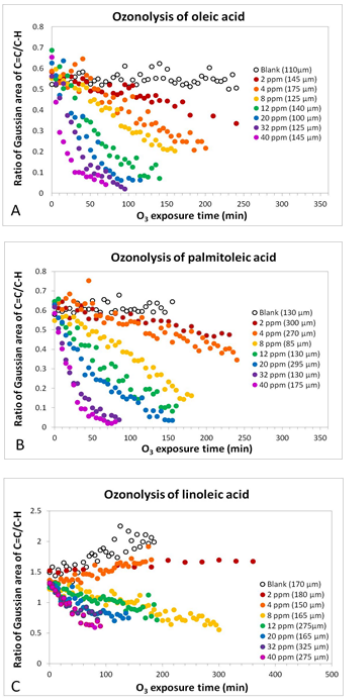

Figure 3. Ozonolysis of various levitated droplets of: A) Oleic acid, B) Palmitoleic acid, and C) Linoleic acid, at ozone concentrations ranging from 2 to 40 ppm (droplet diameters are given in the legend together with [O_3]).

Results

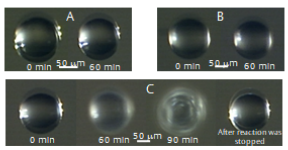

Figure 1. Photographs of levitated droplets of: A) Oleic acid; B) Palmitoleic acid; and C) Linoleic acid.

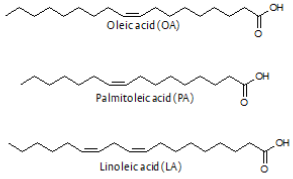

Conclusions and Future Work

In this study, it was found that ozonolysis of OA and PA occurs a higher rate than that of LA, at all ozone concentrations used. LA showed at the lowest O_3 concentrations and in the blank that the ratio C=C/C-H increases. This result was consistent with literature [1] and can be explained by the two double bonds present in LA. It is probable that the particle size can affect the reaction, but future studies will be carried out to elucidate this aspect. Immediate work is focused on the analysis of the products formed during the reaction, by means of GC-MS and Solid Phase Micro-Extraction (SPME).

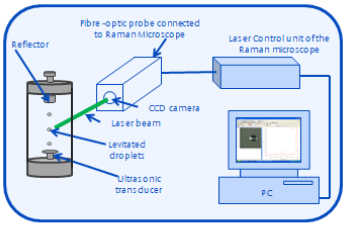

Scheme 1. Experimental set-up for Raman acoustic levitation.

References

1. Lee, A. K. Y. and Chan, C. K. (2007). *J. Phys. Chem. A.* 111: 6285-6295.
2. Pfrang, C.; Shiraiwa, M.; and Pöschl, U. (2011). *Atmos. Chem. Phys.*, 11(14): 7343- 7354.
3. Zahardis, J., and Petrucci, G. A. (2007). *Atmos. Chem. Phys.* 7: 1237-1274.

Acknowledgements

- E. Cabrera-Martinez acknowledges financial support from the Department of Science, Technology and Innovation – Colciencias. Colombia..
- Support for development of the acoustic levitator was provided by NERC (NE/G000883/1) and the Royal Society (2007/R2).

Contact information

- Department of Chemistry, University of Reading, Whiteknights, RG6 6AH
- Email: e.r.cabreramartinez@student.reading.ac.uk

REFERENCES

Almabrok, Sami Hussein (2012) A study of the oxidation of terpenes in levitated droplets and in the gas phase (PhD Thesis) University of Reading, School of Chemistry, Food & Pharmacy. Reading, UK.

Andreae, M. O., & Rosenfeld, D. (2008). Aerosol–cloud–precipitation interactions. Part 1. The nature and sources of cloud-active aerosols. *Earth-Science Reviews, 89*(1), 13-41.

Arthur, C. L., & Pawliszyn, J. (1990). Solid phase microextraction with thermal desorption using fused silica optical fibers. *Analytical chemistry, 62*(19), 2145-2148.

Asad, A., Mmereki, B. T., & Donaldson, D. J. (2004). Enhanced uptake of water by oxidatively processed oleic acid. *Atmospheric Chemistry and Physics, 4*(8), 2083-2089.

Atkinson, R., & Arey, J. (2003). Atmospheric degradation of volatile organic compounds. *Chemical reviews, 103*(12), 4605-4638.

Boucher, O. (2015). *Atmospheric aerosols: Properties and climate impacts.* Springer.

Bowie, B. T., Chase, D. B., Lewis, I. R., & Griffiths, P. R. (2002). Anomalies and artifacts in Raman spectroscopy. *Handbook of vibrational spectroscopy*.

Brandt, E. H. (1989). Levitation in physics. *Science, 243*(4889), 349-355.

Bridge, R. E., & Hilditch, T. P. (1950). 492. The seed fat of Macadamia ternifolia. *Journal of the Chemical Society (Resumed)*, 2396-2399.

Brimblecombe, P. (1996). *Air composition and chemistry*. Cambridge University Press.

Buehler, R. E., Staehelin, J., & Hoigné, J. (1984). Ozone decomposition in water studied by pulse radiolysis. 1. Perhydroxyl (HO2)/hyperoxide (O2-) and HO_3/O_3-as intermediates. *The Journal of Physical Chemistry, 88*(12), 2560-2564.

Cai, C., Stewart, D. J., Reid, J. P., Zhang, Y. H., Ohm, P., Dutcher, C. S., & Clegg, S. L. (2015). Organic component vapor pressures and hygroscopicities of aqueous aerosol measured by optical tweezers. *Journal of Physical Chemistry A, 119*(4), 704-718.

Carey, D. M., & Korenowski, G. M. (1998). Measurement of the Raman spectrum of liquid water. *The Journal of chemical physics, 108*(7), 2669-2675.

Chemical Analysis Facility (n.d.) Spectroscopy. Retrieved 20 May 2018, from https://www.reading.ac.uk/caf/OpticalSpectroscopy/caf_Spectroscopy.aspx

Confocal Raman Microscopy General Overview (n.d) [PDF file]. Retrieved on 2 June 2017, from: http://forum.sci.ccny.cuny.edu/cores/microscopy-imaging/raman/Confocal-raman-note.pdf.

Criegee, R. (1975). Mechanism of ozonolysis. *Angewandte Chemie International Edition, 14*(11), 745-752.

Czamara, K., Majzner, K., Pacia, M. Z., Kochan, K., Kaczor, A., & Baranska, M. (2015). Raman spectroscopy of lipids: a review. *Journal of Raman Spectroscopy*, *46*(1), 4-20.

Davies, J. F., Haddrell, A. E., Miles, R. E., Bull, C. R., & Reid, J. P. (2012). Bulk, surface, and gas-phase limited water transport in aerosol. *The Journal of Physical Chemistry A, 116*(45), 10987-10998.

Dennis-Smither, B. J., Hanford, K. L., Kwamena, N. O. A., Miles, R. E., & Reid, J. P. (2012). Phase, morphology, and hygroscopicity of mixed oleic acid/sodium chloride/water aerosol particles before and after ozonolysis. *The Journal of Physical Chemistry A, 116*(24), 6159-6168.

Ellison, G. B., Tuck, A. F., & Vaida, V. (1999). Atmospheric processing of organic aerosols. *Journal of Geophysical Research: Atmospheres, 104*(D9), 11633-11641.

Fei, L. I. U., Feng-Kui, D. U. A. N., Hai-Rong, L. I., Yong-Liang, M. A., Ke-Bin, H. E., & ZHANG, Q. (2015). Solid Phase Microextraction/Gas Chromatography-Tandem Mass Spectrometry for Determination of Polycyclic Aromatic Hydrocarbons in Fine Aerosol in Beijing. *Chinese Journal of Analytical Chemistry, 43*(4), 540-546.

Feingold, G., & Chuang, P. Y. (2002). Analysis of the influence of film-forming compounds on droplet growth: Implications for cloud microphysical processes and climate. *Journal of the Atmospheric Sciences, 59*(12), 2006-2018.

Finlayson-Pitts, B. J., & Pitts, J. N. (2000). *Chemistry of the Upper and Lower Atmosphere : Theory, Experiments, and Applications.* San Diego: Academic Press.

Frankel, E. N. (1998). *Lipid oxidation (Vol. 10)* Scotland: The Oily Press.

Galliard, T., Phillips, D. R., & Reynolds, J. (1976). The formation of cis-3-nonenal, trans-2-nonenal and hexanal from linoleic acid hydroperoxide isomers by a hydroperoxide cleavage enzyme system in cucumber (Cucumis sativus) fruits. *Biochimica et Biophysica Acta (BBA)-Lipids and Lipid Metabolism, 441*(2), 181-192.

Gallimore, P. J., Achakulwisut, P., Pope, F. D., Davies, J. F., Spring, D. R., & Kalberer, M. (2011). Importance of relative humidity in the oxidative ageing of organic aerosols: case study of the ozonolysis of maleic acid aerosol. *Atmospheric Chemistry and Physics, 11*(23), 12181-12195.

Guo, S., Hu, M., Guo, Q., Zhang, X., Zheng, M., Zheng, J., ... & Zhang, R. (2012). Primary sources and secondary formation of organic aerosols in Beijing, China. *Environmental science & technology*, *46*(18), 9846-9853.

Hallquist, M., Wenger, J. C., Baltensperger, U., Rudich, Y., Simpson, D., Claeys, M., ... & Hamilton, J. F. (2009). The formation, properties and impact of secondary organic aerosol: current and emerging issues. *Atmospheric Chemistry and Physics, 9*(14), 5155-5236.

He, L. Y., Lin, Y., Huang, X. F., Guo, S., Xue, L., Su, Q., ... & Zhang, Y. H. (2010). Characterization of high-resolution aerosol mass spectra of primary organic aerosol emissions from Chinese cooking and biomass burning. *Atmospheric Chemistry and Physics, 10*(23), 11535-11543.

He, X., Leng, C., Pang, S., & Zhang, Y. (2017). Kinetics study of heterogeneous reactions of ozone with unsaturated fatty acid single droplets using micro-FTIR spectroscopy. *RSC Advances, 7*(6), 3204-3213.

Hearn, J. D., & Smith, G. D. (2004). Kinetics and product studies for ozonolysis reactions of organic particles using aerosol CIMS. *The Journal of Physical Chemistry A, 108*(45), 10019-10029.

Hearn, J. D., Lovett, A. J., & Smith, G. D. (2005). Ozonolysis of oleic acid particles: evidence for a surface reaction and secondary reactions involving Criegee intermediates. *Physical Chemistry Chemical Physics, 7*(3), 501-511.

Hiraoka-Yamamoto, J., Ikeda, K., Negishi, H., Mori, M., Hirose, A., Sawada, S., ... & Miki, T. (2004). Serum lipid effects of a monounsaturated (palmitoleic) fatty acid-rich diet based on macadamia nuts in healthy, young Japanese women. Clinical and *Experimental Pharmacology and Physiology*, *31*(s2).

Hobbs, P. V. (2000). *Introduction to atmospheric chemistry.* Cambridge University Press.

Horie, O., & Moortgat, G. K. (1991). Decomposition pathways of the excited Criegee intermediates in the ozonolysis of simple alkenes. *Atmospheric Environment. Part A. General Topics, 25*(9), 1881-1896.

Huff Hartz, K. E., Weitkamp, E. A., Sage, A. M., Donahue, N. M., & Robinson, A. L. (2007). Laboratory measurements of the oxidation kinetics of organic aerosol mixtures using a relative rate constants approach. *Journal of Geophysical Research: Atmospheres, 112*(D4).

Hung, H. M., & Tang, C. W. (2010). Effects of temperature and physical state on heterogeneous oxidation of oleic acid droplets with ozone. *The Journal of Physical Chemistry A, 114*(50), 13104-13112.

Hung, H. M., & Ariya, P. (2007). Oxidation of oleic acid and oleic acid/sodium chloride (aq) mixture droplets with ozone: Changes of hygroscopicity and role of secondary reactions. *The Journal of Physical Chemistry A, 111*(4), 620-632.

Hung, H. M., Katrib, Y., & Martin, S. T. (2005). Products and mechanisms of the reaction of oleic acid with ozone and nitrate radical. *The Journal of Physical Chemistry A, 109*(20), 4517-4530.

Kanakidou, M., Seinfeld, J. H., Pandis, S. N., Barnes, I., Dentener, F. J., Facchini, M. C., ... & Swietlicki, E. (2005). Organic aerosol and global climate modelling: a review. *Atmospheric Chemistry and Physics*, *5*(4), 1053-1123.

Katrib, Y., Martin, S. T., Hung, H. M., Rudich, Y., Zhang, H., Slowik, J. G., ... & Worsnop, D. R. (2004). Products and mechanisms of ozone reactions with oleic acid for aerosol particles having core− shell morphologies. *The Journal of Physical Chemistry A, 108*(32), 6686-6695.

Kawamura, K., Ishimura, Y., & Yamazaki, K. (2003). Four years' observations of terrestrial lipid class compounds in marine aerosols from the western North Pacific. *Global Biogeochemical Cycles, 17*(1).

Kerminen, V. M., Paramonov, M., Anttila, T., Riipinen, I., Fountoukis, C., Korhonen, H., ... & Svenningsson, B. (2012). Cloud condensation nuclei production associated with atmospheric nucleation: a synthesis based on existing literature and new results. *Atmospheric Chemistry and Physics, 12*(24), 12037-12059.

King, M. D., Thompson, K. C., & Ward, A. D. (2004). Laser tweezers Raman study of optically trapped aerosol droplets of seawater and oleic acid reacting with ozone: implications for cloud-droplet properties. *Journal of the American chemical society, 126*(51), 16710-16711.

Kitson, F. G., Larsen, B. S., & McEwen, C. N. (1996). *Gas chromatography and mass spectrometry: a practical guide*. Academic Press.

Kroll, J. H., & Seinfeld, J. H. (2008). Chemistry of secondary organic aerosol: Formation and evolution of low-volatility organics in the atmosphere. *Atmospheric Environment, 42*(16), 3593-3624.

Kuo, S. C., Tsai, Y. I., Tsai, C. H., & Hsieh, L. Y. (2011). Carboxylic acids in PM 2.5 over Pinus morrisonicola forest and related photoreaction mechanisms identified via Raman spectroscopy. *Atmospheric environment, 45*(37), 6741-6750.

Latif, M. T., & Brimblecombe, P. (2004). Surfactants in atmospheric aerosols. *Environmental science & technology, 38*(24), 6501-6506.

Lee, A. K., & Chan, C. K. (2007a). Heterogeneous reactions of linoleic acid and linolenic acid particles with ozone: Reaction pathways and changes in particle mass, hygroscopicity, and morphology. *The Journal of Physical Chemistry A*, 111(28), 6285-6295.

Lee, A. K., & Chan, C. K. (2007b). Single particle Raman spectroscopy for investigating atmospheric heterogeneous reactions of organic aerosols. *Atmospheric environment, 41*(22), 4611-4621.

Lee, A. K., Ling, T. Y., & Chan, C. K. (2008). Understanding hygroscopic growth and phase transformation of aerosols using single particle Raman spectroscopy in an electrodynamic balance. *Faraday discussions, 137*, 245-263.

Lee, J. W., Carrascón, V., Gallimore, P. J., Fuller, S. J., Björkegren, A., Spring, D. R., ... & Kalberer, M. (2012). The effect of humidity on the ozonolysis of unsaturated compounds in aerosol particles. *Physical Chemistry Chemical Physics, 14*(22), 8023-8031.

Lierke, E. G. (1996). Acoustic levitation–a comprehensive survey of principles and applications. *Acta Acustica united with Acustica, 82*(2), 220-237.

Limbeck, Andreas, and Hans Puxbaum. "Organic acids in continental background aerosols." *Atmospheric Environment 33.12* (1999): 1847-1852.

Lohmann, U., & Feichter, J. (2005). Global indirect aerosol effects: a review. *Atmospheric Chemistry and Physics, 5*(3), 715-737.

Mendez, M., Visez, N., Gosselin, S., Crenn, V., Riffault, V., & Petitprez, D. (2014). Reactive and nonreactive ozone uptake during aging of oleic acid particles. *The Journal of Physical Chemistry A*, 118(40), 9471-9481.

Mochida, M., Kawamura, K., Umemoto, N., Kobayashi, M., Matsunaga, S., Lim, H. J., ... & Simoneit, B. R. (2003). Spatial distributions of oxygenated organic compounds (dicarboxylic acids, fatty acids, and levoglucosan) in marine aerosols over the western Pacific and off the coast of East Asia: Continental outflow of organic aerosols during the ACE-Asia campaign. *Journal of Geophysical Research: Atmospheres, 108*(D23).

Mohr, C., DeCarlo, P. F., Heringa, M. F., Chirico, R., Slowik, J. G., Richter, R., ... & Peñuelas, J. (2012). Identification and quantification of organic aerosol from cooking and other sources in Barcelona using aerosol mass spectrometer data. *Atmospheric Chemistry and Physics, 12*(4), 1649-1665.

Mohr, C., Huffman, J. A., Cubison, M. J., Aiken, A. C., Docherty, K. S., Kimmel, J. R., ... & Jimenez, J. L. (2009). Characterization of primary organic aerosol emissions from meat cooking, trash burning, and motor vehicles with high-resolution aerosol mass spectrometry and comparison with ambient and chamber observations. *Environmental science & technology, 43*(7), 2443-2449.

Moise, T., & Rudich, Y. (2000). Reactive uptake of ozone by proxies for organic aerosols: Surface versus bulk processes. *Journal of Geophysical Research: Atmospheres, 105*(D11), 14667-14676.

Moise, T., & Rudich, Y. (2002). Reactive uptake of ozone by aerosol-associated unsaturated fatty acids: kinetics, mechanism, and products. *The Journal of Physical Chemistry A, 106*(27), 6469-6476.

Morris, J. W., Davidovits, P., Jayne, J. T., Jimenez, J. L., Shi, Q., Kolb, C. E., ... & Cass, G. (2002). Kinetics of submicron oleic acid aerosols with ozone: A novel aerosol mass spectrometric technique. *Geophysical Research Letters, 29*(9).

Nájera, J. J. (2007). Phase transition behaviour of sodium oleate aerosol particles. *Atmospheric Environment, 41*(5), 1041-1052.

Nájera, J. J., Percival, C. J., & Horn, A. B. (2015). Infrared Spectroscopic Evidence for a Heterogeneous Reaction between Ozone and Sodium Oleate at the Gas–Aerosol Interface: Effect of Relative Humidity. *International Journal of Chemical Kinetics*, *47*(4), 277-288.

Nash, D. G., Tolocka, M. P., & Baer, T. (2006). The uptake of O 3 by myristic acid–oleic acid mixed particles: evidence for solid surface layers. *Physical Chemistry Chemical Physics*, *8*(38), 4468-4475.

NIST Mass Spec Data Center, S.E. Stein, director, "Mass Spectra" in NIST Chemistry WebBook, NIST Standard Reference Database Number 69, Eds. P.J. Linstrom and W.G. Mallard, National Institute of Standards and Technology, Gaithersburg MD, 20899,doi:10.18434/T4D303, (retrieved May 9, 2017).

Pack, A., Kremer, K., Albrecht, N., Simon, K., & Kronz, A. (2010). Description of an aerodynamic levitation apparatus with applications in Earth sciences. *Geochemical*

transactions, *11*(1), 4.

Petters, M. D., Prenni, A. J., Kreidenweis, S. M., DeMott, P. J., Matsunaga, A., Lim, Y. B., & Ziemann, P. J. (2006). Chemical aging and the hydrophobic-to-hydrophilic conversion of carbonaceous aerosol. *Geophysical research letters*, *33*(24).

Pfrang, C., Rastogi, K., Cabrera-Martinez, E. R., Seddon, A. M., Dicko, C., Labrador, A., ... & Squires, A. M. (2017). Complex three-dimensional self-assembly in proxies for atmospheric aerosols. *Nature communications*, *8*(1), 1724.

Pfrang, C., Sebastiani, F., Lucas, C. O., King, M. D., Hoare, I. D., Chang, D., & Campbell, R. A. (2014). Ozonolysis of methyl oleate monolayers at the air–water interface: oxidation kinetics, reaction products and atmospheric implications. *Physical Chemistry Chemical Physics, 16*(26), 13220-13228.

Pfrang, C., Shiraiwa, M., & Pöschl, U. (2011). Chemical ageing and transformation of diffusivity in semi-solid multi-component organic aerosol particles. *Atmospheric Chemistry and Physics*, *11*(14), 7343-7354.

Pope, F. D., Gallimore, P. J., Fuller, S. J., Cox, R. A., & Kalberer, M. (2010). Ozonolysis of maleic acid aerosols: Effect upon aerosol hygroscopicity, phase and mass. *Environmental science & technology, 44*(17), 6656-6660.

Pöschl, U. (2005). Atmospheric aerosols: composition, transformation, climate and health effects. *Angewandte Chemie International Edition, 44*(46), 7520-7540.

Priego-Capote, F., & de Castro, L. (2006). Ultrasound-assisted levitation: Lab-on-a-drop. *TrAC Trends in Analytical Chemistry, 25*(9), 856-867.

Pryor, W. A. (1994). Mechanisms of radical formation from reactions of ozone with target molecules in the lung. *Free Radical Biology and Medicine, 17*(5), 451-465.

Pryor, W. A., Squadrito, G. L., & Friedman, M. (1995). The cascade mechanism to explain ozone toxicity: the role of lipid ozonation products. *Free Radical Biology and Medicine, 19*(6), 935-941.

Raman Spectroscopy Explained. March 2017 [Brochure]. [PDF file]. Retrieved on 20 March 2017 from: http://www.renishaw.com/en/raman-spectroscopy-explained--25801

Raman, C. V., & Krishnan, K. S. (1928). A new type of secondary radiation. *Nature, 121*(3048), 501-502.

Rastogi, Kunal. (2015). Study of atmospheric aerosol in an ultrasonic trap (PhD Thesis). University of Reading, School of Chemistry, Food & Pharmacy. Reading, UK.

Robinson, A. L., Subramanian, R., Donahue, N. M., Bernardo-Bricker, A., & Rogge, W. F. (2006). Source apportionment of molecular markers and organic aerosol. 3. Food cooking emissions. *Environmental science & technology*, *40*(24), 7820-7827.

Rogge, W. F., Hildemann, L. M., Mazurek, M. A., Cass, G. R., & Simoneit, B. R. (1991). Sources of fine organic aerosol. 1. Charbroilers and meat cooking operations. *Environmental Science & Technology*, *25*(6), 1112-1125.

Rudich, Y., Donahue, N. M., & Mentel, T. F. (2007). Aging of organic aerosol: Bridging the gap between laboratory and field studies. *Annu. Rev. Phys. Chem., 58*, 321-352.

Schauer, J. J., Rogge, W. F., Hildemann, L. M., Mazurek, M. A., Cass, G. R., & Simoneit, B. R. (1996). Source apportionment of airborne particulate matter using organic compounds as tracers. *Atmospheric Environment*, *30*(22), 3837-3855.

Schultz, L., de Haas, O., Verges, P., Beyer, C., Rohlig, S., Olsen, H., ... & Funk, U. (2005). Superconductively levitated transport system-the SupraTrans project. *IEEE transactions on applied superconductivity*, *15*(2), 2301-2305.

Schwier, A. N., Sareen, N., Lathem, T. L., Nenes, A., & McNeill, V. F. (2011). Ozone oxidation of oleic acid surface films decreases aerosol cloud condensation nuclei activity. *Journal of Geophysical Research: Atmospheres*, *116*(D16).

Schwier, A., Mitroo, D., & McNeill, V. F. (2012). Surface tension depression by low-solubility organic material in aqueous aerosol mimics. *Atmospheric environment*, *54*, 490-495.

Seddon, A. M., Richardson, S. J., Rastogi, K., Plivelic, T. S., Squires, A. M., & Pfrang, C. (2016). Control of nanomaterial self-assembly in ultrasonically levitated droplets. *The journal of physical chemistry letters*, *7*(7), 1341-1345.

Seinfeld, J. H., & Pandis, S. N. (2006). *Atmospheric chemistry and physics: from air pollution to climate change*. John Wiley, 2006

Shiraiwa, M., Garland, R. M., & Pöschl, U. (2009). Kinetic double-layer model of aerosol surface chemistry and gas-particle interactions (K2-SURF): degradation of polycyclic aromatic hydrocarbons exposed to O 3, NO 2, H 2 O, OH and NO 3. *Atmospheric Chemistry and Physics*, *9*(24), 9571-9586.

Skoog, D. A., Holler, F. J., & Crouch, S. R. (2007). *Instrumental analysis*. Australia: Thomson Brooks/Cole

Smekal, A. (1925). Zur Quantentheorie der Streuung und Dispersion. *Zeitschrift für Physik*, *32*(1), 241-244.

Smith, G. D., Woods, E., DeForest, C. L., Baer, T., & Miller, R. E. (2002). Reactive uptake of ozone by oleic acid aerosol particles: Application of single-particle mass spectrometry to heterogeneous reaction kinetics. *The Journal of Physical Chemistry A*, *106*(35), 8085-8095.

Socrates, G. (2004). *Infrared and Raman characteristic group frequencies: tables and charts*. John Wiley & Sons.

Song, C., Zaveri, R. A., Alexander, M. L., Thornton, J. A., Madronich, S., Ortega, J. V., ... & Maughan, D. A. (2007). Effect of hydrophobic primary organic aerosols on secondary organic aerosol formation from ozonolysis of α-pinene. *Geophysical Research Letters*, *34*(20).

Spencer, G. F., & Kleiman, R. (1978). Palmitoleic acid in Roureopsis obliquifoliata (Connaraceae) seed oil. *Journal of the American Oil Chemists' Society*, *55*(10), 689-689.

Spietelun, A., Pilarczyk, M., Kloskowski, A., & Namieśnik, J. (2010). Current trends in solid-phase microextraction (SPME) fibre coatings. *Chemical Society Reviews*, *39*(11), 4524-4537.

Spiteller, P., Kern, W., Reiner, J., & Spiteller, G. (2001). Aldehydic lipid peroxidation products derived from linoleic acid. *Biochimica et Biophysica Acta (BBA)-Molecular*

and Cell Biology of Lipids, 1531(3), 188-208.

Staehelin, J., & Hoigne, J. (1982). Decomposition of ozone in water: rate of initiation by hydroxide ions and hydrogen peroxide. *Environmental Science & Technology, 16*(10), 676-681.

Sun, Q. (2009). The Raman OH stretching bands of liquid water. *Vibrational Spectroscopy, 51*(2), 213-217.

Sun, Q. (2012). Raman spectroscopic study of the effects of dissolved NaCl on water structure. *Vibrational Spectroscopy, 62*, 110-114.

Tabazadeh, A. (2005). Organic aggregate formation in aerosols and its impact on the physicochemical properties of atmospheric particles. *Atmospheric Environment, 39*(30), 5472-5480.

Thornberry, T., & Abbatt, J. P. D. (2004). Heterogeneous reaction of ozone with liquid unsaturated fatty acids: detailed kinetics and gas-phase product studies. *Physical Chemistry Chemical Physics, 6*(1), 84-93.

Tiddy, G. J. (1980). Surfactant-water liquid crystal phases. *Physics reports, 57*(1), 1-46.

Ultrasonic levitator manual. PDF file (n.d). [PDF file]. Retrieved on 16 September 2017, from: https://www.tec5.com/adbimage/575/asset-original/levitator_manual.pdf

Vandaele, V., Lambert, P., & Delchambre, A. (2005). Non-contact handling in microassembly: Acoustical levitation. *Precision engineering, 29*(4), 491-505.

Vesna, O., Sax, M., Kalberer, M., Gaschen, A., & Ammann, M. (2009). Product study of oleic acid ozonolysis as function of humidity. *Atmospheric environment, 43*(24), 3662-3669.

Vesna, O., Sjogren, S., Weingartner, E., Samburova, V., Kalberer, M., Gäggeler, H. W., & Ammann, M. (2008). Changes of fatty acid aerosol hygroscopicity induced by ozonolysis under humid conditions. *Atmospheric chemistry and physics, 8*(16), 4683-4690.

Wade, L. G. (2013). *Organic Chemistry: Pearson New International Edition*: Pearson

Education Limited

Wang, G., Kawamura, K., Watanabe, T., Lee, S., Ho, K., & Cao, J. (2006). High loadings and source strengths of organic aerosols in China. *Geophysical research letters, 33*(22).

Weitkamp, E. A., Hartz, K. E. H., Sage, A. M., Donahue, N. M., & Robinson, A. L. (2008). Laboratory measurements of the heterogeneous oxidation of condensed-phase organic molecular makers for meat cooking emissions. *Environmental science & technology*, *42*(14), 5177-5182.

Winborne, D. A., Nordine, P. C., Rosner, D. E., & Marley, N. F. (1976). Aerodynamic levitation technique for containerless high temperature studies on liquid and solid samples. *Metallurgical and Materials Transactions B, 7*(4), 711-713.

Wire 4 Training Modules Compilation (n.d). [PDF file]. Retrieved on April 2015 from: http://www.ccmr.cornell.edu/wp-content/uploads/sites/2/2016/08/Wire4_Training_Modules_Compilation-Part-1.pdf.

Wong, P. T. T., & Mantsch, H. H. (1983). Temperature-induced phase transition and structural changes in micellar solutions of sodium oleate observed by Raman scattering. *The Journal of Physical Chemistry*, *87*(13), 2436-2443.

Worsnop, D. R., Morris, J. W., Shi, Q., Davidovits, P., & Kolb, C. E. (2002). A chemical kinetic model for reactive transformations of aerosol particles. *Geophysical research letters, 29*(20).

Zahardis, J., & Petrucci, G. A. (2007). The oleic acid-ozone heterogeneous reaction system: products, kinetics, secondary chemistry, and atmospheric implications of a model system–a review. *Atmospheric Chemistry and Physics, 7*(5), 1237-1274.

Zahardis, J., LaFranchi, B. W., & Petrucci, G. A. (2006). Photoelectron resonance capture ionization mass spectrometry of fatty acids in olive oil. *European Journal of Lipid Science and Technology, 108*(11), 925-935.

Zeng, G., Holladay, S., Langlois, D., Zhang, Y., & Liu, Y. (2013). Kinetics of heterogeneous reaction of ozone with linoleic acid and its dependence on temperature,

physical state, RH, and ozone concentration. *The Journal of Physical Chemistry A*, *117*(9), 1963-1974.

Zhao, X., Wang, X., Ding, X., He, Q., Zhang, Z., Liu, T., ... & Deng, X. (2014). Compositions and sources of organic acids in fine particles (PM2. 5) over the Pearl River Delta region, south China. *Journal of Environmental Sciences*, *26*(1), 110-121.

Zhao, Y., Hu, M., Slanina, S., & Zhang, Y. (2007a). Chemical compositions of fine particulate organic matter emitted from Chinese cooking. *Environmental science & technology*, *41*(1), 99-105.

Zhao, Y., Hu, M., Slanina, S., & Zhang, Y. (2007b). The molecular distribution of fine particulate organic matter emitted from Western-style fast food cooking. *Atmospheric Environment*, *41*(37), 8163-8171.

Zhou, S., Gonzalez, L., Leithead, A., Finewax, Z., Thalman, R., Vlasenko, A., ... & Furutani, H. (2014). Formation of gas-phase carbonyls from heterogeneous oxidation of polyunsaturated fatty acids at the air–water interface and of the sea surface microlayer. *Atmospheric Chemistry and Physics*, *14*(3), 1371-1384.

Ziemann, P. J. (2005). Aerosol products, mechanisms, and kinetics of heterogeneous reactions of ozone with oleic acid in pure and mixed particles. *Faraday Discussions*, *130*, 469-490.